SEGREGATION OF A BINARY MIXTURE OF GRANULAR PARTICLES

A Dissertation

Presented to the Faculty of the Graduate School

of Cornell University

in Partial Fulfillment of the Requirements for the Degree of

Doctor of Philosophy

by

Kook-Young Yoon

May 2006

SEGREGATION OF A BINARY MIXTURE OF GRANULAR PARTICLES

Kook-Young Yoon, Ph.D.

Cornell University 2006

Kinetic theory for a binary mixture of slightly inelastic particles, based on Maxwellian velocity distribution with corrections due to high density, is used to predict segregation of a binary mixture with species differing in sizes and material densities. The relative mean species velocities indicates segregation for a mixture uniformly agitated under gravity. Molecular dynamics simulations of elastic hard spheres and physical experiments with inelastic spheres in a cylindrical container vibrated at high normalized acceleration support this prediction. An analysis for a non-uniformly agitated mixture under gravity provides a general criterion for segregation. We establish the validity of equipartition assumption in this problem.

Then, we introduce kinetic theory for mono-disperse disks with a friction model differentiating sticking and sliding collisions and derive a simple way of incorporating friction into theory with effective normal restitution coefficient.

We linearize Revised Enskog Theory for a binary mixture of disks with small differences in sizes and masses. By solving a boundary value problem of the mixture sheared between two bumpy circular cells, we provide experimenters a concrete way of testing the theory.

We then compare dense Maxwellian theory, from the first problem, with Revised Enskog Theory to see differences and their consequences on the prediction of segregation. In the absence of temperature gradient, with gravity present, they yield similar

predictions. However, in the presence of temperature gradient, with gravity absent, they only agree at high volume fractions.

Then, we describe a steady fully-developed flow on a bumpy incline, with a kinetic theory for mono-disperse spheres. We test the theory by attempting to reproduce three features of inclined flows from physical experiments and numerical simulations. On failing this, we describe modifications that may salvage the core of the theory with a few assumptions. A chain theory is introduced as a promising modification.

With the solutions of the chain theory, we predict segregation on an inclined plane using Revised Enskog Theory. Using density profiles for various sizes and material densities in the mixture, we compare its prediction with the prediction based on dense Maxwellian in the first problem and find that the agreement is good.

BIOGRAPHICAL SKETCH

The author was born in Seoul, Korea in 1978. He entered University of Waterloo in Canada in 1997 and graduated with a Bachelor's degree in Mathematics in 2001. On his graduation, he came to Theoretical and Applied Mechanics at Cornell University to study granular mechanics under the supervision of Professor James T. Jenkins.

ACKNOWLEDGEMENTS

I like to thank all the committee members for this study: Professor Michel Louge, Professor Carl Franck, Professor Zellman Warhaft and Professor James Jenkins. I also thank NASA for the financial support (Microgravity Grant NCC3-797) in the form of Graduate Research Assistantship. Especially, my thank goes, among all the members, to my advisor Professor Jenkins without whom the thesis would have been utterly impossible. Over the past four years, he demonstrated, by his own example, what it means to be passionate, hard working and precise in doing research. Furthermore, he exposed me to various research scenes around the world, which earned me the title of the most traveled graduate student in Theoretical and Applied Mechanics Department. His caring and understanding nature as a person has left a lasting impression on me all these years; what other graduate student would get a chance to go on a tube riding in Cayuga lake with his advisor?

And I like to thank all friends at TAM who have been a great source of stimulating and entertaining conversations in the hallway of Thurston Hall in the middle of night. My special thank goes to Luigi La Ragione who successfully ingrained in my brain the Italian life style; David, this is life! Life is wonderful! Do you not agree, David? Without the joy of life, I would not be here.

TABLE OF CONTENTS

LIST OF FIGURES

Chapter 1

INTRODUCTION

Granular mechanics is the study of a collection of inelastic particles, whether this collection is in motion or in stasis.[31] What distinguishes granular particles from a molecular gas is the loss of energy as a result of collisions of particles, the sources of this loss being either inelasticity in a collision, viscosity due to air between the particles or friction due to the interaction of rough particle surfaces. Common examples of granular particles and regimes of behavior include a pile of sand forming a pyramid, a constantly shaken box of cereals and granules of rice being processed in a factory. Though a particle can take any shape, typically in modeling a granular particle, it is common to assume it to be a sphere (or a disk in the case of two dimensional study) for the sake of simplicity. Experiments by Savage and Sayed[61] indicate that the same scaling of the shear and normal stresses with shear rate are observed in homogeneous collisional shearing flows of glass spheres and crushed walnut shells. However, details of the flow are certain to be influenced by the enhancement of the coupling between the rotational and translational degrees of freedom associated with departures from spherical or circular shape. In addition, we assume that particles are massive enough so that the effect of air friction can be ignored, as in particles in vacuum. In his pioneering experiments on shearing flows of neutrally buoyant spheres, Bagnold[8] introduces a dimensionless measure of the relative importance of viscous and collisional momentum transfer. Later studies by Koch and Sangani[44] characterize the influence of viscosity on the dissipation of particle fluctuation energy. Consequently, information is available to evaluate the neglect of viscosity in a given situation.

Although this collection of granular particles can behave as a solid or fluid, this

thesis concerns the latter behavior of the collection: in particular, rapid flow of granular particles.[13][23] Rapid flow of granular particles deals with particles interacting through collisions in which the mean time between collisions is much greater than the time taken in a single collision. That is, the collision can be assumed to be instantaneous. This implies that the dominant mechanism of momentum transfer between particles occurs through collisions. The possibility of lasting or rolling contacts between particles is ignored. Experiments carried out on steady, homogeneous shearing flows of dry granular materials in annular shear cells[61][18][26] give shear and normal stresses close to those predicted by theories based on instantaneous, binary collisions. In steady, fully-developed, but inhomogeneous shear flows in other geometries[71], the predictions of a kinetic theory based on instantaneous, binary interactions are in excellent agreement with experiments and discrete numerical simulations.

One of the most interesting phenomena of granular particles is their segregation. For example, when a mixture of different types of particles in a circular cylinder is rotated with its axis horizontal, after a few rotations the mixture tends to separate into regions of homogeneous types of particles, radially as well as axially.[64]

As a simpler case, imagine a box of baseballs and softball. If the box is shaken strongly enough, one will find that softballs, which are bigger, are found at the top, while baseballs, which are smaller, will be found at the bottom. This phenomenon where the bigger particles end up at the top is called “Brazil Nut Effect”[60][43] and this phenomenon is the motivation of this thesis.

To model the behavior of rapid flows, we adopt a kinetic theory of dense gases in which the particle velocity distribution function is assumed rather than solved for.[33] The approach we take through the thesis is to evaluate mean values of, for example, number density and velocity using the distribution function and then to use these in

balance equations for momentum and fluctuation energy. Either by looking at a certain variable in the balance equations or by numerically solving them in a boundary value problem, predictions of the direction of segregation are made. Through the study, we confine ourselves with either a binary mixture (a mixture with two types of particles) or a mono-disperse flow (one type of particle); in the latter case, the purpose of the study is to find out general properties of granular flows, excluding segregation.

The kinetic theory of a binary mixture of hard, nearly elastic particles, developed by Jenkins and Mancini[36], assumes a Maxwellian velocity distribution function and takes the high density of the mixture into account by distinguishing the centers of particles and by correcting the collision frequency with radial distribution functions. In addition, the theory assumes that only binary collisions are possible and the velocities of colliding particles are not correlated with each other. This theory is an extension of the approach of Thorne[15] who used Chapman-Enskog method to derive a theory for hard, elastic particles. The difference between these two theories is the term having to do with dissipation of energy as a result of inelastic collisions, which were modelled with a restitution coefficient in the theory of Jenkins and Mancini.[36]

Once Barajas, Garcia-Colin and Pina[9] found that the arbitrary choice for evaluating the radial distribution functions in the theory of Thorne[15] and in other competing theories led to a conflict with irreversible thermodynamics, van Beijeren and Ernst[66] and López de Haro, Cohen and Kincaid[46] developed a kinetic theory that is consistent with irreversible thermodynamics. With this revised theory and with a perturbed form of Maxwellian velocity distributions, Jenkins and Mancini[37] and subsequently Arnarson and Willits[7][70][1] improved the existing theory[36] for inelastic particles. However, as this revised theory was too complicated to use because of its lengthy equations, a simplification was introduced by Arnarson and Jenkins[6] who linearized the revised

theory for small differences in masses and radii of the mixture for spheres.

Xu, Louge and Reeves[71] compared the predictions of this simplified theory[6] with numerical simulations for a binary mixture of spheres in a circular Couette cell with bumpy boundaries moving in opposite directions, with and without plane side walls. They found very good agreements in mean and fluctuation velocities, but they also noted that the theory tended to over-estimate segregation effects, especially in a dense region. Louge *et al*.[47] employed the same theory, with modifications to account for flat side walls, in race track geometry. Using this cell, they performed experiments in micro-gravity, with moving inner wall and stationary bumpy outer wall. By looking at flows in the straight section of the cell close to the side wall, they compared the fluctuation velocities and number densities measured from experiments and predicted from numerical simulations and saw good agreement. They found very good agreement between the theory and the simulation for steady, fully developed flows in the straight section of the track. They did not compare the experiment with the theory because of their uncertainty whether the flow was fully-developed. However, they did determine the numerical simulation was able to reproduce the developing flow and the theory was able to predict what was measured in the numerical simulations of a fully-developed flow.

There are on-going developments on theories for a mixture with multi-components [19], but we limit our attention to a mixture of two components in this thesis.

Chapter 2, following the Introduction, discusses a simple way of predicting segregation in a binary mixture in an ideal situation. An ideally large container containing a homogeneous mixture of small and large particles, differing in masses, is assumed to be going through strong collisions, uniformly agitated throughout the container. To make the study simpler, we assume that the large particles are dilute in a dense collection of small particles. We imagine, then, that we can suddenly "turn on" gravity. In such a

case, we obtain a simple formula for the mean motion of the bigger particles with respect to the smaller particles as soon as gravity is turned on. We use it to predict the direction of segregation. We discuss a relevant numerical simulation and physical experiments. This chapter discusses a few more issues pertaining to the assumption of equipartition of granular temperatures and the prediction of segregation in the presence of gravity and the temperature gradient. The prediction of the initial direction of segregation using an algebraic condition is compared with steady concentration profiles obtained as solutions to boundary-value problems for segregation. Relevant discrete numerical simulations have been carried out by Hong, Quinn and Luding[30] and experiments that involve the segregation of a binary mixture above a vibrating base[12][21] provide a test of the theory.

When modeling the rapid flow of granular particles, we typically look at the translational motion of particles, primarily because it saves us the trouble of studying additional equations of angular momentum and rotational energy balances. However, if the model is to describe the frictional nature of particles, it is necessary to incorporate the effects of friction at the surface of particles. Chapter 3 accomplishes this with the friction model that classifies a collision either as sticking or sliding. Modeling the sticking collision with a constant tangential restitution coefficient and the sliding one with a constant Coulomb friction coefficient[67], we look at the balance equations of a flow of mono-disperse disks for their translational as well as rotational motions. We simplify the problem by assuming that the friction is small. Then after some assumptions, that having a small friction is equivalent to having no friction, but with a smaller normal restitution coefficient.[42] Hence, the picture becomes dramatically simpler. We incorporate the rotational motion by including frictional dissipation and then deal exclusively with the translation motion with a new normal restitution coefficient, an effective

restitution coefficient.

Chapter 4 returns to a binary mixture, but a more refined theory is introduced. Whereas Chapter 2 uses a binary mixture theory, which we call dense Maxwellian, Chapter 4 employs Revised Enskog Theory.[66][46][7] The first part of this chapter is mere improvement of a similar discussion appearing in an unpublished work of Arnarson. We pick up where he left off and slightly improve it by including gravity, which was not considered in his study. The later part of this chapter provides examples of a boundary value problem for a mixture sheared between two bumpy circular walls and for a mixture on a vibrated bottom boundary. We show in detail how to set up the flow equations and the boundary conditions in order to solve them using bvp4c in MATLAB.

Chapter 5 serves to compare dense Maxwellian and Revised Enskog Theory, discussed in Chapter 4. Revised Enskog Theory, more refined than dense Maxwellian, suffers the drawback of being very complicated. This limits its use only to cases where its expressions can be greatly simplified, such as when the constituents of the mixture do not differ much in sizes and masses.[6] Naturally, we are interested to see whether this complicated theory differs in any significant way from dense Maxwellian, which is simpler. Thus, we set about comparing these two theories, in the analytically tractable case of similar sizes and masses.

In Chapter 6, we challenge the limit of the kinetic theory for dense gases by looking at steady fully developed inclined flows of mono-disperse spheres on a bumpy incline, which are typically at a density where the assumptions of kinetic theory break down. First, three characteristic features of an inclined flow found in physical experiments[55] and numerical simulations[63] are stated and we attempt to reproduce these features using kinetic theory. After failings in all attempts to reproduce solutions in agreement with those features, a few possible modifications to kinetic theory are mentioned, with

the hope of salvaging the theory with the bulk of the existing framework intact. In particular, the chain theory which seems to have the most success to this date is discussed in greater details.

Chapter 7 wraps up the story of the segregation of a binary mixture by looking at an inclined flow of a binary mixture. The prediction from the simple approach in Chapter 2 is compared to numerical solutions from solving this boundary value problem, the kinetic theory having been modified with the chain theory introduced in the previous chapter. The key point of this chapter is the agreement between the analytical prediction using the initial motion of bigger particles in the dense Maxwellian theory and the numerical prediction of steady fully developed state flows of Revised Enskog Theory. Although there is currently no experimental work on segregation on steady, fully developed inclined flows that we can use to compare with our predictions, Berton *et al*.[11] studied experimentally a binary mixture of disks flowing on a bumpy 2-D inclined chute. By carefully following trajectories of large and small disks in quasi-fully-developed flows for a mixture of same materials, but different sizes, they tried to identify possible mechanisms of segregation on inclined flows.

Chapter 2

THE INFLUENCE OF DIFFERENT SPECIES' GRANULAR TEMPERATURES ON SEGREGATION IN A BINARY MIXTURE OF DISSIPATIVE GRAINS

When a binary mixture of particles differing in sizes and material densities is agitated, the mixture has a tendency to segregate into homogeneous regions of one type of particle. Jenkins and Yoon[41] studied this problem of segregation in a binary mixture by considering a case where large particles are dilute in a dense gas of small particles; that is, a few large particles among many small particles. The mixture was assumed to be homogeneous and agitated uniformly in the absence of gravity. Then gravity was imagined to be turned on[30] and the initial motion of the large particles with respect to the small particles was used as an indicator of segregation. Using a kinetic theory for a binary mixture derived by Jenkins and Mancini[36], Jenkins and Yoon[41] derived an algebraic relation between the initial mean velocity of intruder particles with respect to the mean velocity of background particles and the ratios of particle radii and material densities. In deriving this expression for the motion of the intruder particles, they assumed that the gradients of the number densities and the partial pressures could be ignored. In addition, they assumed that the granular temperature of each species was equal to the mixture granular temperature.

However, Wildman and Parker[68] and Feitosa and Menon[21] found in physical experiments that when a binary mixture of granular particles is vibrated, each species

achieved its own granular temperature, different from that of the other species, and the ratio of these temperatures depended strongly on the ratio of material densities. The partition of granular temperatures has also been studied in numerical simulations by Barrat and Trizac[10], Alam and Luding[49], Galvin, Dahl and Hrenya[25] and others, who report failure of equipartition and emphasize the importance of including differences in species' temperatures when studying a mixture.

In this work, we test the importance of incorporating the difference in granular temperatures on segregation due to gravity. Using the expressions provided by Jenkins and Mancini[36] for this difference, we compare the predictions of segregation with different species temperatures to those with equipartition, in a fashion similar to Jenkins and Yoon[41].

2.1 Preliminaries

We consider a mixture of large and small particles. We later specialize to the case in which large particles are dilute in a dense gas of small particles. The small and the large species are denoted by A and B, respectively, and have radius r_i, mass m_i and material density ρ_i^s, where $i = A$ or B. We assume that the mixture is agitated uniformly through its depth, so that the granular temperature is constant, and that the variation in fields occurs only along the z-axis, directed upward opposite to the gravitational acceleration g. A prime is used to denote a derivative with respect to z.

The particles are smooth, nearly elastic spheres (or disks) with a constant restitution coefficient e. The number density is

$$n_i(z) \equiv \int f_i^{(1)}(\mathbf{c}_i, z)\, \mathbf{dc}_i,$$

where the integration is done over velocities $\mathbf{c}$ and $f_i^{(1)}$ is the single particle veloc-

ity distribution function, assumed to be Maxwellian, as in the calculations of Jenkins and Mancini[36]. The volume fraction (or the area fraction for disks) is $\nu_i \equiv 2\left(D-1\right)\pi r_i^D n_i/D$, where D is 2 for disks and 3 for spheres, and the mass density is given by $\rho_i \equiv m_i n_i$. The total number density is $n \equiv n_A + n_B$ and the total volume fraction (or area fraction) is $\nu \equiv \nu_A + \nu_B$. We also introduce $r_{ik} \equiv r_i + r_k$ and $m_{ik} \equiv m_i + m_k$.

The granular temperature of species i is

$$T_i \equiv \frac{1}{D} m_i \int \left(\mathbf{c}_i - \mathbf{u}\right)^2 f_i^{(1)}\left(\mathbf{c}, z\right) \mathbf{dc},$$

where $\mathbf{u}$ is the mass averaged velocity of the mixture. The mixture temperature is $T \equiv n^{-1}\left(n_A T_A + n_B T_B\right)$.

The deviation in species temperature from the mean, which was ignored in Jenkins and Yoon[41], is $\theta_i \equiv T_i - T$ and it follows from the definition of T that $0 = n_A\theta_A + n_B\theta_B$.

2.1.1 Momentum equations

The momentum equation of each species, ignoring inertia and viscous contributions to the stress, is given by

$$\pi_i' = -n_i m_i g + \phi_i, \tag{2.1}$$

where the partial pressure π_i, assuming here and elsewhere that $1 + e \cong 2$ for nearly elastic particles, is[36]

$$\pi_i \equiv n_i \left(T + \theta_i\right) + \sum_{k=A,B} \pi \frac{D-1}{D} g_{ik} r_{ik}^D n_i n_k \times \left(T + \frac{m_i \theta_k + m_k \theta_i}{m_{ik}}\right),$$

and the rate of exchange of momentum per unit volume (or area for disks) ϕ_i is[36]

$$\phi_A \equiv \pi \frac{D-1}{D} g_{AB} r_{AB}^D n_A n_B T \left[\frac{m_B - m_A}{m_{AB}} \left(\ln T\right)' + \left(\ln \frac{n_A}{n_B}\right)' + \frac{4}{r_{AB}} \left(\frac{2 m_A m_B}{\pi m_{AB} T}\right)^{1/2} w_{BA}\right],$$

where w_{BA} is the mean velocity of B with respect to the mean velocity of A, and $\phi_A = -\phi_B$. The radial distribution functions for contacting pairs are, for spheres[14]:

$$g_{ik} \equiv \frac{1}{1-\nu} + \frac{6 r_i r_k}{r_{ik}} \frac{2\pi \left(n_A r_A^2 + n_B r_B^2\right)}{3\left(1-\nu\right)^2} + 8 \left(\frac{r_i r_k}{r_{ik}}\right)^2 \frac{4\pi^2 \left(n_A r_A^2 + n_B r_B^2\right)^2}{9\left(1-\nu\right)^3}$$

and, for disks[36]:

$$g_{ik} \equiv \frac{1}{1-\nu} + \frac{9}{8} \frac{r_i r_k}{r_{ik}} \frac{\pi \left(n_A r_A + n_B r_B\right)}{\left(1-\nu\right)^2}.$$

Upon dividing the momentum equation of each species by ρ_i and subtracting one from the other, we obtain the weighted difference of momentum equations:

$$0 = -\pi'_A \frac{\rho_B}{\rho} + \pi'_B \frac{\rho_A}{\rho} + \phi_A. \tag{2.2}$$

With the introduction of $R \equiv \pi_A n_B / (\pi_B n_A)$ and with the expression for π'_A from (2.1), we can write

$$\pi'_B = \pi_B \left(\ln \frac{n_B}{n_A} \right)' - \frac{m_A n_B g}{R} + \frac{n_B}{n_A} \frac{\phi_A}{R} - \pi_B \left(\ln R \right)'.$$

Upon substituting this and the expression for π'_A from (2.1) into (2.2), as in Jenkins and Yoon[41], we obtain the equation that determines the difference w_{BA} between the mean motion of B and the mean motion of A:

$$\begin{aligned} &\left(R^{-1} n_B + n_A \right) \pi \frac{D-1}{D} g_{AB} r_{AB}^D n_B T \left[\frac{m_B - m_A}{m_{AB}} \left(\ln T \right)' \right. \\ &\left. + \left(\ln \frac{n_A}{n_B} \right)' + \frac{4}{r_{AB}} \left(\frac{2 m_A m_B}{\pi m_{AB} T} \right)^{1/2} w_{BA} \right] \\ &= \pi_B \left(\ln \frac{\pi_A}{\pi_B} \right)' + \left(m_A - R m_B \right) \frac{n_B g}{R}. \end{aligned} \tag{2.3}$$

2.1.2 Energy equations

We next write energy equation of each species, ignoring the time derivative, the energy fluxes associated with the species mean velocities, the gradients of the species energy fluxes and the product between diffusion velocities and the gradient of the total pressure. The result is given by[36]

$$0 = \gamma_i + \rho_i s, \tag{2.4}$$

where s is an energy source that maintains the temperatures constant, similar to the thermal reservoir used in the simulations[30], and the dissipation rate γ_i, due to the

difference in temperatures and the collision, is[36]:

$$\begin{aligned}\gamma_i = & \sum_{k=A,B} 4 g_{ik} r_{ik}^{D-1} n_i n_k T \left(D-1\right) \\ & \times \left\{ \left(\frac{2\pi m_i m_k T}{m_{ik}} \right)^{1/2} \left(\frac{\theta_k - \theta_i}{m_{ik} T} \right) \right. \\ & - \frac{m_k}{m_{ik}} \left(1-e\right) \left[\frac{1}{2} \left(\frac{2\pi m_{ik} T}{m_i m_k} \right)^{1/2} \right. \\ & \left. \left. + \frac{3}{4} \left(\frac{2\pi m_{ik} T}{m_i m_k} \right)^{1/2} \left(\frac{m_i \theta_k + m_k \theta_i}{m_{ik} T} \right) \right] \right\}.\end{aligned}$$

Upon dividing (2.4) by the species density and taking the difference of the results, we have

$$\frac{\gamma_A}{\rho_A} = \frac{\gamma_B}{\rho_B},$$

from which the expression for the difference of temperature deviations can be calculated [36]:

$$\begin{aligned}& \theta_B - \theta_A \\ & = \frac{n m_{AB}}{\rho} D_{AB} \left(1-e\right) \pi \left(\frac{T}{\pi} \right)^{1/2} \left[m_B n_A r_{AA}^{D-1} \right. \\ & \times \frac{g_{AA}}{m_A^{1/2}} + \sqrt{2} \left(m_B^2 n_B - m_A^2 n_A \right) r_{AB}^{D-1} \\ & \left. \times \frac{g_{AB}}{\left(m_A m_B m_{AB} \right)^{1/2}} - m_A n_B r_{BB}^{D-1} \frac{g_{BB}}{m_B^{1/2}} \right],\end{aligned}$$

where

$$D_{AB} \equiv \frac{1}{2 n r_{AB}^{D-1} g_{AB}} \left(\frac{m_{AB} T}{2\pi m_A m_B} \right)^{1/2}.$$

With $0 = n_A \theta_A + n_B \theta_B$, we can rewrite this difference in terms of θ_B alone:

$$\left(1+\frac{n_B}{n_A}\right)\theta_B \tag{2.5}$$
$$= \frac{nm_{AB}}{\rho} D_{AB}\left(1-e\right)\pi n_A \left(\frac{T}{\pi}\right)^{1/2} \left[m_B r_{AA}^{D-1}\right.$$
$$\times \frac{g_{AA}}{m_A^{1/2}} + \sqrt{2}\left(m_B^2 \frac{n_B}{n_A} - m_A^2\right) r_{AB}^{D-1}$$
$$\left.\times \frac{g_{AB}}{\left(m_A m_B m_{AB}\right)^{1/2}} - m_A \frac{n_B}{n_A} r_{BB}^{D-1} \frac{g_{BB}}{m_B^{1/2}}\right].$$

2.2 Assumptions

Assuming that the mixture is uniformly agitated through the depth, we ignore T' in the equation (2.3). Furthermore, because the mixture is assumed to be homogeneous before the gravity is turned on, we neglect terms that involve derivatives of the logarithms of the ratios of number densities and partial pressures:

$$\pi \frac{D-1}{D} g_{AB} r_{AB}^D n_B T \frac{4}{r_{AB}} \left(\frac{2m_A m_B}{\pi m_{AB} T}\right)^{1/2} w_{BA}$$
$$= \frac{1}{n_B R^{-1} + n_A}\left(m_A - R m_B\right)\frac{n_B g}{R}.$$

This can be written more compactly as

$$k^2 w_{BA} = \frac{m_A}{m_B} - R \tag{2.6}$$

where $k^2 > 0$. This provides an algebraic characterization of initial segregation; B will rise if $m_A/m_B - R > 0$ and fall if $m_A/m_B - R < 0$. We note that R, which contains the ratio of partial pressures, is the only quantity that is sensitive to the differences in temperatures.

2.2.1 B dilute in A

To simplify the expressions for R and θ_B, we assume that large particles of B are dilute in a dense gas of small particles of A. With this assumption, we ignore terms proportional to n_B/n_A and replace ν_A by ν.

The radial distribution functions for spheres can then be approximated by

$$g_{AA} \approx \frac{1}{1-\nu} + \frac{3\nu}{2(1-\nu)^2} + \frac{\nu^2}{2(1-\nu)^3},$$
$$g_{AB} \approx \frac{1}{1-\nu} + \frac{3\nu}{(\eta+1)(1-\nu)^2} + \frac{2\nu^2}{(\eta+1)^2(1-\nu)^3},$$

where $\eta = r_A/r_B$ and those for disks by

$$g_{AA} \approx \frac{1}{1-\nu} + \frac{9}{16}\frac{\nu}{(1-\nu)^2}$$

$$g_{AB} \approx \frac{1}{1-\nu} + \frac{9}{8}\frac{1}{\eta+1}\frac{\nu}{(1-\nu)^2}.$$

Because $n_A\theta_A + n_B\theta_B = 0$, we see that $\theta_A/\theta_B = -n_B/n_A$ can be ignored and (2.5) simplifies to

$$\theta_B = \left(\frac{\eta^D+\mu}{\eta^D}\right)^{3/2} \frac{1-e}{2^{3/2}} \frac{T}{g_{AB}} \frac{\mu^{1/2}}{\eta^{D/2}} \times \left[\left(\frac{2\eta}{\eta+1}\right)^{D-1} g_{AA} - \frac{\sqrt{2}\eta^{2D}}{\mu^{3/2}(\eta^D+\mu)^{1/2}} g_{AB}\right] \tag{2.7}$$

where $\mu \equiv \rho_B^s/\rho_A^s$.

With this, the ratio of temperatures can be calculated

$$\frac{T_A}{T_B} = \left\{1 + \left(\frac{\eta^D + \mu}{\eta^D}\right)^{3/2} \frac{1-e}{2^{3/2}} \times \left[\left(\frac{2\eta}{\eta+1}\right)^{D-1} \frac{\mu^{1/2}}{\eta^{D/2}} \frac{g_{AA}}{g_{AB}} - \frac{\sqrt{2}\eta^{3D/2}}{\mu\left(\eta^D+\mu\right)^{1/2}}\right]\right\}^{-1}.$$

Note that when collisions are perfectly elastic, the temperatures are equal. An additional simplification can be made by evaluating g_{ij} at a representative dense solid fraction: $\nu = 1/2$ for spheres and $\nu = 3/4$ for disks. In Figure 2.1, we show how the temperature ratio T_A/T_B varies with the diameter ratio $r_A/r_B = \eta$ for spheres of the same material ($\mu = 1$) and in Figure 2.2, we plot T_A/T_B against $m_B/m_A = \mu/\eta^D$ for particles of the same size ($\eta = 1$), with fixed values of e in both cases.

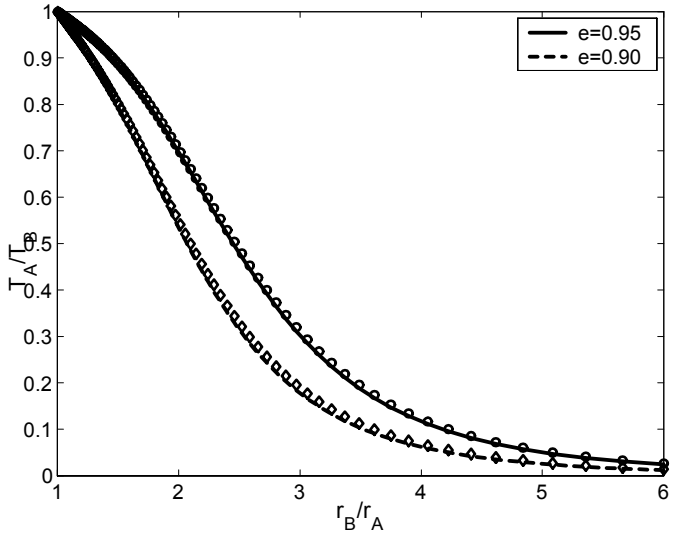

Figure 2.1: Ratio of temperatures versus ratio of radii.

The simulations of Galvin, Dahl and Hrenya[25] and the predictions of Barrat and Trizac[10] are in good agreement with these results. As an example, Figure 2.3 illustrates the ratio of temperatures for a mixture with equal material density and $e = 0.95$

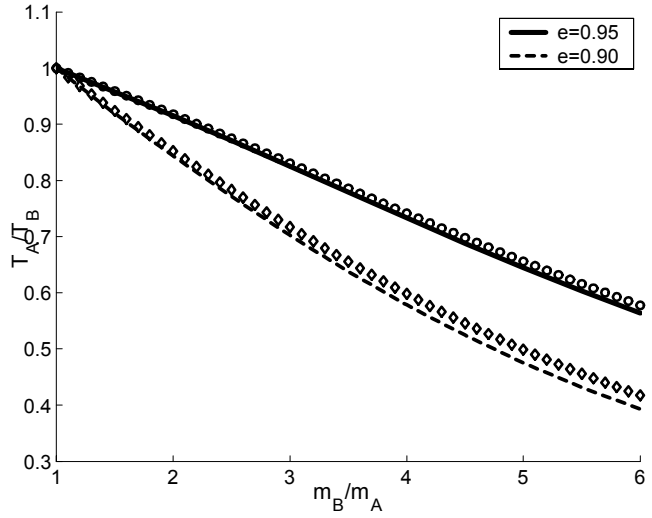

Figure 2.2: Ratio of temperatures versus ratio of masses.

from our calculation and the calculation of Barrat and Trizac[10], whose results are in excellent agreement with numerical simulations and physical experiments.

2.3 Segregation

Recalling (2.6), we can incorporate the role of the temperature difference in predicting segregation by employing (2.7) in the expression for R. Ignoring the kinetic contribution to π_i, we obtain

$$R = \frac{g_{AA}}{g_{BA}} \frac{r_{AA}^D}{r_{BA}^D} \frac{1}{1 + \frac{\theta_B/T}{m_B/m_A+1}}.$$

Plotting $w_{BA} = 0$ or $m_A/m_B - R = 0$ in $\eta - \mu$ plane for a fixed value of e, we can characterize the role that non-equipartition plays in the initial motion of the large intruder particles.

In Figure 2.4, we see that the difference in temperatures modifies the segregation curve slightly. The straight line ($e = 1$) is the segregation criterion when there is

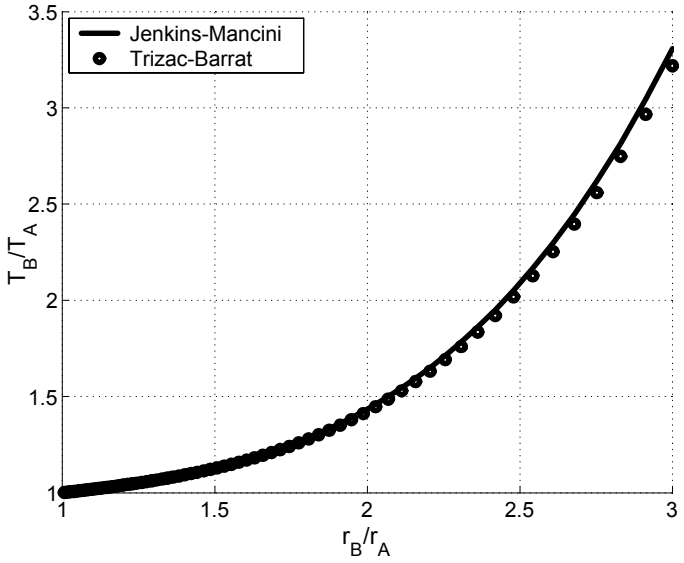

Figure 2.3: Comparison of temperature ratios between Jenkins and Mancini[36] and Barrat and Trizac[10].

no difference in granular temperatures. With decreasing values of e, the difference in temperatures increases and yet the segregation criteria change little.

We have to emphasize, however, that the theory of Jenkins and Mancini[36] that we employ here assumes that the deviation of species temperature from the mixture temperature, θ_i , is a small quantity. However, as shown in Figure 2.1 and 2.2, for small values of e and large differences in masses and sizes, this assumption of small θ_i does not hold and this theory should not apply. Thus, though Figure 2.4 displays parameters beyond the valid range of the theory, this prediction should be used for values of e, μ and η such that the ratio of the temperatures stays greater than, say 0.9.

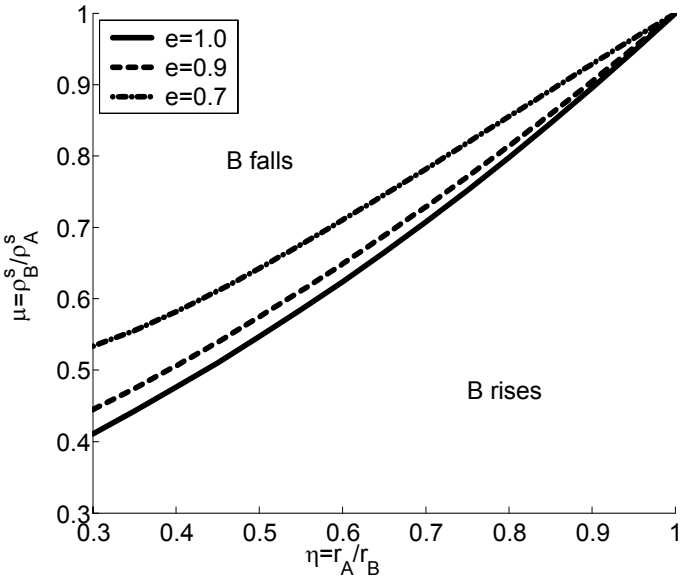

Figure 2.4: Material density ratio versus radii ratio for spheres.

2.4 Segregation with gravity and the temperature gradient

When a binary mixture undergoes segregation, segregation takes place because there exists some asymmetry in the mixture. Such asymmetry is introduced through the existence of a body force, such as gravity, and/or through a gradient of granular temperature. However, in the presence of both effects, it is possible to minimize or maximize the phenomenon of segregation, by adjusting gravity and temperature gradient. In this section, we look at two limiting cases: first with gravity, but with no gradient in temperature, as in the previous Section; then with temperature gradient, but no gravity.

By combining what these two extreme cases predict about segregation, one can gather more information about segregation when both gravity and temperature play roles in segregation.

2.4.1 Case 1: $g \neq 0$ and $T' = 0$

As this is a case that we have just looked at, but now with $e = 1$, we briefly review the prediction. By looking at w_{BA}, the initial velocity of B with respect to A, the direction of segregation is indicated. As before, if $w_{BA} > 0$, B moves up against gravitational pull and down if $w_{BA} < 0$.

When the inhomogeneities are neglected in the difference of momentum equation and the limit $n_B/n_A \ll 1$ is taken, we obtain a very simple equation relating the relative velocity to the difference in the ratios of the partial pressures and densities:

$$\begin{aligned} \frac{4TK_{AB}}{r_{AB}}\left(\frac{2m_Am_B}{\pi m_{AB}T}\right)^{1/2} w_{BA} &= \frac{n_B}{Rn_A+n_B}(m_A - Rm_B)g \\ &= \frac{m_An_An_B}{\pi_A+\pi_B}\left(\frac{\pi_B}{\rho_B}-\frac{\pi_A}{\rho_A}\right)g \end{aligned} \tag{2.8}$$

If we were dealing with an ideal gas, the quantity $\pi_B/\rho_B - \pi_A/\rho_A$ would correspond to difference in temperatures. Thus, it is conceivable that the segregation is due to a difference in temperatures.

Figure 2.5 plots the line $w_{AB} = 0$ from (2.8) for $\nu = 0.5$, which is a typical volume fraction for a dense gas of spheres. The solid line is the prediction from kinetic theory, while the dotted line is from Hong *et al*.'s numerical simulations[30] and symbols are from physical experiments of Breu *et al*.[12]

The molecular dynamics simulation of Hong *et al*.[30], for elastic hard spheres in 3D systems and disks in 2D systems, begins with a homogeneous binary mixture without gravity at a high temperature. Then, gravity is turned on and the system is taken to be in contact with a thermal reservoir that provides a uniform agitation to the entire system. Based on the final segregated configuration in the simulation, Hong *et al*.[30] provided the criterion shown in Figure 2.5. We note that while the prediction of the

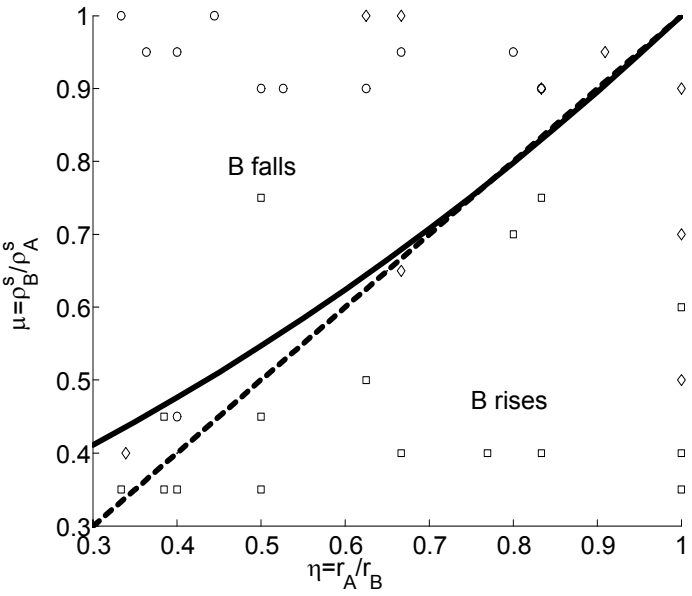

Figure 2.5: Comparison of the current theory with numerical simulation and physical experiments. Solid line is the prediction of the current theory. Dashed line is that of Hong *et al*.[30] Symbols are from the experiment of Breu *et al*.[12]: circles when bigger particles fall, squares when bigger particles rise and diamonds when the mixture stays mixed.

current work is based on the initial motion of large particles, the segregation criterion of the simulation is based on the final segregated configuration. The agreement between the two is quite good.

Breu *et al*.[12], in attempting to reproduce the predictions of the simulation of Hong *et al*.[30] in a physical experiment, prepared a cylinder containing a binary mixture of granular particles on a plate that was excited by vertical vibrations. The cylinder was first filled with layers of identical particles and on top of them were placed several layers of another type of particle. The granular particles they used were chosen from glass, aluminum, bronze, steel and so forth, with typical diameter being around 10 mm,

about one tenth of the diameter of the container. The bottom particles were predicted to rise from the simulations of Hong *et al*.[30] in all situations. After testing various combinations of different types of particles and determining the final position of the larger particles, Breu *et al*.[12] concluded that the prediction of Hong *et al*.[30] agreed with their experiments, provided that the normalized acceleration of the vibration was sufficiently high.

Feitosa and Menon[21] studied a similar system experimentally that differed from Breu *et al*.[12] in that their system was two dimensional. It consisted of a binary mixture of spherical balls of the same size, but different masses and restitution coefficients, between two parallel plates, the distance between the plates being 1.2 particle diameter. They vibrated the cage vertically at accelerations greater than $32g$ and velocities greater than 0.86 m/s, they measured the density profiles of each species. When the masses of the particles of each species were the same, the density profiles of both species was the same, regardless of the restitution coefficient of each species. However, when the masses differed, they observed that the heavier particles were found about mid-way between the top and the bottom of the cell, whereas the lighter particles were found uniformly spread through the depth of the cage. This finding is not expected of our simple theory of the initial segregation, the simulation of Hong *et al*.[30] and the experiment of Breu *et al*.[12], where we expect the heavier particles would sink below lighter particles. It is not clear at this point what the source of the difference is. We note that Feitosa and Menon[21] found that, at this range of high acceleration, no particular type of cluster was formed and that there was no horizontal gradient in velocity or density. In Chapter 4, we will solve a boundary value problem of segregation of disks on a vibrated bottom boundary, using a different kinetic theory for a binary mixture. For the vibrating boundary condition for kinetic theory, we adopt that of Richman[59] who considers a bumpy

boundary which moves up and down from the rest position with a specified fluctuation velocity and derives the appropriate boundary conditions by calculating the momentum and the energy exchange rates between the flow and the boundary.

2.4.2 Case 2: $g = 0$ and $T' \neq 0$

In the absence of gravity, it is rather well known that in systems that consist of particles of the same material, but two different sizes, or particles of the same size, but two different masses, the more massive particles move to the regions of lower temperature.[71][47] This is also predicted in steady fully-developed flows through solutions of boundary-value problems based on the kinetic theory.[71][6] Here, we wish to obtain this result as a simple algebraic condition that governs the initial direction of segregation in a system subjected to a sudden temperature gradient in the absence of gravity. As in the previous Section, we make the assumption of equipartition.

With the same physical setup and assumptions as in Case 1, except now with $g = 0$ and $T' \neq 0$, a similar routine calculation from momentum equations gives the following expression, showing how w_{BA} is related to temperature gradient, masses and radii of A and B.

$$\frac{4T}{r_{AB}}\left(\frac{2m_A m_B}{\pi m_{AB} T}\right)^{1/2} w_{BA} = T' \frac{m_A - m_B}{m_A + m_B}$$

As in Case 1, w_{BA} indicates how segregation occurs initially. We see that it only depends on the mass difference of A and B, not on their difference in size.

If B is less massive than A, then w_{BA} shares the same sign as T'. This implies that B goes to a region of higher temperature. This is, when gravity is absent but only a temperature gradient is imposed, the segregation exclusively depends on the masses of the particles of A and B, not individually on size or material density. Heavier particles

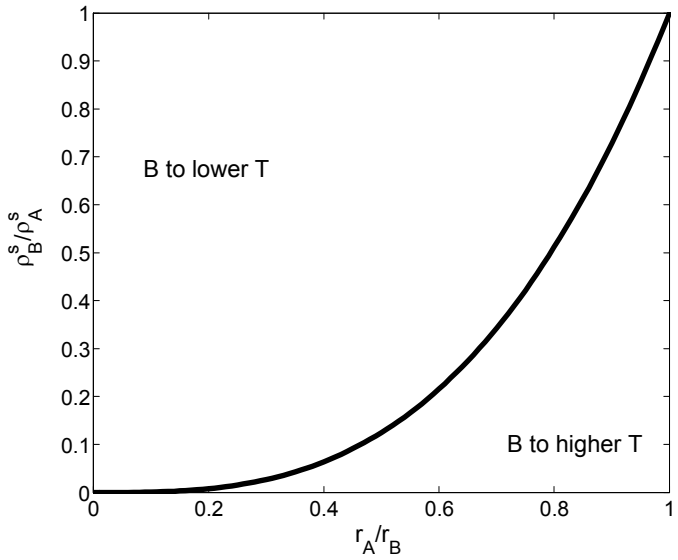

Figure 2.6: $g = 0$ and $T' \neq 0$.

migrate to a colder region and lighter particles to a hotter region. Figure 2.6 shows in what direction particles segregate.

2.4.3 Segregation with $g \neq 0$ and $T' \neq 0$

Now that the two limiting cases, $g \neq 0$ with $T' = 0$ and $g = 0$ and $T' \neq 0$, have been studied, the general case with $g \neq 0 \neq T'$ needs to be addressed. By superposing the two results obtained from the extreme cases (Figure 2.5 and 2.6), we can gather some useful information about the general case, Figure 2.7. In R1, B particles go with gravity and seek lower T. In R2, B goes against gravity and, yet, seeks lower T. In R3, B goes against gravity and seeks higher T.

To clarify the meaning of Figure 2.7, assume a temperature profile, with T high near the top and low near the bottom. In R1 of Figure 2.7, gravity tends to bring B downward and also, because T is lower at the bottom, the temperature gradient also forces B down. Hence, B will sink because both gravity and the temperature gradient

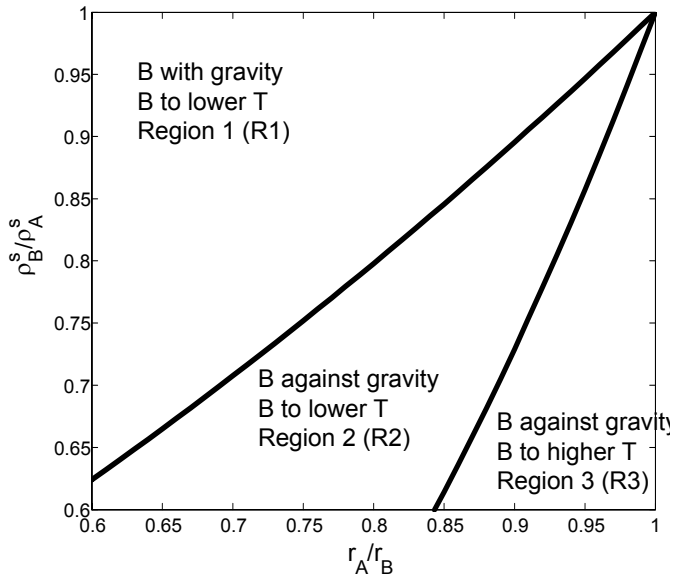

Figure 2.7: By knowing the profile of T and sizes and material densities of particles, it is possible to determine the direction of segregation.

are acting together. Thus, for ratio of radii and material densities in R1 of Figure 2.7, B falls.

For a mixture in R2, B rises against gravity, yet B wants to fall to a place with low T. Here, two mechanisms of segregation act in opposition. In this case, this graph cannot say anything about the direction of segregation. Numerical calculations of the full mixture theory would also be required to determine whether B rises or falls.

In R3 of Figure 2.7, B rises against gravity and also up because T is high at the top. Thus, B rises to the top. These three results are summarized in Figure 2.8.

If the temperature profile is to be reversed so that T is low at the top and high at the bottom, similar argument as above will indicate how segregation occurs (Figure 2.9).

We have just seen that given only a qualitative temperature profile, the superposed Figure 2.7 gives information on the direction of segregation for a mixture with certain ratios of radii and material densities. At the same time, it is seen that for some mixtures,

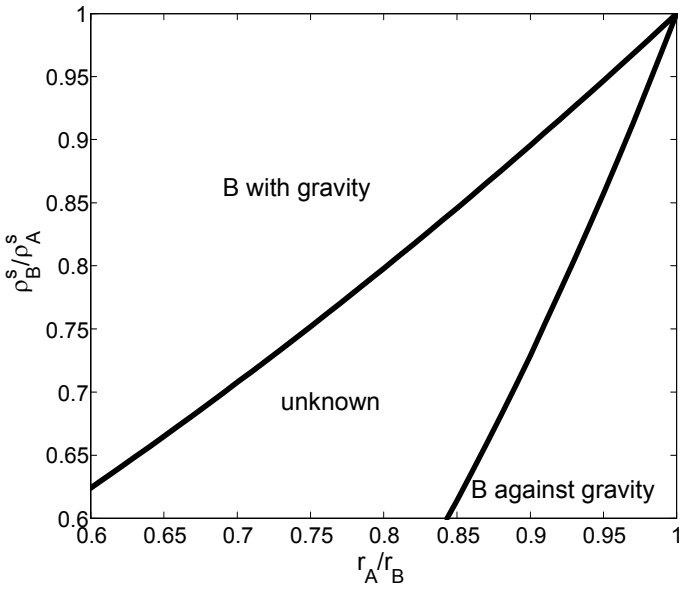

Figure 2.8: For T high at the top and T low at the bottom.

it is not possible to determine the direction of segregation from this simple diagram.

Before finishing this section, we recall that this simple theory predicts how B particles will move with respect to A particles in a homogeneous mixture as soon as gravity is turned on. It is our inference that this initial motion also agrees with the final steady state where the mixture has already segregated. It is to be verified that the prediction of this simple theory agrees with the the final steady state by comparing it with the predictions bases on numerical solutions. Thus, the last three Chapters of the thesis are concerned with checking the prediction of Figure 2.7, by solving the full kinetic equations numerically and comparing the predictions. In the last Chapter, by looking at numerical solutions of steady fully developed inclined flows, we show that the initial motion of the large particles is a good indicator of the final segregation.

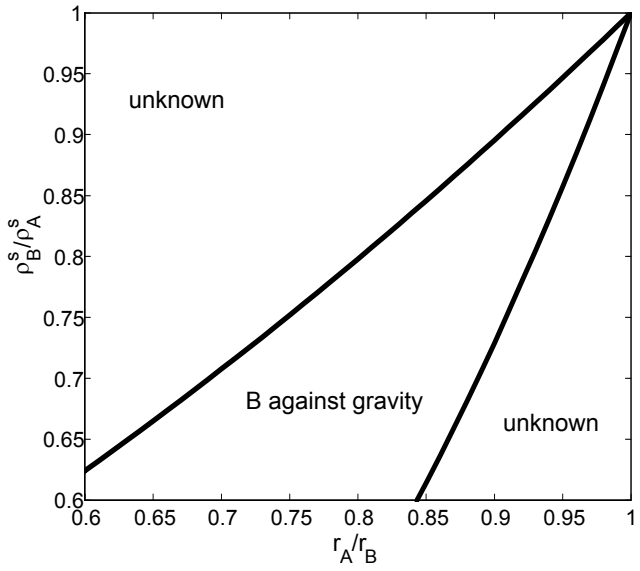

Figure 2.9: For T low at the top and T high at the bottom.

2.5 Conclusion

Using a simple kinetic theory for a binary mixture, we considered a relatively homogeneous agitated mixture of two species of particles with different temperatures and showed that when the temperature differences is not large, the prediction on segregation is not significantly affected by the difference in species temperatures. Therefore, when studying uniformly agitated systems under gravity and where large particles are dilute in a dense gas of small particles, the assumption of equipartition is appropriate for a range of parameters where the ratio of temperatures remains close to unity.

Assuming equipartition, we extended this analysis to the case when not only gravity but also temperature gradient is present and provided a general criterion on the direction of segregation based on sizes and material densities of the binary mixture.

Chapter 3

KINETIC THEORY FOR IDENTICAL, FRICTIONAL, NEARLY ELASTIC DISKS[72]

Most kinetic theories of granular particles have been developed with only the translational motion of particles in mind.[50][38][62] This is natural, considering the complexity of equations that describe the translational motion. When the rotational degrees of freedom are taken into account, the governing equations become even more complicated and the generation of solutions for this set of equations is, without question, a daunting task.[51]

Yet the need to take friction into account in modeling the interactions of granular particles forces kinetic theories to consider the rotational degrees of freedom. For example, Jenkins and Richman[39] developed a kinetic theory for rough disks; however, their model used only a tangential restitution coefficient to account for friction, thereby leaving the possibility of Coulomb friction unexplored.

Walton[67] proposed a friction model that distinguished a collision as either sliding or sticking. In a sliding collision, a constant normal restitution coefficient e and a constant friction coefficient μ are used to describe the interaction between particles. In a sticking collision, the same e and a constant tangential restitution coefficient β_0 are employed. The validity of this model has been tested experimentally by Foerster *et al.*[24] who carried out experiments on binary collisions of spheres and collisions of spheres with a flat plate. They showed that the model of collisions with three constant parameters describes real collisions for a wide range of incident angles.

Herbst *et al*.[28] calculated the rotational and the translational energy dissipation rates for spheres using this friction model. Their results were adopted by Jenkins and Zhang[42], who took a simple approach to the problem of incorporating friction into a kinetic theory. As an approximation, they employed solutions for the angular momentum balance and the rotational energy balance for steady homogeneous shearing and incorporated the influence of small friction on the exchange and dissipation of translation fluctuation energy. In doing so, they used the explicit expressions for the rates of the dissipation of the translational and the rotational fluctuation energies per unit volume, derived by Herbst *et al*.[28] By setting the rotational energy dissipation rate to zero as in a steady, homogeneous shear flow, they were able to solve for the ratio of the rotational granular temperature to the translational granular temperature, assuming small friction. This ratio was then used to determine an effective coefficient of normal restitution. In this way, small friction could be accounted for in a kinetic theory with the same structure as that for the translational degrees of freedom alone.

In this paper, we first present the interaction model for a binary collision of two frictional disks. Then, we derive changes in translational and rotational energies associated with either a sticking or a sliding collision. We write balance equations for mass, linear and angular momentums and translational and rotational energies that result from the Boltzmann equation. Terms related to the dissipation of energy appear in the energy balances. The bulk of this paper consists of the calculation of these dissipation terms. Once they are evaluated, the rotational dissipation term is approximated to be zero by ignoring terms involving unsteady and inhomogeneous contributions[42], as if the flow is in a steady, homogeneous shearing state, so that the ratio of rotational to translational temperatures can be obtained. With this, we replace e in the translational dissipation term with an effective coefficient. For small friction, the effective coefficient of restitu-

tion is given as a function of the Coulomb friction coefficient μ.

3.1 Binary collision

We consider two disks of mass m and diameter σ, undergoing an instantaneous collision in $x-y$ plane. Each disk has a moment of inertia $I = m\sigma^2/\alpha$, where α depends on the mass distribution within the disk. For the special case of a homogeneous disk, I is $m\sigma^2/8$. The velocity and the angular velocity of a disk are, respectively, $\mathbf{c}_i$ and $\mathbf{w}_i$, where $i = 1$ or 2. Note that $\mathbf{w}_i$ has only one non-zero component, which is along z axis.

Linear momentum conservation gives

$$\mathbf{c}_1' = \mathbf{c}_1 + \mathbf{J} \quad \text{and } \mathbf{c}_2' = \mathbf{c}_2 - \mathbf{J}, \tag{3.1}$$

where $\mathbf{J}$ is the impulse divided by m and the prime denotes post-collisional quantities.

Angular momentum conservation gives

$$\mathbf{w}_1' = \mathbf{w}_1 + \frac{m\sigma}{2I}\mathbf{k} \times \mathbf{J} \text{ and } \mathbf{w}_2' = \mathbf{w}_2 + \frac{m\sigma}{2I}\mathbf{k} \times \mathbf{J},$$

where the unit normal vector $\mathbf{k}$ is directed from from the center of disk 1 to the center of 2.

The relative velocity of centers of the disks is defined as

$$\mathbf{g} \equiv \mathbf{c}_1 - \mathbf{c}_2.$$

The values of $\mathbf{g}$ before and after the collision are assumed to be related by a constant coefficient of normal restitution e, with $0 \leq e \leq 1$:

$$\mathbf{g}^{'} \cdot \mathbf{k} = -e\left(\mathbf{g} \cdot \mathbf{k}\right).$$

The mean angular velocity is

$$\mathbf{s} \equiv \frac{1}{2}\left(\mathbf{w}_1 + \mathbf{w}_2\right).$$

The relative velocity of contact points is

$$\mathbf{G} \equiv \mathbf{g} + \sigma \mathbf{s} \times \mathbf{k}. \tag{3.2}$$

The impulse, divided by m, can be decomposed into two orthogonal components:

$$\mathbf{J} = A\mathbf{k} + B\mathbf{j},$$

where the unit tangent vector is

$$\mathbf{j} = \frac{(\mathbf{G} \times \mathbf{k}) \times \mathbf{k}}{|\mathbf{G} \times \mathbf{k}|}$$

and the coefficient A is found by taking a dot product of the difference of (3.1), using the definition of e: $A = -\frac{1}{2}(1+e)\,\mathbf{g} \cdot \mathbf{k}$**.**

3.1.1 Sliding versus sticking collisions

Walton[67] proposed a collision model involving three parameters: the normal and the tangential restitution coefficients e and β_0, respectively, and the Coulomb friction coefficient μ. When the angle between the relative velocity of the points of contact and the line of centers is small, particles stick during the contact and the tangential velocities at the contact can be reversed in direction. When this angle is larger, particles slip at the point of contact. Roughly, near head-on collisions gives rise to sticking collisions and grazing collisions to sliding collisions.

We can state this more precisely. If $|\mathbf{J} \cdot \mathbf{j}| \leq \mu\,|\mathbf{J} \cdot \mathbf{k}|$, then the collision is sticking. Otherwise, the collision is sliding and $|\mathbf{J} \cdot \mathbf{j}| = \mu\,|\mathbf{J} \cdot \mathbf{k}|$. See Figure 3.1. Whether

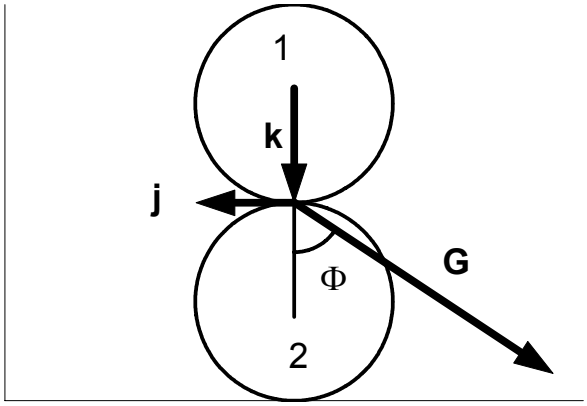

Figure 3.1: In a binary collision between disk 1 and 2, $\mathbf{k}$ is the unit vector pointing from 1 to 2. $\mathbf{G}$ is the relative velocity of contact of 1 with respect to 2. Φ is the angle between $\mathbf{k}$ and $\mathbf{G}$ and lies between 0 and $\pi/2$. $\mathbf{j}$ is the unit vector perpendicular to $\mathbf{k}$, as shown. If $\Phi > \Phi^*$, a sliding collision takes place. If $\Phi < \Phi^*$, a sticking collisions takes place. The positive z axis comes out of the paper.

a collision is sliding or sticking depends on the angle Φ between $\mathbf{k}$ and $\mathbf{G}$. Above a critical angle Φ^*, the collision is sliding; otherwise, it is sticking.

A sliding collision is modelled with Coulomb friction

$$\begin{aligned} B &= -\mu A \\ &= \frac{1}{2}\mu\left(1+e\right)\mathbf{g}\cdot\mathbf{k}. \end{aligned}$$

For a sticking collision, the values of $\mathbf{G}$ before and after a collision are assumed to be related by a coefficient of tangential restitution β_0, with $0 \leq \beta_0 \leq 1$:

$$\mathbf{G}'\cdot\mathbf{j} \equiv -\beta_0\left(\mathbf{G}\cdot\mathbf{j}\right).$$

This gives

$$B = -\frac{1+\beta_0}{2\left(1+m\sigma^2/4I\right)}\mathbf{G}\cdot\mathbf{j}.$$

For the expressions for B to agree at the critical angle Φ^*,

$$\beta_0 = -1 + \mu\,(1+e)\left(1 + \frac{m\sigma^2}{4I}\right)\cot\Phi^*.$$

The tangent of the critical angle, written in terms of β_0, is

$$\mu_0 \equiv \tan\Phi^* = \mu\frac{1+e}{1+\beta_0}\left(1 + \frac{m\sigma^2}{4I}\right), \tag{3.3}$$

and because $\alpha = m\sigma^2/I$,

$$\begin{aligned}\Phi^* &= \arctan\mu_0 \\ &= \arctan\left[\left(1+\frac{\alpha}{4}\right)\mu\frac{1+e}{1+\beta_0}\right].\end{aligned} \tag{3.4}$$

The set $e,\ \mu$ and β_0, or $e,\ \mu$ and μ_0, specifies the nature of a collision.

3.2 Kinetic equations

The average $\langle\phi\rangle$ of a quantity ϕ is defined in terms of the single particle distribution function $f\,(\mathbf{c},\boldsymbol{\omega};\mathbf{x},t)$ discussed in the next section,

$$\langle\phi\rangle \equiv \frac{1}{n}\int \phi f\,(\mathbf{c},\boldsymbol{\omega};\mathbf{x},t)\,d\mathbf{c}d\boldsymbol{\omega},$$

where n is the number density related to the area fraction ν by $\nu \equiv \pi\sigma^2 n/4$.

The velocity fluctuation is $\mathbf{C} \equiv \mathbf{c} - \mathbf{u}$, where $\mathbf{u}$ is the mean translation velocity, and the angular velocity fluctuation is $\boldsymbol{\Omega} \equiv \boldsymbol{\omega} - \bar{\boldsymbol{\omega}}$, where $\bar{\boldsymbol{\omega}}$ is the mean rotational velocity. The translational temperature is given by $T \equiv \langle C^2\rangle/2$ and the rotational temperature is $\Theta \equiv I\langle\Omega^2\rangle/m$.

We define the total change in a particle property ϕ in a binary collision as $\Delta\phi \equiv \phi_1' + \phi_2' - \phi_1 - \phi_2$.

3.2.1 Change in translational fluctuation energy

For a sliding collision, the total change in the translational fluctuation energy, $mC^2/2$, is

$$\begin{aligned}\Delta\frac{1}{2}mC^2 = &-\frac{1}{2}m\hat{e}\left(1-e\right)\left(\mathbf{g}\cdot\mathbf{k}\right)^2\\ &+m\mu\hat{e}\left(\mathbf{g}\cdot\mathbf{k}\right)\left(\mathbf{g}\cdot\mathbf{j}\right)\\ &+m\mu^2\hat{e}^2\left(\mathbf{g}\cdot\mathbf{k}\right)^2,\end{aligned}$$

where $\hat{e}$ is $\left(1+e\right)/2$ and equal to one for perfectly elastic collisions. For a sticking collision, it is

$$\begin{aligned}\Delta\frac{1}{2}mC^2 = &-\frac{1}{2}m\hat{e}\left(1-e\right)\left(\mathbf{g}\cdot\mathbf{k}\right)^2\\ &-m\frac{1+\beta_0}{2\left(1+\alpha/4\right)}\left(\mathbf{G}\cdot\mathbf{j}\right)\left(\mathbf{g}\cdot\mathbf{j}\right)\\ &+m\left[\frac{1+\beta_0}{2\left(1+\alpha/4\right)}\right]^2\left(\mathbf{G}\cdot\mathbf{j}\right)^2.\end{aligned}$$

3.2.2 Change in rotational fluctuation energy

For a sliding collision, the total change in the rotational fluctuation energy, $I\Omega^2/2$, is

$$\begin{aligned}\Delta\frac{1}{2}I\Omega^2 = &\,m\mu\hat{e}\sigma\left(\mathbf{g}\cdot\mathbf{k}\right)\left(\mathbf{k}\times\mathbf{j}\right)\cdot\mathbf{s}\\ &+\frac{\alpha}{4}m\mu^2\hat{e}^2\left(\mathbf{g}\cdot\mathbf{k}\right)^2.\end{aligned}$$

For sticking collisions, it is

$$\begin{aligned}\Delta\frac{1}{2}I\Omega^2 = &\,m\frac{1+\beta_0}{2\left(1+\alpha/4\right)}\sigma\left|\mathbf{k}\times\mathbf{G}\right|\left(\mathbf{k}\times\mathbf{j}\right)\cdot\mathbf{s}\\ &+\frac{\alpha}{4}m\left[\frac{1+\beta_0}{2\left(1+\alpha/4\right)}\right]^2\left(\mathbf{k}\times\mathbf{G}\right)^2.\end{aligned}$$

3.2.3 Balance equations

Boltzmann equation

The balance equation for a quantity ϕ can be obtained by taking the product of ϕ with Boltzmann's equation and integrating over $\mathbf{c}$ and $\boldsymbol{\omega}$:[42]

$$\begin{aligned}
&\frac{Dn\left\langle\phi\right\rangle}{Dt}+n\left\langle\phi\right\rangle\frac{\partial u_i}{\partial x_i}+\frac{\partial n\left\langle\phi C_i\right\rangle}{\partial x_i}\\
&-n\left[\left(F_i-\frac{Du_i}{Dt}\right)\left\langle\frac{\partial\phi}{\partial C_i}\right\rangle-\frac{\partial u_i}{\partial x_j}\left\langle\frac{\partial\phi}{\partial C_i}C_j\right\rangle\right.\\
&\left.-\frac{D\omega_i}{Dt}\left\langle\frac{\partial\phi}{\partial\Omega_i}\right\rangle-\frac{\partial\bar{\omega}_i}{\partial x_j}\left\langle\frac{\partial\phi}{\partial\Omega_i}C_j\right\rangle\right]\\
&=\chi\left[\phi\right]-\frac{\partial}{\partial x_i}\theta_i\left[\phi\right]-\frac{\partial u_j}{\partial x_i}\theta_i\left[\frac{\partial\phi}{\partial C_j}\right]-\frac{\partial\bar{\omega}_j}{\partial x_i}\theta_i\left[\frac{\partial\phi}{\partial\Omega_j}\right],
\end{aligned}\tag{3.5}$$

where $\chi\left[\phi\right]$ and $\boldsymbol{\theta}\left[\phi\right]$ are

$$\begin{aligned}
\chi\left[\phi\right]\equiv\frac{1}{2}\sigma&\int\limits_{\mathbf{g}\cdot\mathbf{k}\geq 0}\left(\mathbf{g}\cdot\mathbf{k}\right)\Delta\phi\\
&\times f^{(2)}\left(\mathbf{c}_1,\boldsymbol{\omega}_1,\mathbf{x}_1,\mathbf{c}_2,\boldsymbol{\omega}_2,\mathbf{x}_2;t\right)\\
&\times d\mathbf{k}d\mathbf{c}_1d\boldsymbol{\omega}_1d\mathbf{c}_2d\boldsymbol{\omega}_2
\end{aligned}\tag{3.6}$$

and

$$\begin{aligned}
\boldsymbol{\theta}\left[\phi\right]\equiv-\frac{1}{2}\sigma^2&\int\limits_{\mathbf{g}\cdot\mathbf{k}\geq 0}\mathbf{k}\left(\mathbf{g}\cdot\mathbf{k}\right)\\
&\times\left(\phi_1'-\phi_1\right)\left[1-\frac{1}{2}\left(\sigma\mathbf{k}\cdot\boldsymbol{\nabla}\right)\cdot\cdot\right]\\
&\times f^{(2)}\left(\mathbf{c}_1,\boldsymbol{\omega}_1,\mathbf{x}_1,\mathbf{c}_2,\boldsymbol{\omega}_2,\mathbf{x}_2;t\right)\\
&\times d\mathbf{k}d\mathbf{c}_1d\boldsymbol{\omega}_1d\mathbf{c}_2d\boldsymbol{\omega}_2.
\end{aligned}$$

The material derivative is $D/Dt\equiv\partial/\partial t+\mathbf{u}\cdot\boldsymbol{\nabla}$, where $\mathbf{u}$ is the mean velocity. The complete pair distribution function $f^{(2)}\left(\mathbf{c}_1,\boldsymbol{\omega}_1,\mathbf{x}_1,\mathbf{c}_2,\boldsymbol{\omega}_2,\mathbf{x}_2;t\right)$ is discussed in the following section.

Translational motion

From (3.5), the mass balance is

$$\frac{D\rho}{Dt} + \rho \boldsymbol{\nabla} \cdot \mathbf{u} = 0,$$

where the mass density ρ is $\rho \equiv mn$. The linear momentum balance is

$$\rho \frac{D\mathbf{u}}{Dt} = \boldsymbol{\nabla} \cdot \mathbf{t} + \rho \mathbf{F},$$

where the stress tensor is

$$\mathbf{t} \equiv -\rho \left\langle \mathbf{C}\mathbf{C} \right\rangle - \boldsymbol{\theta} \left[m\mathbf{C} \right].$$

The translational fluctuation energy balance is

$$\rho \frac{DT}{Dt} = -\boldsymbol{\nabla} \cdot \mathbf{q} + \frac{\partial u_i}{\partial x_j} t_{ij} - \gamma,$$

where the flux of translational fluctuation energy is

$$\mathbf{q} \equiv \rho \left\langle \mathbf{C} C^2/2 \right\rangle + \boldsymbol{\theta} \left[mC^2/2 \right]$$

and the rate of dissipation of translational fluctuation energy per unit area is

$$\gamma \equiv -\chi \left[mC^2/2 \right].$$

Rotational motion

From (3.5), the angular momentum balance is

$$nI \frac{D\bar{\boldsymbol{\omega}}}{Dt} = \boldsymbol{\nabla} \cdot \mathbf{l} + \chi \left[I\boldsymbol{\Omega} \right], \tag{3.7}$$

where the couple stress $\mathbf{l}$ is

$$\mathbf{l} \equiv -nI \left\langle \mathbf{C}\boldsymbol{\Omega} \right\rangle - \boldsymbol{\theta} \left[I\boldsymbol{\Omega} \right].$$

The rotational fluctuation energy balance is

$$\rho\frac{D\Theta}{Dt} = -\boldsymbol{\nabla}\cdot\mathbf{Q} + \frac{\partial\bar{\omega}_i}{\partial x_j}l_{ij} - \Gamma, \tag{3.8}$$

where the flux of rotational fluctuation energy is

$$\mathbf{Q} \equiv nI\left\langle \mathbf{C}\Omega^2/2\right\rangle + \boldsymbol{\theta}\left[I\Omega^2/2\right],$$

and the rate of dissipation of rotational fluctuation energy per unit area is

$$\Gamma \equiv -\chi\left[I\Omega^2/2\right].$$

Recall that the rotational velocity has only one non-zero component and the above expressions can be written with that in mind. However, they are presented in the above form to maintain the parallel with Jenkins and Zhang[42].

In a steady, uniform shearing flow, the rotational fluctuation energy balance (3.8) simplifies to $\Gamma = 0$. From now on, we take Γ to be zero, with the assumption that as far as the rotational temperature is concerned, the flow can be approximated by this simple shear flow.

3.3 Complete pair distribution function

With the assumption of molecular chaos for dense gases, the complete pair distribution function is

$$\begin{aligned} &f^{(2)}\left(\mathbf{c}_1,\boldsymbol{\omega}_1,\mathbf{x}_1,\mathbf{c}_2,\boldsymbol{\omega}_2,\mathbf{x}_2;t\right) \\ &= g_0\left(\nu\right) f\left(\mathbf{c}_1,\boldsymbol{\omega}_1;\mathbf{x}_1,t\right) f\left(\mathbf{c}_2,\boldsymbol{\omega}_2;\mathbf{x}_1+\sigma\mathbf{k},t\right) \end{aligned}$$

where the radial distribution function[39] is

$$g_0\left(\nu\right) \equiv -\frac{1}{16}\frac{7\nu-16}{\left(\nu-1\right)^2}.$$

We should use a distribution function that includes a small perturbation of the Maxwell distribution function, but to the order of approximation we are interested in, that is, to the first order in small gradients, the perturbations of the Maxwellian do not enter into the calculation of the energy sources. Thus, it is appropriate to take the single particle velocity distribution to be Maxwellian, $f = f^{(0)}$:

$$f^{(0)} \equiv \frac{n}{(2\pi T)\,(2\pi\Theta)^{1/2}} \exp\left[-\frac{1}{2}\left(\frac{C^2}{T} + \frac{I\Omega^2}{m\Theta}\right)\right].$$

Jenkins and Zhang[42] provide more detailed discussion of the choice of the distribution function.

3.4 Dissipation: functional form

We determine the functional forms of translational and rotational dissipation terms and set the latter equal to zero to find the ratio of the rotational and the translational temperatures and use this in the former to calculate an effective coefficient of restitution. As do Jenkins and Zhang[42], we wish to incorporate small friction into an effective coefficient of normal restitution e_{eff}.

With $\mathbf{g}\cdot\mathbf{k} = G\cos\Phi$ and $\mathbf{g}\cdot\mathbf{j} = -G\sin\Phi + \sigma s$ from (3.2) and Figure 3.1, where $G = |\mathbf{G}|$ and s is the z-component of $\mathbf{s}$, we can express the changes of translational and rotational energies for sliding and sticking collisions in terms of $\Phi,\ s$ and G and apply these expressions in the definition of the rates of the energy dissipation $\gamma = -\chi\,[mC^2/2]$

and $\Gamma = -\chi\left[I\Omega^2/2\right]$ and obtain (see Appendix A and B for details)

$$\begin{aligned}
&\chi\left[\frac{1}{2}I\Omega^2\right]\left[\frac{mn^2g_0}{\left(2\pi T\right)^2 2\pi\Theta}\right]^{-1}\frac{\left[\hat{R}+2\left(\mu_0^2+1\right)^{-1}\right]^{3/2}}{16T^3K\pi^2\left(\hat{R}+2\right)}\\
&=\left[-2\frac{\mu\hat{e}}{\mu_0}+\frac{\alpha}{4}\left(\hat{R}+2\right)\left(\frac{\mu\hat{e}}{\mu_0}\right)^2\right]\frac{\mu_0^3/\left(\mu_0^2+1\right)^{3/2}}{\hat{R}+2}\\
&-2\mu\hat{e}\frac{\left(\mu_0^2+1\right)^{-3/2}}{\hat{R}}\\
&+\frac{\alpha}{4}\mu^2\hat{e}^2\left\{\frac{2\left[\hat{R}+2\left(\mu_0^2+1\right)^{-1}\right]^{3/2}}{\left(\hat{R}+2\right)\hat{R}^{1/2}}+\frac{\mu_0^3}{\left(\mu_0^2+1\right)^{3/2}}\right.\\
&\left.-\frac{3\hat{R}-4\mu_0^2/\left(\mu_0^2+1\right)+6}{\hat{R}+2}\frac{\mu_0}{\sqrt{\mu_0^2+1}}\right\}
\end{aligned}\tag{3.9}$$

and

$$\begin{aligned}
&\chi\left[\frac{1}{2}mC^2\right]\left[\frac{mn^2g_0}{\left(2\pi T\right)^2 2\pi\Theta}\right]^{-1}\frac{\left[\hat{R}+2\left(\mu_0^2+1\right)^{-1}\right]^{3/2}}{16T^3K\pi^2\left(\hat{R}+2\right)}\\
&=-\hat{e}\left(1-e\right)\frac{\left[\hat{R}+2\left(\mu_0^2+1\right)^{-1}\right]^{3/2}}{\left(\hat{R}+2\right)\hat{R}^{1/2}}\\
&+\frac{\mu\hat{e}}{\mu_0}\left[\left(\hat{R}+2\right)\left(-1+\frac{\mu\hat{e}}{\mu_0}\right)+2\right]\frac{\mu_0^3/\left(\mu_0^2+1\right)^{3/2}}{\hat{R}+2}\\
&+\mu^2\hat{e}^2\left\{2\frac{\left[\hat{R}+2\left(\mu_0^2+1\right)^{-1}\right]^{3/2}}{\left(\hat{R}+2\right)\hat{R}^{1/2}}\right.\\
&\left.-\frac{\mu_0}{\sqrt{\mu_0^2+1}}\left[\frac{3\hat{R}-4\mu_0^2/\left(\mu_0^2+1\right)+6}{\hat{R}+2}-\frac{\mu_0^2}{\mu_0^2+1}\right]\right\}\\
&-\mu\hat{e}\left(\mu_0^2+1\right)^{-3/2}.
\end{aligned}\tag{3.10}$$

where $R\equiv T/\Theta$, $\hat{R}\equiv 8R/\alpha$ and β_0 has been replaced by μ_0 using the relation

$$\frac{1+\beta_0}{2\left(1+m\sigma^2/4I\right)}=\frac{\mu\hat{e}}{\mu_0}.$$

If we know the Coulomb friction coefficient μ, the tangential restitution coefficient

β_0 (or equivalently μ_0, given e) and the moment of inertia of the disk, we can solve for $1/R \equiv \Theta/T$ by setting the rotational dissipation (3.9) equal to zero, as discussed before.

3.4.1 Relationship among μ, β_0 and R

When (3.9) is set equal to zero, (3.9) can be solved analytically for μ and the relationship between μ and β_0, for fixed R, is plotted in Figure 3.2.

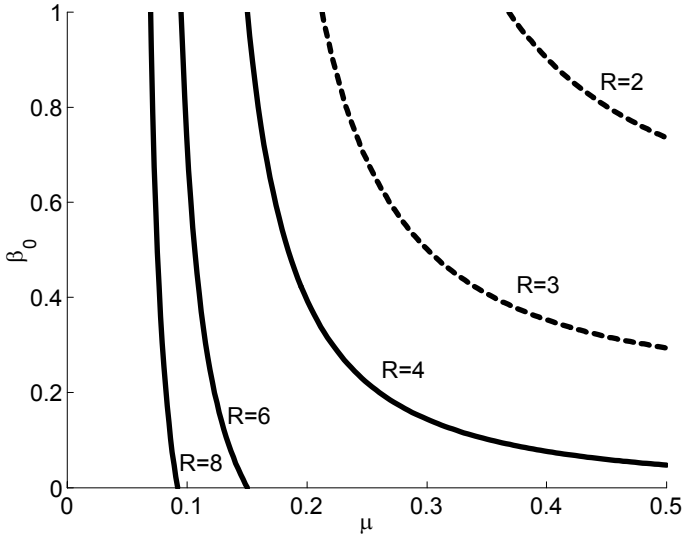

Figure 3.2: For given $R = T/\Theta$, the relationship between μ and β_0 (or equivalently μ and μ_0) can be determined by setting (3.9) to zero. For homogeneous disks ($\alpha = 8$) with $e = 0.92$. For large R, the curve shows little dependence on β_0; that is, R becomes a function of μ only, consistent with our approximate result $R = 1/2\hat{e}\mu$.

Though not shown in the figure, in the case of equipartition, $R = 1$, β_0 quickly approaches 1 for increasing μ. This is expected because when $\beta_0 = 1$ and μ is very large, all collisions will be sticking and the tangential velocity of contacting particles will be completely reversed without loss of any energy, not influenced by translational motion. That is, rotational and translational energies are independent, resulting in equipartition.

In Figure 3.3, we plot the contribution to the restitution coefficient e due to friction, resulting from (3.10). We rewrite (3.10) in a form of $1 - e$ plus a contribution from friction and equate this expression to $1 - e_{eff}$. What is shown in Figure 3.3 is the contribution to this from friction: $e_{eff} - e$.

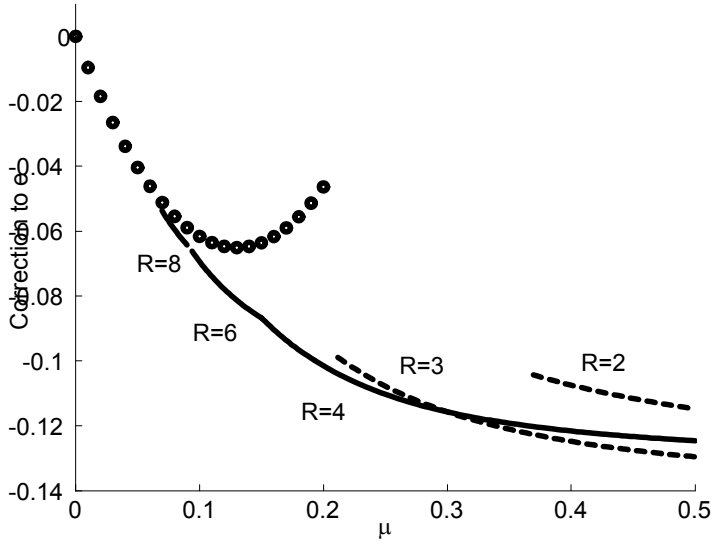

Figure 3.3: By finding the contribution to e by μ and β_0 (or equivalently μ and μ_0) in (3.10), the correction to e to obtain e_{eff} can be calculated. For homogeneous disks ($\alpha = 8$) with $e = 0.92$. μ has upper and/or lower bounds because, as shown in Figure 3.2, $0 \leq \beta_0 \leq 1$. The line of circles represents the approximate expression for the correction to e in the limit of small μ.

In Figure 3.3, when $R = 8$, the correction to the restitution coefficient is near -0.06 with μ near 0.08. That is, $e_{eff} = e - 0.06 = 0.86$, resulting in a lower value of the effective restitution coefficient. After the tangential interactions have been incorporated into e_{eff}, the resulting theory treats more inelastic disks with no regard to the rotational degrees of freedom.

Chou and Richman[16] provided a constitutive theory for smooth and highly in-

elastic spheres. Because of the highly dissipative collisions, they used an anisotropic Maxwellian velocity distribution function, instead of an isotropic one. Thus, instead of a single translational granular temperature, they dealt with all of the components of the second moments of fluctuation velocity. In a homogeneous shear flow, the theory predicted that the difference in the diagonal component of the second moment tensor differed more as the value of e decreased. At a fixed volume fraction of $\nu = 0.4$, the difference of the eigenvalues of this tensor increased to about fifty percent of their sum as e was changed from 0.9 to 0.6, Other predictions also indicated that for small values of e, the use of Maxwellian velocity distribution function is inappropriate. As a consequence, we should limit the application of our theory to effective coefficients of restitution no less than, say, 0.70.

3.4.2 Prediction of the value of Θ/T

Mitarai and Nakanishi[53] have performed a numerical simulation of inhomogeneous frictional disks, with $\alpha = 10$, flowing down an inclined plane, with periodic boundary conditions at the beginning and at the end of the flow. To model the contact between disks, they used the linear spring-dashpot model and the Coulomb friction with the coefficient $\mu = 0.5$ and with the normal restitution coefficient $e = 0.92$. Their tangential restitution coefficient was not constant in the simulation.

Their simulation with these parameters suggested that the ratio Θ/T lies in the range between 0.456 and 0.696, the values depending on the angle of inclination. When we take $\Gamma = 0$ in (3.9) as before and solve for Θ/T with $\mu = 0.5,\ e = 0.92$ and β_0 from 0.8 to 1, we find values of Θ/T between 0.642 and 0.755. Both the measurements of Mitarai and Nakanishi and our predictions indicate Θ/T is a value roughly between $1/2$ and $3/4$. However, our prediction does not depend on the angle of inclination.

3.4.3 Slightly frictional case

When the friction coefficient μ is small, we expect the translational fluctuation T to be greater than the rotational fluctuation Θ. With this in mind, we can expand (3.9) and (3.10) in small $r \equiv \Theta/T$. We retain terms up to the order μ^2.

In the case of frictional spheres of Jenkins and Zhang[42], r is shown to be of order μ. Thus, by including terms up to order r^2, we ensure that the expansion is consistent with our expectation that r is of order μ and with the premise of keeping terms up to μ^2.

Thus, when (3.9) is expanded in $r = \Theta/T$ with the error of $O\left(r^3\right)$, we have

$$\chi\left[\frac{1}{2}I\Omega^2\right]\left[\frac{mn^2g_0}{\left(2\pi T\right)^2 2\pi\Theta}\right]^{-1}\frac{\left(\hat{R}+2\left(\mu_0^2+1\right)^{-1}\right)^{3/2}}{16\pi^2KT^3\left(\hat{R}+2\right)\hat{e}\mu\alpha}$$
$$= E + rF + r^2G + O\left(r^3\right),$$

where

$$E = \frac{1}{2}\hat{e}\mu\left(1-\frac{\mu_0}{\sqrt{\mu_0^2+1}}\right),$$
$$F = \frac{1}{4}\hat{e}\mu\alpha\left[-\frac{1}{2}+\frac{3}{4}\frac{1}{\mu_0^2+1}+\frac{1}{2}\frac{\mu_0^3}{\left(\mu_0^2+1\right)^{3/2}}\right]$$
$$-\frac{1}{4}\frac{1}{\left(\mu_0^2+1\right)^{3/2}}-\frac{1}{4}\frac{\mu_0^2}{\left(\mu_0^2+1\right)^{3/2}},$$
$$G = \frac{\mu_0^2}{\left(\mu_0^2+1\right)^{3/2}}\frac{\alpha}{16}+\frac{1}{4}\hat{e}^2\mu^2\alpha^2\left[\frac{1}{8}-\frac{3}{16}\frac{1}{\mu_0^2+1}\right.$$
$$\left.+\frac{3}{64}\frac{1}{\left(\mu_0^2+1\right)^2}-\frac{1}{8}\frac{\mu_0^3}{\left(\mu_0^2+1\right)^{3/2}}\right].$$

By substituting $\mu_0 = \mu\left(1+e\right)\left(1+\alpha/4\right)/\left(1+\beta_0\right)$ and expanding in μ, we obtain

$$\begin{aligned}
E &= \frac{1}{2}\hat{e}\mu - \frac{\hat{e}^2\mu^2}{\beta_0+1}\left(\frac{1}{4}\alpha+1\right) + O\left(\mu^3\right), \\
F &= -\frac{1}{4} + \frac{1}{16}\hat{e}\mu\alpha \\
&\quad + \frac{1}{2}\frac{\hat{e}^2\mu^2}{\left(\beta_0+1\right)^2}\left(\frac{1}{4}\alpha+1\right)^2 + O\left(\mu^3\right), \\
G &= -\frac{1}{256}\hat{e}\mu\alpha^2 \\
&\quad + \frac{1}{4}\alpha\frac{\hat{e}^2\mu^2}{\left(\beta_0+1\right)^2}\left(\frac{1}{4}\alpha+1\right)^2 + O\left(\mu^3\right).
\end{aligned}$$

Now, setting $\chi\left[I\Omega^2/2\right] = 0$ and, we can solve the quadratic equation for r and retain the root that gives a positive ratio

$$r = \frac{\Theta}{T} = 2\hat{e}\mu + \hat{e}^2\mu^2\frac{\alpha\left(\beta_0-1\right)-8}{2\left(\beta_0+1\right)} + O\left(\mu^3\right).$$

When a similar expansion is done to the translational dissipation, we find

$$\begin{aligned}
&\chi\left[\frac{1}{2}mC^2\right]\left[\frac{mn^2g_0}{\left(2\pi T\right)^2 2\pi\Theta}\right]^{-1}\frac{1}{16T^3K\pi^2}\left(\frac{1}{r}\frac{8}{\alpha}\right)^{1/2} \\
&= -1 + e + L + rM + r^2N + O\left(r^3\right) \qquad (3.11)
\end{aligned}$$

where

$$\begin{aligned}
L &= -\mu + 2\hat{e}\mu^2 + O\left(\mu^3\right) \\
M &= \frac{1}{8}\alpha\mu + O\left(\mu^3\right) \\
N &= -\frac{3}{128}\alpha^2\mu + O\left(\mu^3\right).
\end{aligned}$$

The effective coefficient restitution is then $e_{eff} = e + L + rM + r^2N$. With error $O\left(\mu^3\right)$, we have

$$e_{eff} = e - \mu + \mu^2\hat{e}\left(\frac{1}{4}\alpha+2\right).$$

In particular, for homogeneous disks ($\alpha = 8$) and $e_{eff} = e - \mu + 4\hat{e}\mu^2$. Note the dependence of e_{eff} on μ, but not on β_0 which would appear in μ^3 term. With $e = 0.92$, the approximation does quite well for $\mu < 0.1$ as can be seen in Figure 3.3.

3.4.4 Near reversal of tangential velocity

If the Coulomb friction coefficient μ is infinitely large, we have from our definition (3.4) that $\Phi^* = \arctan \mu_0 = \arctan \left[(1+e)\,(1+\alpha/4)\,\mu/\,(1+\beta_0) \right] = \pi/2$. This shows all collisions are sticking, as can be seen from (A.6) and (A.7). By setting (3.9) to zero, we find $\Theta/T = 4\,(\beta_0+1)\,/\,[8+\alpha\,(1-\beta_0)]$. For $\beta_0 = 1$, we see that $\Theta/T = 1$, independent of α or e. That is, when all collisions are sticking and $\beta_0 = 1$, no rotational energy is lost in a collision and an equipartition of the translational and the rotational temperatures is established.

3.5 Conclusion

We have considered a kinetic theory for nearly elastic, slightly frictional disks. We began with a two-parameter friction model that distinguished the tangential interaction either as sliding or sticking. We focused on first evaluating the exact expressions for the rates of dissipation of both the translational and rotational fluctuation energies per unit area. To do this, we adopted the Maxwellian distribution function, with the assumption of molecular chaos for the complete pair distribution function, and evaluated the dissipation terms.

After the rotational dissipation Γ and the translational dissipation γ were found exactly, we assumed that the rotational energy equation could be approximated as in a steady, homogeneous shear flow. Setting $\Gamma = 0$, we solved for the ratio of temperatures, Θ/T. The resulting relationship between Θ/T, μ and β_0 was shown, as was the correction due to friction on the normal restitution coefficient.

The theory was then used to compare our prediction of Θ/T with that of numerical simulations. The simulations dealt with inclined flows of disks whose collisions were

modelled with the linear spring-dashpot and Coulomb friction. Our prediction of Θ/T fell near the range of the findings in the simulations.

Two simple cases were also investigated. The first was when the Coulomb friction coefficient μ was sufficiently small such that Θ/T could be considered small. In such a case, the dissipation expressions were expanded to the order of μ^2 and the value of Θ/T was found. This value was used to determine an analytic expression of an effective coefficient of normal restitution for the small friction.

The second case dealt with the opposite situation when μ is infinitely large. Here, we found all collisions to be sticking and determined an expression relating Θ/T to β_0. In particular, when $\beta_0 = 1$, the equipartition of the rotational and the translational temperatures was established. This was to be expected because, in this case, no rotational energy is dissipated in a collision.

Chou and Richman[16] showed that for small values of e_{eff}, the adoption of a Maxwellian distribution function becomes inappropriate and our theory is no longer applicable. However, the analytic expressions we have found for the translational and the rotational dissipations should be useful in studying general flows of slightly frictional, nearly elastic disks.

Chapter 4

SIMPLIFIED KINETIC THEORY OF A BINARY MIXTURE OF NEARLY ELASTIC, SMOOTH DISKS

Few studies exist on the kinetic theory of mixtures of inelastic disks. Jenkins and Mancini[36] derived constitutive laws for a dense binary mixture of smooth, nearly elastic disks by assuming the equipartition of energy between species and a Maxwellian velocity distribution, introducing Enskog's correction to the collision frequency, and distinguishing between the position of the centers of two colliding disks. Willits and Arnarson[70] developed a more precise theory using the Revised Enskog Theory derived by van Beijeren and Ernst[66]. They followed the path set by López de Haro *et al*.[46] and Jenkins and Mancini[37] who worked with sphere mixtures. They used the Chapman-Enskog procedure to solve the appropriate kinetic equations and derived explicit expressions for the transport coefficients. Their theory was in remarkable agreement with numerical simulations for systems of moderate densities.

The transport coefficients obtained by Willits and Arnarson[70], later corrected by Alam *et al*.[1], are very complicated functions of the species radii, species masses, and species number densities. Because of this, it is very difficult to get an understanding of how these functions depend on the difference of the radii and masses. However, if we consider mixtures with components that differ only slightly in mass and diameter, substantial simplifications are obtained. We derive the governing equations for a steady, fully-developed and rectilinear flow of a binary mixture of smooth, nearly elastic disks. Then we consider perturbations in the radii, $\delta r = r_A/r_B - 1$, and masses,

$\delta m = (m_A - m_B) / (m_A + m_B)$, retaining terms to first order only in the resulting expressions for the transport coefficients. Once the simple expressions for the transport coefficients are obtained, we write down the governing equations for a steady, fully-developed and rectilinear flow of mixtures that differ only slightly in mass and diameter. Then, we apply these expressions to solve boundary value problems of a steady, fully-developed flow of a binary mixture in a circular shear cell between two bumpy walls, with adjustments to account for the non-rectilinearity of this flow and then of a steady flow on a vibrated bottom boundary.

4.1 Steady, fully-developed rectilinear flow

In this section, we derive the governing equations for a steady, fully-developed and rectilinear flow of a binary mixture of nearly elastic disks using the constitutive theory of Willits and Arnarson[70]. We take X to be the coordinate in the flow direction, assumed to be perpendicular to the direction of gravity. We then take Y to be the coordinate perpendicular to X. Spatial variations occur only in the Y direction. In this coordinate system, our assumptions of the flow allow us to consider a velocity field of the form $\mathbf{u} = (u_X(Y), 0)$ and to ignore the spatial change, d/dX.

The two species in the binary mixture are denoted by A and B, species radii are r_i, species masses are m_i, and species number densities are n_i, where $i = A$ or B.

The balance of linear momentum requires the shear stress, S, and the pressure, P, to be constant. The constitutive relation for the pressure is

$$P = (n + K_{AA} + K_{BB} + 2K_{AB})\, T, \tag{4.1}$$

where $n = n_A + n_B$, T is the mixture granular temperature defined by

$$nT \equiv n_A T_A + n_B T_B,$$

where T_i is the kinetic energy of the velocity fluctuations of species i, and

$$K_{ij} = \frac{\pi}{2} n_i n_j r_{ij}^2 g_{ij_c}.$$

Here, $r_{ij} = r_i + r_j$, and the radial distribution function for particles of species i and j in contact[36] is,

$$g_{ij_c} = \frac{1}{1-\nu} + \frac{9}{8}\frac{r_i r_j}{r_i + r_j}\frac{\zeta}{(1-\nu)^2},$$

where the area fraction, ν, is given by $\nu = \pi\left(n_A r_A^2 + n_B r_B^2\right)$, and $\zeta = \pi\left(n_A r_A + n_B r_B\right)$.

The balance of fluctuation energy is

$$q' - Su' + \gamma = 0, \tag{4.2}$$

where the heat flux is given by

$$q = -\kappa T'. \tag{4.3}$$

κ is the coefficient of thermal conduction, and u is the center of mass velocity given by

$$\rho u \equiv \rho_A u_A + \rho_B u_B,$$

where $\rho_i = m_i n_i$, $\rho = \rho_A + \rho_B$, and γ is the collisional rate of energy dissipation due to inelasticity. u_i is the mean velocity of species i along X axis. Here, prime denotes differentiation with respect to Y. The velocity gradient is related to the shear stress via the viscosity, μ, by

$$S = \mu u'. \tag{4.4}$$

An expression for the difference in species diffusion velocities, $\mathbf{v}_i = \mathbf{u}_i - \mathbf{u}$, was found by Willits and Arnarson[70]. The resulting expression is

$$\mathbf{v}_A - \mathbf{v}_B = -\frac{n^2}{n_A n_B} D_{AB} \left(\mathbf{d}_A + K_T^{(A)} \nabla \ln T \right), \tag{4.5}$$

where D_{AB} is the ordinary diffusion coefficient given by $K_T^{(A)}$ is the coefficient of thermal diffusion, and $\mathbf{d}_A$ is the diffusion force of species A given by

$$\begin{aligned} \mathbf{d}_A = &-\frac{\rho_A}{n\rho T} \nabla P + \frac{1}{n} \left(n_A + 2M_{AB} K_{AB} + K_{AA} \right) \\ &\times \nabla \ln T + \frac{n_A}{nT} \left(\frac{\partial \mu_A}{\partial n_A} \nabla n_A + \frac{\partial \mu_A}{\partial n_B} \nabla n_B \right), \end{aligned}$$

where $M_{ij} \equiv m_i / m_{ij}$, $m_{ij} \equiv m_i + m_j$. By considering two dimensional analog of multicomponent chemical potentials for spheres found in Reed and Gubbins[57], Mancini[52] found the chemical potentials, μ_i, corresponding to the radial distribution functions g_{ij_c} to be

$$\begin{aligned} \frac{\mu_i}{T} = &\ln n_i - \ln\left(1-\nu\right) \left(\frac{r_i^2 \zeta^2}{8\nu^2} - \frac{r_i \zeta}{4\nu} + 1 \right) \\ &- \frac{r_i \zeta}{2\left(1-\nu\right)} \left[\frac{r_i \zeta}{4\nu} - \frac{2\pi r_i n}{\zeta} - \frac{9}{2} - \frac{9 r_i \zeta}{4\left(1-\nu\right)} \right]. \end{aligned}$$

Using the assumptions of a fully-developed and rectilinear flow, one can show that the right hand side of (4.5) is equal to zero. The same conclusion follows when we consider a fully-developed and axisymmetric flow in a circular geometry which we study later in the paper. Differentiating the pressure with respect to Y using the chain rule yields

$$P' = \frac{\partial P}{\partial n_A} n_A' + \frac{\partial P}{\partial n_B} n_B' + \frac{\partial P}{\partial T} T' = -\rho g, \tag{4.6}$$

where g is the gravitational constant. This equation, together with equation (4.5), forms a set of two equations that can be used to solve for the gradients of number density. The

resulting expressions are

$$n'_A = -n\frac{T'}{T}\left(\frac{1}{T}\frac{\partial P}{\partial n_A}\right)^{-1} \times \left[\beta + \left(\frac{1}{T}\frac{\partial P}{\partial n_B}\right)\left(n\frac{T'}{T}\right)^{-1} n'_B + \frac{P}{nT}\right] \tag{4.7}$$

and

$$n'_B = \frac{n}{J}\frac{T'}{T}\left[\frac{n}{n_A}\left(\frac{1}{T}\frac{\partial P}{\partial n_A}\right)\frac{\rho_A}{\rho}\beta + \frac{1}{n}\left(n_A + K_{AA} + 2M_{AB}K_{AB}\right) + K_T^{(A)} - \left(\frac{n}{T}\frac{\partial \mu_A}{\partial n_A}\right)\left(\beta + \frac{P}{nT}\right)\right], \tag{4.8}$$

where

$$J \equiv \det\begin{bmatrix} \frac{n}{T}\frac{\partial \mu_A}{\partial n_A} & \frac{n}{T}\frac{\partial \mu_A}{\partial n_B} \\ \frac{1}{T}\frac{\partial P}{\partial n_A} & \frac{1}{T}\frac{\partial P}{\partial n_B} \end{bmatrix},$$

and $\beta \equiv \rho g/nT'$.

4.2 Transport coefficients

In this section, we simplify the transport coefficients calculated by Willits and Arnarson [70] given in the previous section. Although we focus attention on steady, fully-developed and rectilinear flow, these transport coefficients also apply in more general flow situations[70], although the balance of the fluctuation energy (4.2) needs additional terms associated with the rate of the change of temperature and the flux of energy to describe general flow situations. We obtain the expressions for the transport coefficients in terms of the perturbations $\delta r \equiv r_A/r_B - 1$ and $\delta m \equiv (m_A - m_B)/(m_A + m_B)$, retaining terms to first order only. When $\delta r = \delta m = 0$, we recover the transport coefficients corresponding to a single constituent with diameter r_{AB} and mass $m_{AB}/2$.

4.2.1 Thermal conductivity

The coefficient of thermal conductivity is given by

$$\kappa = \sum_{i=A,B} \frac{n_i}{n} K_i a_{i1} + 2 \sum_{i,j=A,B} K_{ij} r_{ij} \left(\frac{2T m_i m_j}{\pi m_{ij}^3} \right)^{1/2},$$

where

$$K_i = 1 + \sum_{j=A,B} \frac{3\pi}{2} n_j r_{ij}^2 g_{ij_c} M_{ji} M_{ij},$$

for $i \neq j$, and the quantities a_{i1} arise in the Chapman-Enskog procedure which is used to derive the explicit constitutive relations. The Nth Enskog approximation of a_{i1} is denoted by $a_{i1}[N]$ and refers to the number of terms kept in the infinite series expansion in the Chapman-Enskog procedure. Alam *et al.*[1] corrected the second Enskog approximation for a_{i1} calculated by Willits and Arnarson[70]. The resulting expression is

$$\begin{aligned} a_{i1}[2] = & \frac{4nT}{m_i n_i n_k r_{ik} g_{ik_c} \lambda_{ik} M_{kl}} \\ & \times \left[\frac{\alpha_i n_i K_i + 13 M_{ik} M_{ki} n_k K_k}{\alpha_i \alpha_k - 169 M_{ik}^2 M_{kl}^2} \right], \end{aligned} \tag{4.9}$$

where

$$\begin{aligned} \alpha_i \equiv & \, 12 M_{ki}^2 + 4 M_{ik} M_{ki} + 5 M_{ik}^2 \\ & + \frac{n_k}{n_i} \frac{r_{kk}}{r_{ik}} \frac{g_{kk_c}}{g_{ik_c}} \frac{1}{M_{ik}} \left(\frac{M_{ik}}{M_{kk}} \right)^{1/2}, \end{aligned} \tag{4.10}$$

for $i \neq k$, and

$$\lambda_{ij} = \left(\frac{2\pi T m_{ij}}{m_i m_j} \right)^{1/2}.$$

Introducing the dimensionless thermal conductivity,

$$\lambda = \frac{m_{AB}^{1/2}}{n r_{AB} (2T)^{1/2}} \kappa, \tag{4.11}$$

and expanding in powers of δr and δm keeping only terms to first order, we find

$$\lambda = \frac{2GM}{\sqrt{\pi}} \left[1 + \frac{1}{2} \left(\frac{n_A}{n} - \frac{n_A}{n} \right) (\delta r - \delta m) \right], \tag{4.12}$$

where

$$G(\nu) = \frac{\nu (16 - 7\nu)}{16 (1 - \nu)^2} \tag{4.13}$$

and

$$M(\nu) = 1 + \frac{\pi}{4} \left(\frac{3}{2} + \frac{1}{G} \right)^2. \tag{4.14}$$

4.2.2 Energy dissipation

Willits and Arnarson[70] derived the total rate of energy dissipation. The expression is

$$\gamma = \sum_{i,j=A,B} 2 g_{ij_c} r_{ij} n_i n_j M_{ji} (1 - e_{ij}) \left(\frac{2\pi T^3 m_{ij}}{m_i m_j} \right)^{1/2},$$

where e_{ij} is the normal coefficient of restitution in a collision between a disk of type i and a disk of type j. For simplicity, we assume that $e_{ij} = e$, i.e., that the coefficients of restitution are all the same.

Introducing the dimensionless rate of energy dissipation

$$\tilde{\gamma} \equiv \frac{m_{AB}^{1/2} r_{AB} \gamma}{n 2^{1/2} T^{3/2}},$$

we expand in powers of δr and δm retaining only terms to first order. The resulting expression is

$$\tilde{\gamma} = \frac{8G (1 - e)}{\sqrt{\pi}} \left[1 - \frac{1}{2} \left(\frac{n_A}{n} - \frac{n_B}{n} \right) (\delta r + \delta m) \right], \tag{4.15}$$

where G is given by (4.13).

4.2.3 Shear Viscosity

The expression for the shear viscosity is

$$\mu = \frac{1}{2}\left[\sum_{i=A,B}\frac{n_i}{n}Tb_{i0}K_i' + \sum_{i,j=A,B}K_{ij}r_{ij}\left(\frac{2Tm_im_j}{\pi m_{ij}}\right)^{1/2}\right],$$

where

$$K_i' = 1 + \sum_{j=A,B}\frac{\pi}{2}n_j r_{ij}^2 g_{ij_c}M_{ji}\ ,$$

and $i \neq k$. The coefficients b_{i0} arise in a similar way as the a_{i1} above. Alam *et al*.[1], in correcting the expression given by Willits and Arnarson[70], found the first Enskog approximation to be

$$b_{i0}\left[1\right] = \frac{n}{\lambda_{ik}n_in_kg_{ik_c}}\left(\frac{n_iK_i'\beta_i + n_kK_k'M_{ik}M_{ki}}{\beta_i\beta_k - M_{ik}^2M_{ki}^2}\right),$$

where

$$\beta_i = M_{ik}\left(1 + M_{ki}\right) + \frac{1}{2}\frac{n_k}{n_i}\frac{r_{kk}}{r_{ik}}\frac{g_{kk_c}}{g_{ik_c}}\left(\frac{M_{ik}}{M_{kk}}\right)^{1/2},$$

and $i \neq k$.

Upon introducing the dimensionless viscosity

$$\eta = \frac{\mu}{nr_{AB}m_{AB}^{1/2}T^{1/2}},$$

expanding this in powers of δr and δm, and keeping only terms to first order, we find

$$\eta = \frac{GJ}{\sqrt{2\pi}}\left[1 + \frac{1}{2}\left(\frac{n_A}{n} - \frac{n_B}{n}\right)\left(\delta r + \delta m\right)\right], \tag{4.16}$$

where

$$J\left(\nu\right) \equiv 1 + \frac{\pi}{8}\left(1 + \frac{1}{G}\right)^2,$$

and where G is given by equation (4.13).

4.2.4 Thermal Diffusion coefficient

The thermal diffusion coefficients are given by the formula

$$K_T^{(i)} = \frac{a_{i0}}{t_{i0}},$$

where the t_{i0} and a_{i0} arise in a similar context as a_{i1}. Since $t_{i0}\,[2]$ does not differ significantly from $t_{i0}\,[1]$, we will use the latter. However, the second Enskog approximation is necessary for the calculation of a_{i0}. For a discussion on the accuracy of the Enskog approximations for diffusion coefficients, see Hirschfelder *et al.*[29], p. 480. The formulas for these coefficients were found by Willits and Arnarson[70]. They are

$$a_{i0}\,[2] = \frac{\rho_k}{2\rho}\left(M_{ik}a_{k1}\,[2] - M_{ki}a_{i1}\,[2]\right),$$

where $a_{j1}\,[2]$ are given by equations (4.9) and (4.10), and

$$t_{i0}\,[1] = \frac{n^2\rho_k T}{\rho n_i n_k r_{ik} g_{ik_c}\lambda_{ik} m_i M_{ki}},$$

and $i \neq k$. Expanding in powers of δr and δm, and keeping only terms to first order, we find

$$K_T^{(A)} = \frac{2n_A n_B}{21n^2}\left[\left(1 + \frac{9\nu}{16-7\nu} - \frac{3}{2}G\right)\delta r + \frac{65}{4}\left(1 + \frac{3}{2}G\right)\delta m\right].$$

The term $9\nu/\left(16-7\nu\right)$ arises in the perturbations of the radial distribution functions and G is given by equation (4.13).

4.3 Simplified equations

We focus attention on a steady, fully-developed and rectilinear flow of a binary mixture of nearly elastic, smooth disks. Expanding the constitutive relation for the pressure,

equation (4.1), in δr yields

$$\frac{P}{nT} = 2FG + O\left(\delta r^2\right), \tag{4.17}$$

or, upon introducing

$$w \equiv \left(\frac{2T}{m_{AB}}\right)^{1/2},$$

we find

$$P = \frac{4m_{AB}}{\pi r_{AB}^2} w^2 \nu FG \left(1 - 2x\delta r\right),$$

where $F(\nu) \equiv 1 + 1/2G$, G is given by equation (4.13), and we have introduced a new variable that appears frequently in the perturbations of the transport coefficients:

$$x \equiv \frac{1}{2}\left(\frac{n_A}{n} - \frac{n_B}{n}\right).$$

In order to find a differential equation for x, we need to expand the differential equations for the number densities, equations (4.7) and (4.8), in δr and δm. This requires, among other things, the expansion of the derivatives of the chemical potentials. The perturbations of the chemical potentials are

$$\begin{aligned}\frac{n}{T}\frac{\partial \mu_A}{\partial n_A} = {} & \frac{n}{n_A} + 2G + 2\nu H \\ & + \frac{n_B}{n}\left(2G + 6\nu H\right)\delta r,\end{aligned}$$

and

$$\begin{aligned}\frac{n}{T}\frac{\partial \mu_A}{\partial n_B} = {} & 2G + 2\nu H + \Big[2\left(\frac{n_B}{n} - \frac{n_A}{n}\right)\nu H \\ & -2\frac{n_A}{n}\left(G + \nu H\right)\Big]\delta r,\end{aligned}$$

where

$$H(\nu) \equiv \frac{dG}{d\nu} = \frac{8 + \nu}{8\left(1 - \nu\right)^3}.$$

The resulting expansions for the gradients in number density are

$$n_A' = -n\frac{T'}{T}\frac{n_A}{n}\frac{1+2G+\beta_0}{1+2G+2\nu H} + \Big(\frac{n_A n_B}{n^2}\Gamma\delta m + \frac{n_A}{n}\frac{\beta_m}{1+2G+2\nu H}\Big) + \frac{n_A n_B}{n^2}\hat{R}\delta r$$

and

$$n_B' = -n\frac{T'}{T}\frac{n_B}{n}\frac{1+2G+\beta_0}{1+2G+2\nu H} + \Big(-\frac{n_A n_B}{n^2}\Gamma\delta m + \frac{n_B}{n}\frac{2\beta_m}{1+2G+2\nu H}\Big) - \frac{n_A n_B}{n^2}\hat{R}\delta r,$$

where $\beta_0 = g/2ww'$, $\beta_m = 2x\beta_0$ and

$$\Gamma \equiv \frac{121}{28}G + \frac{65}{42} + 2\beta_0, \tag{4.18}$$

$$\hat{R} \equiv \frac{2}{21}\left(1 - \frac{3}{2}G + \frac{9\nu}{16-7\nu}\right) + \frac{(1+2G)(2G-1)}{2G+2H\nu+1} + \frac{9}{16}\frac{\nu^2}{(1-\nu)^2} - 1 - \frac{2(1+H\nu)\beta_0}{2G+2H\nu+1}. \tag{4.19}$$

Using the differential equations for the number densities, equations (4.7) and (4.8), we find a differential equation for x :

$$x' = -\left(\frac{1-4x^2}{2}\right)\frac{w'}{w}\left(\hat{R}\delta r + \Gamma\delta m\right), \tag{4.20}$$

where Γ and R are given by equations (4.18) and (4.19). We note that this equation is identical to its three dimensional analog, except that Γ and R have different forms in three dimensions[6]. Also note that (4.20) can be integrated for x as a function of Y once $w(Y)$ and $\nu(Y)$ are determined from the mixture equations.

Note that $x' = O(\delta r) + O(\delta m)$; so whenever x is multiplied with either δr or δm, we can replace x with its average, $\bar{x}$. This is convenient in the perturbation of the transport coefficients where x is always multiplied with either δr or δm. This fact decouples equation (4.20) from the system of equations for w, u and ν.

4.4 Boundary value problem

In this section, we apply the previous results to study segregation of a binary mixture in a circular cell with a bumpy outer wall and a bumpy inner wall when, in the absence of an external force, the walls are used to shear the flow by rotating them in opposite directions. The goal is to find out how the densities of species A and B are distributed when the mixture reaches a steady, fully-developed state. Because the example we consider is not rectilinear, we must make some modifications to the equations that we have derived. A similar problem for the mixture sheared between two parallel bumpy walls is discussed elsewhere.[73]

The boundaries are flat walls to which equally spaced disks of diameter d are attached, with s the distance between their edges. At each plate or wall, we specify the bumpiness, θ, and the restitution coefficient of the bumps with the flowing disks, e_w. The bumpiness θ is given as

$$\sin\theta \equiv \frac{d+s}{d+r_{AB}}.$$

The boundary conditions are applied at a distance $(d + r_{AB})/2$ into the flow from the center of a wall disk. We use subscript I and O to denote the inner boundary and the outer boundary, respectively.

4.4.1 Circular shear cell

Note that the equations need to be written in polar coordinates. We assume there is no external body force and the flow is axisymmetric, steady and fully-developed. Here, let $R \equiv Y/r_{AB}$ and let prime denote a derivative with respect to R. The variables of interest are $I(R) \equiv (1/L)\int_{R_I}^{R} \nu d\zeta,\ \nu,\ w,\ q,\ u,\ S,\ x$ and $J(R) \equiv (1/L)\int_{R_I}^{R} x d\zeta$, where $L \equiv R_O - R_I$. We non-dimensionalize the variables in the following way:

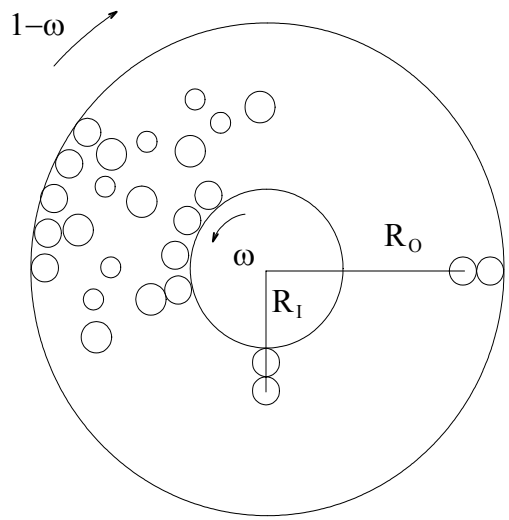

Figure 4.1: Circular shear cell. Velocities and length made non-dimensional by U and r_{AB}.

$$\tilde{u} = \frac{u}{U},\ \tilde{w} = \frac{w}{U},$$
$$\tilde{S} = \frac{S}{U^2}\frac{\pi r_{AB}^2}{2m_{AB}},$$
$$\tilde{q} = \frac{q}{U^3}\frac{\pi r_{AB}^2}{2m_{AB}},$$

where U is a typical velocity associated with the moving boundary. Once made without dimensions, the outer boundary moves clockwise with velocity $1-\omega$, while the inner boundary moves counter clockwise with velocity ω. See Figure 4.1.

From now on, we drop all the hats and use the variables used for dimensional quantities to represent their non-dimensional counterparts.

Governing equations

From the definitions of I and J, we have

$$I' = \frac{\nu}{L},$$
$$J' = \frac{x}{L}.$$

The normal momentum balance (4.6) in circular geometry with the constitutive relation (4.17) gives us

$$\nu' = -\left[-\left(1+2x\delta m\right)\nu\frac{u^2}{R} - q\frac{\sqrt{\pi}}{M}\left(1+x\delta r+x\delta m\right)\frac{F}{w}\right]\frac{GF\nu}{p\hat{H}}.$$

The constitutive relation for the flux of fluctuation energy (4.3) with the expression for thermal conductivity (4.12) yields

$$w' = -q\sqrt{\pi}\frac{F}{2Mp}\left(1+x\delta r+x\delta m\right). \tag{4.21}$$

Similarly, from (4.4) and (4.16), the velocity gradient is found to be,

$$u' = \frac{u}{R} + 2SF\sqrt{\pi}\frac{w}{pJ}\left(1+x\delta r-x\delta m\right).$$

The energy balance (4.2) with the expression for the dissipation (4.15) and the above expression for u' result in

$$q' = -\frac{q}{R} - \left[\left(1-e\right)\left(1-3x\delta r-x\delta m\right) - \frac{1}{2}\pi\frac{F^2S^2}{p^2J}\left(1+x\delta r-x\delta m\right)\right]\frac{4pw}{F\sqrt{\pi}}.$$

We also have from (4.20)

$$x' = -\left(\frac{1-4x^2}{4}\right)\left[-\frac{1}{w}q\sqrt{\pi}\frac{F}{Mp}\left(\hat{R}_1\delta r+\hat{g}_1\delta m\right) + \frac{1}{w^2}\left(\hat{R}_2\delta r+\hat{g}_2\delta m\right)\right], \tag{4.22}$$

where

$$\begin{aligned}
\hat{R}_1 &= \frac{2}{21}\left(1-\frac{3}{2}G+\frac{9\nu}{16-7\nu}\right) \\
&\quad +\frac{(1+2G)(2G-1)}{2G+2H\nu+1}+\frac{9}{16}\frac{\nu^2}{(1-\nu)^2}-1, \\
\hat{R}_2 &= \frac{2(1+H\nu)}{2G+2H\nu+1}\frac{u^2}{R}, \\
\hat{g}_1 &= \frac{121}{28}G+\frac{65}{42}, \\
\hat{g}_2 &= -2\frac{u^2}{R}.
\end{aligned} \tag{4.23}$$

We note that $\hat{R}_1$ is the first four terms of $\hat{R}$ in (4.19) and $\hat{R}_2$ is the last term of $\hat{R}$ with g replaced by $-u^2/R$. Similarly, $\hat{g}_1$ and $\hat{g}_2$ are related to Γ in (4.18). The tangential momentum balance gives

$$S' = -2\frac{S}{R}.$$

Note that the appearance of R in the denominators of some terms is due to the circular geometry.

Boundary conditions

Because we have eight first order differential equations, we need to impose eight boundary conditions. We have two conditions on I:

$$I(R_I) = 0 \text{ and } I(R_O) = \bar{\nu},$$

where $\bar{\nu}$ is the known average area fraction. Similarly, we have two conditions on J

$$J(R_I) = 0 \text{ and } J(R_O) = \bar{x}.$$

Each bumpy boundary provides two conditions, one on the slip velocity and one on the heat flux[6].

Once the solutions are found, the values of ν and x with δr and δm are used to find the area fractions of A and B: ν_A and ν_B, respectively. ν_i is related to n_i through $\nu_i = \pi r_i^2 n_i$. From our approximation

$$n = \frac{1}{r_{AB}^2}\frac{4\nu}{\pi}\left(1 - 2x\delta r\right),$$

and

$$n_A = \left(\frac{1}{2} + x\right) n,$$
$$n_B = \left(\frac{1}{2} - x\right) n,$$

we have

$$\nu_A = \nu\left[\frac{1}{2} + x + \frac{1}{2}\left(1 - 4x^2\right)\delta r\right],$$
$$\nu_B = \nu\left[\frac{1}{2} - x - \frac{1}{2}\left(1 - 4x^2\right)\delta r\right].$$

Sample solution

We choose parameters $e = 0.8,\ e_{wI} = 0.9,\ e_{wO} = 0.9,\ \theta_I = \pi/6$ and $\theta_O = \pi/6$. Boundary conditions are applied at the inner radius of 50 particle diameters and the outer radius of 60 particle diameter. The average area fraction is $\bar{\nu} = 0.7$ and the filling fraction of A is $n_A/n = 0.7$, from which $\bar{x}$ is found. ω is chosen to be 0.65. The mixture has $r_A/r_B = 1$ and $m_A/m_B = 1.1$. MATLAB bvp4c function is employed to solve the system.

The outer wall is moving clockwise at velocity 0.35, while the inner wall is moving counter-clockwise at velocity 0.65. The profile of u shows that slips are present at both

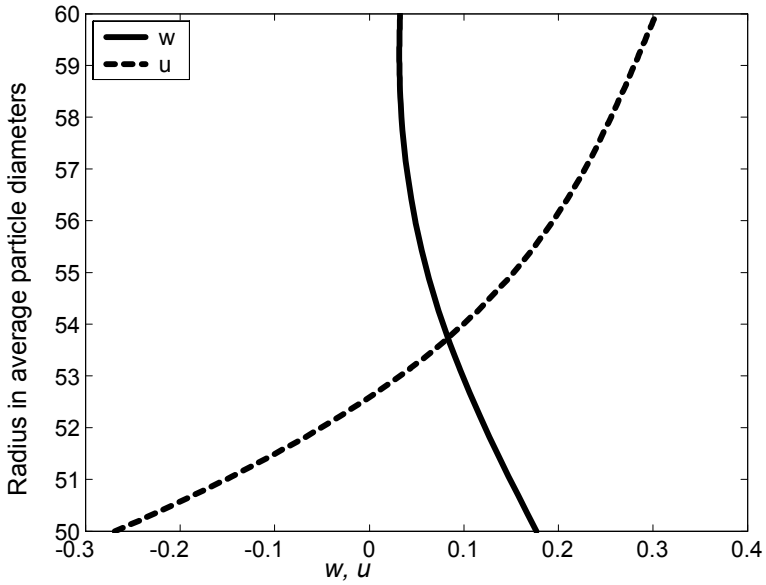

Figure 4.2: Profiles of non-dimensional fluctuation velocity w and mean velocity u.

boundaries. The profile of w shows that the flow is more agitated near the inner wall than near the outer wall. By choosing different values for $e_{wI},\ e_{wO},\ \theta_I$ and θ_O, not only the amount of the slip at the wall, but the general qualitative features of solutions can change.

The profiles of ν_A and ν_B show how A and B segregate in the final state. Here, we note the heavier particles of species A are found near the outer wall where the fluctuation velocity is lower; that is, colder. The total concentration is seen to increase as we move towards the outer wall.

The segregation profile in Figure 4.3 can be understood in terms of the thermal diffusion factor[7]

$$\begin{aligned} \alpha_{AB} &\equiv -\frac{(\ln n_A)' - (\ln n_B)'}{(\ln T)'} \\ &= -\frac{n^2}{n_A n_B}\frac{x'}{2\,(\ln w)'}. \end{aligned} \tag{4.24}$$

From the definition of x and (4.24), we see that if x' and w' have the same sign, the

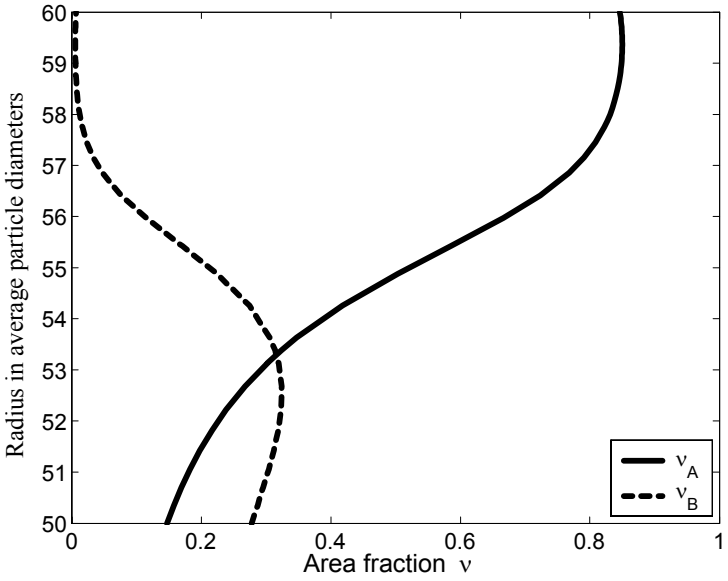

Figure 4.3: Density profiles of A and B.

concentration of A increases with increasing w. That is, if $\alpha_{AB} < 0$, then A moves to a hotter region. Similarly, if x' and w' differ in their signs, the concentration of A decreases with increasing w; A moves to a colder region if $\alpha_{AB} > 0$. If $\alpha_{AB} = 0$, no segregation occurs.

Suppose we have a system where we know the behaviors of the total volume fraction and the fluctuation velocity. Then, it is possible to predict the segregation analytically with the information only on δr and δm. Using (4.21), (4.22) and (4.23), we can write $\alpha_{AB} = 0$ as a relation between the ratio of material densities ρ_A^s/ρ_B^s and the ratio of radii r_A/r_B:

$$\begin{aligned}
&\frac{\rho_A^s}{\rho_B^s} \\
&= -\frac{1}{\left(r_A/r_B\right)^2} \\
&\times \frac{2\left(\hat{R}_1\delta r - \hat{g}_1\right) + \left(\hat{R}_2\delta r - \hat{g}_2\right)/\left(w'w\right)}{2\left(\hat{R}_1\delta r + \hat{g}_1\right) + \left(\hat{R}_2\delta r + \hat{g}_2\right)/\left(w'w\right)}.
\end{aligned}$$

Note that while $\hat{R}_1$ and $\hat{g}_1$ are functions of ν only, $\hat{R}_2$ and $\hat{g}_2$ are functions of ν as well as of u^2/R. Because we know the relative strength of the centripetal force versus the temperature gradient, that is, $(u^2/R)\,/\,(w'w)$, we can determine the relationship between ρ_A^s/ρ_B^s and r_A/r_B. For our example, $(u^2/R)\,/\,(w'w)$ is roughly taken to be $(\langle u^2\rangle\,/\,\langle R\rangle)\,/\,(\langle w'\rangle\,\langle w\rangle) \simeq -0.4$, where the brackets denote an arithmetic average within the circular cell. With ν replaced by $\bar{\nu} = 0.7$, we obtain Figure 4.4.

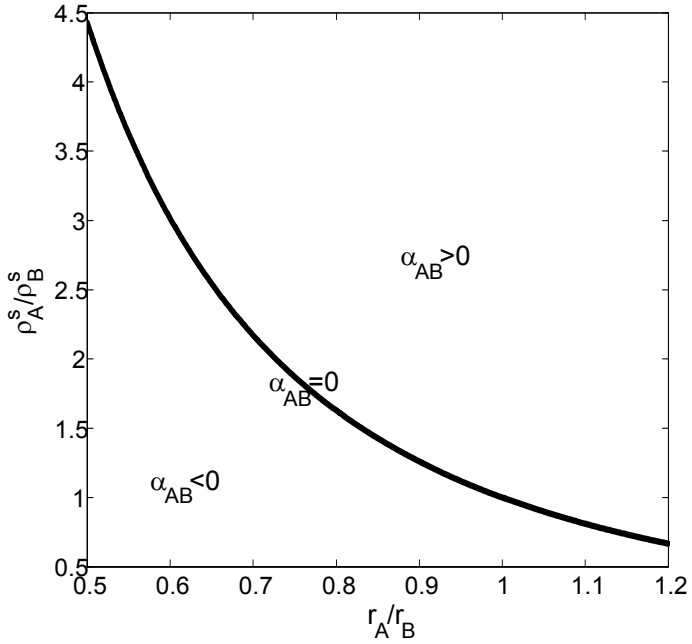

Figure 4.4: $\alpha_{AB} = 0$ can be written as a relation between ρ_A^s/ρ_B^s and r_A/r_B. For $(u^2/R)\,/\,(w'w) \simeq -0.4$ and $\bar{\nu} = 0.7$. Here, $r_A/r_B = 1$ and $m_A/m_B = 1.1$ (that is, $\rho_A^s/\rho_B^s = 1.1$).

With $r_A/r_B = 1$ and $m_A/m_B = 1.1$ (that is, $\rho_A^s/\rho_B^s = 1.1$) , we lie above the line $\alpha_{AB} = 0$ and can show from (4.24) that $\alpha_{AB} > 0$ below this curve. That is, x' and w' have different signs in (4.24). Consequently, the concentration of A increases with decreasing w and there is more of species A in the upper part of the flow, in agreement with Figure 4.3.

Although this is a crude way of determining how A and B segregate, it can be used as a quick and useful rule of thumb on determining the direction of segregation.

4.4.2 Vibrated mixture from the bottom boundary

The experiment of Feitosa and Menon[21] on segregation of a binary mixture vibrated by the bottom boundary motivates this example. We consider two dimensional flow of a binary mixture of disks, with the bottom boundary vibrating at a specified fluctuation velocity from the rest position, in the presence of gravity. Assuming that the flow is steady and only gradient occurs along z-axis, pointing upward opposite to gravity. For this example, we ignore frictional effects due to the flat side walls, though it is possible to account for it[47] and we assume that there is only one coefficient of restitution, e, to describe collisions among all flow particles and e_w to describe the collisions between wall and the flow particles.

As in the previous example, we employ the same governing equations from Revised Enskog Theory, except that we now have gravity in place of centripetal force and thus extra terms involving radius in the previous example all disappear, as in the example of shearing between two parallel plates.[73] For the boundary condition at the base, we use that of Richman[59] who calculated, using Maxwellian velocity distribution, the rates at which linear momentum and kinetic energy are exchanged between the flow and the vibrating boundary, moving up and down from the mean position with a specified fluctuation velocity. Unlike an experimental set-up which requires both the acceleration and the velocity of the moving boundary in order to specify a vibrating bottom condition, Richman's condition requires only the velocity. But, Breu *et al*.[12] observed in a similar experiment that when the acceleration is sufficiently high for a given velocity, only the information on the velocity is sufficient to describe a qualitative behavior of

segregation. This can be also seen in the work of Wildman *et al*.[69] who saw good agreements in comparing the predictions of kinetic theory[6], using Richman's vibrating boundary condition[59], with experimental and numerical findings for a binary mixture of spheres vibrated in a three dimensional cylinder. We use Richman's condition to solve this problem, but it is only an approximation because Richman's calculation was derived for three dimensional flows, while we deal with two dimensional flows.

First, we determine the dimensionless height of the vibrated mixture, H, with the condition that this is the height at which kinetic theory fails; that is, there are so few collisions that the mean free path of a particle is equal to the length of vertical ballistic trajectory. This provides a condition for the non-dimensionalized pressure (See Chapter 6 for more details),

$$p\left(H\right) = \nu\left(H\right) w^2\left(H\right) = 0.04$$

and assuming that there are very few collisions above H, we obtain that $q\left(H\right) = 0$.

Our approximation with the use of Richman's calculation on the vibrating boundary provides a condition on the heat flux at the base,

$$q\left(0\right) = \sqrt{\frac{2}{\pi}} p\left(1 - 3x\delta r\right) \sqrt{w^2 + V^2} \left[\frac{2V^2}{w^2 + V^2} - \left(1 - e_w\right)\right],$$

where $2V^2$ is the mean square velocity of the boundary.

One drawback of the boundary condition on x that we used in our previous example is that $\overline{x}$ cannot be found analytically. To go about that problem, we introduce another variable

$$s = \frac{x\nu}{\overline{n}H}.$$

Differentiating s with respect to z, we get

$$\frac{ds}{dz} = \frac{1}{\overline{n}H}\left(\frac{dx}{dz}\nu + x\frac{d\nu}{dz}\right)$$

From the definition of x,

$$x = \frac{1}{2}\frac{\nu_A - \nu_B}{\nu} + O(\delta r),$$

and we have, ignoring the order of δr in x as before,

$$s = \frac{1}{2}\frac{\nu_A - \nu_B}{\overline{n}H}.$$

Defining an integral of s,

$$J(z) = \frac{2}{\pi r_B^2}\int_0^z s(Y)\,dY,$$

we get boundary conditions $J(0) = 0$ and

$$\begin{aligned} J(H) &= \frac{1}{\pi r_B^2}\frac{\overline{\nu}_A - \overline{\nu}_B}{\overline{n}} \\ &= \frac{N_A - N_B}{N} \\ &= f_A - \frac{1}{2}. \end{aligned}$$

where N_i is the number of particles of species i, $N = N_A + N_B$ and $f_A = N_A/N$ is the filling fraction of A.

Similarly, we define

$$I(z) = \int_0^z \nu(Y)\,dY,$$

which gives us the boundary condition, $I(0) = 0$ and

$$\begin{aligned} I(H) &= \overline{\nu}H \\ &= \frac{\pi r_{AB}^2}{4}\overline{n}H. \end{aligned}$$

Using these boundary conditions, we study two mixtures similar to the ones studied by Feitosa and Menon[21]. For these mixtures, we fix $e = 0.85$ and $e_w = 0.85$, which are typical values of restitution coefficients for materials in their experiment. We also fix the filling fraction $f_A = 1/2$ and $\pi r_{AB}^2\overline{n}H/4$ to be 0.5. Each disk has a radius of

1.6 mm and the fluctuation velocity of the base is taken to be 0.86 m/s, which gives $V = 4.85$.

Figure 4.5 and 4.6 shows the area fractions of each species and the fluctuation velocity of the mixture, for $m_A/m_B = 0.92$ and 0.33, respectively. In both solutions, we see that there is an increase in the fluctuation velocity as we move up from the base to the first ten particle diameters. Above this level, we see that the agitation is nearly constant within the mixture and the assumption of uniform temperature used in Chapter 2 can be justified. We also note that our predictions suggest a more dilute and taller mixture than observed by Feitosa and Menon[21].

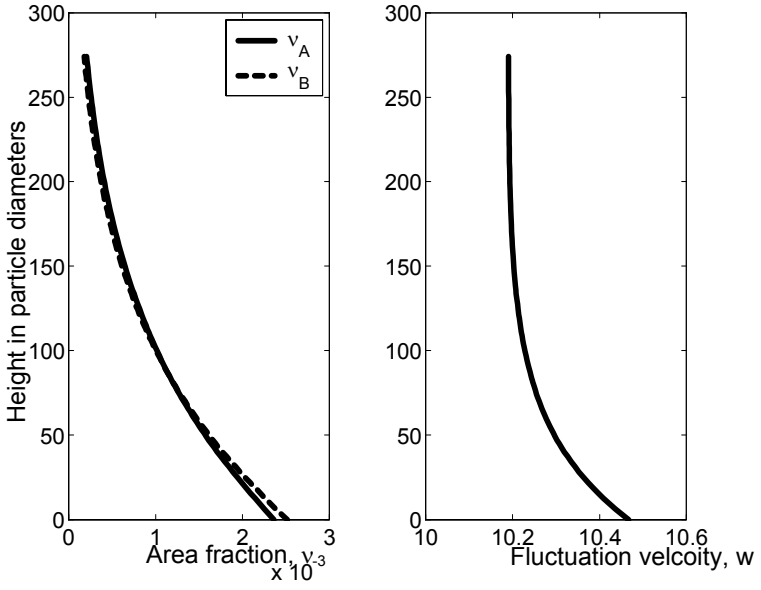

Figure 4.5: $m_A/m_B = 0.92$.

In the case where the species have the same size and similar masses, as in Figure 4.5, the density profiles of A and B are identical to each other, as observed by Feitosa and Menon[21]. When the species have the same size, yet differ in masses, as in Figure 4.6, we see that the heavier particles are found near the base, where there is a gradient of the temperature, and the lighter particles near the core region of the mixture. This is

in agreement with our analytical prediction given in Chapter 2. Feitosa and Menon[21] saw in their experiment that heavier particles tended to be concentrated slightly more in the center of the mixture, whereas the lighter particles were spread uniformly through the mixture.

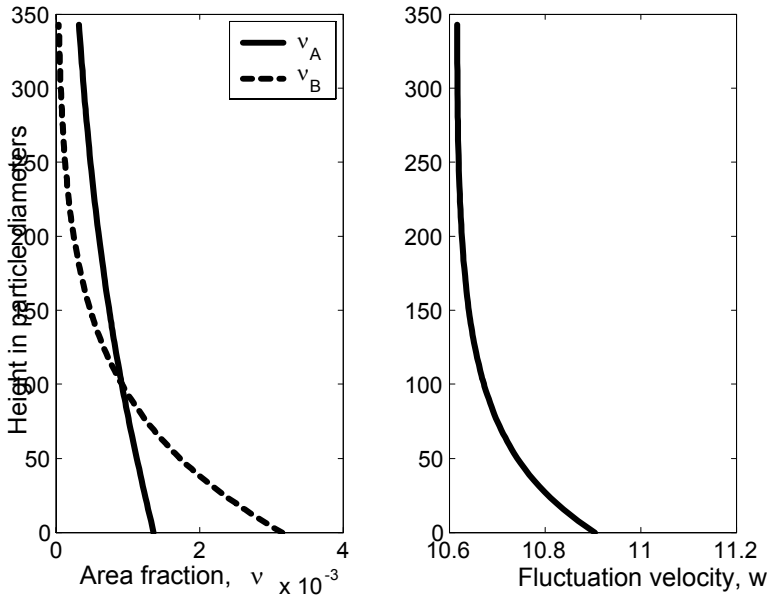

Figure 4.6: $m_A/m_B = 0.33$.

The general shape of the density profiles from our study indicates that there is a gradual decrease in density as we move away from the base. However, Feitosa and Menon[21] found that the density profiles were actually symmetric about the center of the mixture. It is not clear what causes such difference: side wall effect, increased viscosity due to air in the cage or inadequate boundary condition. But we note that in the experimental and numerical works of Wildman *et al*.[68] on a binary mixture in a vibrated cylinder, they saw profiles of fluctuation velocities and densities similar to the ones found here.

4.5 Conclusion

We have linearized the kinetic equations for a binary mixture of disks, derived by Willits and Arnarson[70] with the corrections by Alam *et al*.[1], in small δr and δm and found explicit expressions for transport coefficients. By using terms linearized in δr and δm, we were able to compactly formulate the governing equations and prescribe the boundary conditions for a steady, fully-developed and axisymmetric flow of a binary mixture of disks sheared by bumpy inner and outer walls in a circular cell. With MATLAB bvp4c function, we solved the two point boundary value problem in this particular geometry to study segregation and predicted the velocity and the temperature profiles as well as how the species segregate. In the course of solving this system, we found that the nature of the solutions are very sensitive to the choice of parameters e_w and θ. We used thermal diffusion factor, α_{AB}, as a measure of segregation by showing how the sign of α_{AB} is related to the density profiles of A and B. Then, we introduced a crude way of determining the segregation using α_{AB}.

To study a binary mixture of disks vibrated at the base, we used Richman's fluctuating bottom boundary condition, in a very crude way. We solved for densities for a binary mixture differing in masses, but not in sizes. Though the features our solutions are in qualitative agreement with findings of Wildman *et al*.[68], the general shape of the density profiles we found are quite different the ones found by Feitosa and Menon[21]. It is possible that the friction between the disks and the side walls, or the interstitial air between disks in the cage may have reduced the role of gravity in their experiment and thus making the mixture more uniform in densities as well as in agitation.

An indication of the limits of the approximate kinetic theory and the more general theory from which it was derived can be obtained from the results of recent numerical simulations. Alam and Luding[2] showed for a shearing flow of binary mixtures

of frictionless disks that for particles with different sizes, but with the same mass, the assumption of the equipartition of energy and the predictions of the kinetic theory of Willits and Arnarson[70] apply for diameter ratios up to five and coefficients of restitution as low as 0.70. However, Clelland and Hrenya[17] and Alam and Luding[3] found that for particles of the same density, but with different diameters, the difference in mass amplifies the difference in the energies of species. Within the limits where the assumption of the equipartition is reasonable, say diameter ratios less than two, mass ratios less than four and coefficients of restitution greater than 0.80, this kinetic theory of binary of Willits and Arnarson[70] mixture should give a plausible description of transport and segregation[6]. And as the current study focuses on expressions linearized in small size and mass differences, we believe the assumption of equipartition to be valid.

Chapter 5

COMPARISON BETWEEN DENSE MAXWELLIAN THEORY AND REVISED ENSKOG THEORY

Binary mixtures of granular materials reveal interesting phenomena, such as segregation due to size and/or material density differences. To study rapid flows of such mixtures, kinetic theories have been developed[46][22][36][37][7] in the past, but no explicit comparison of the predictions of these theories exists.

The mixture theory of Jenkins and Mancini[36], which we will call DMAX, treats smooth, slightly inelastic particles. It assumes Maxwellian single velocity distribution functions and molecular chaos and employs dense corrections using the radial distribution functions for contacting particles. It does not assume equipartition of granular energy of each species, but considers the difference in energies to be small.

As the choice of Maxwellian distribution function is inappropriate for gradients in the mean fields, an extension was made by Jenkins and Mancini[37] who calculated field variables with a perturbed form of Maxwellian distribution from the revised Enskog theory of López de Haro *et al.*[46] who derived a mixture theory for elastic spheres and who assumed the equipartition of energy between species. The revised Enskog theory resolved the issue of at what point along the line of centers the radial distribution functions are to be evaluated for contacting particles. As theories prior to this evaluated these functions at arbitrary points, they all disagreed with one another and were in conflict with irreversible thermodynamics. By taking the radial distributions functions as nonlocal functionals of the density fields, van Beijeren and Ernst resolved these

issues.[46][66]

Arnarson and Willits[7], whose theory we will call RET, reexamined the theory of Jenkins and Mancini[37] and corrected two errors in the transport coefficients. Using this theory, Arnarson and Jenkins[6] studied a boundary value problem for a binary mixture of spheres whose sizes and masses do not differ much. They simplified the theory of Arnarson and Willits by linearizing all expressions in small $\delta r = r_A/r_B - 1$ and $\delta m = (m_A - m_B) / (m_A + m_B)$.

Though RET is more refined than DMAX, the complexity of the terms appearing in RET makes it difficult to use, and for this reason, the actual difference in the prediction of segregation between RET and DMAX has not yet been explicitly studied. When Jenkins and Yoon[41] used DMAX to predict segregation criteria for an agitated collection of particles under gravity with uniform temperature, they found their prediction to agree well with numerical simulation of Hong *et al*.[30] and with RET.[6] Hence, we are interested to see how DMAX compares with RET in the presence of temperature gradient.

Consequently, we propose to compare these theories. If RET and DMAX give similar predictions, it is more natural to implement DMAX, which is simpler in appearance and in use, compared to RET. To proceed with the comparison, we study a steady flow of a binary mixture of smooth, nearly elastic spheres, whose sizes and masses do not differ much. The variation in fields is along the vertical direction z only and the only external force is gravity. First, we show that density variations are governed by gravity and the temperature gradient. Then, we compare DMAX of Jenkins and Mancini[36] and RET of Arnarson and Willits[7] for their predictions of density variations. Finally, we compare the predictions of segregation for small δr and δm.

5.1 Segregation

5.1.1 Preliminaries

We consider a mixture of spherical particles, where there exist two species of spheres, A and B. The spheres are assumed to be nearly elastic, smooth and homogeneous. Spheres of type i, where i is either A or B, have radius r_i and mass m_i. We also introduce $r_{ij} \equiv r_i + r_j$ and $m_{ij} \equiv m_i + m_j$.

To define mean values, we employ the single particle velocity distribution functions $f_i^{(1)}(\mathbf{c}, \mathbf{x}, t)$, where $\mathbf{c}$ is the particle velocity, $\mathbf{x}$ is the position of the particle and t is the time. The number density n_i of species i is, then,

$$n_i(\mathbf{x}, t) = \int f_i^{(1)}(\mathbf{c}, \mathbf{x}, t)\mathbf{dc},$$

where the integration is taken over all $\mathbf{c}$. The total number density is $n \equiv n_A + n_B$. The mass density ρ_i of species i is defined as $m_i n_i$ and the total mass density ρ is

$$\rho \equiv \rho_A + \rho_B = m_A n_A + m_B n_B.$$

The mean velocity $\mathbf{u}_i$ of species i is

$$\mathbf{u}_i \equiv \langle \mathbf{c}_i \rangle = \int \mathbf{c}_i f_i^{(1)}(\mathbf{c}, \mathbf{x}, t)\mathbf{dc}.$$

Then, the mass average, or barycentric velocity, $\mathbf{u}$, is defined as the mass-average of the species velocities:

$$\mathbf{u} \equiv \rho^{-1}(\rho_A \mathbf{u}_A + \rho_B \mathbf{u}_B).$$

The diffusion velocity is given by $\mathbf{v}_i = \mathbf{u}_i - \mathbf{u}$.

The temperature, T_i, of species i is defined by

$$T_i \equiv \frac{1}{3} m_i \left\langle (\mathbf{c}_i - \mathbf{u}) \cdot (\mathbf{c}_i - \mathbf{u}) \right\rangle,$$

which is the mean of the kinetic energy of the fluctuations relative to the mass average velocity. The mixture temperature, T, is defined as the number average of the species temperatures:

$$T \equiv n^{-1}(n_A T_A + n_B T_B). \tag{5.1}$$

The partial pressure of species i is

$$p_i = n_i T \left(1 + \sum_{j=A,B} K_{ij}\right), \tag{5.2}$$

where K_{ij} is defined in terms of the species volume fraction ν_i as

$$K_{ij} = \frac{1}{2}\nu_j g_{ij} \left(1 + \frac{r_i}{r_j}\right)^3.$$

The radial distribution function for contacting pairs is given by

$$g_{ij} = \frac{1}{1-\nu} + \frac{6 r_i r_j}{r_{ij}} \frac{\xi}{(1-\nu)^2} + 8 \left(\frac{r_i r_j}{r_{ij}}\right)^2 \frac{\xi^2}{(1-\nu)^3},$$

where the mixture volume fraction is $\nu = \nu_A + \nu_B$ and $\nu_i = 4\pi n_i r_i^3/3$ and $\xi_i = 2\pi n_i r_i^2/3$ and $\xi = \xi_A + \xi_B$. The total pressure is simply the sum of partial pressures,

$$p = p_A + p_B.$$

5.2 Jenkins and Mancini (DMAX)

The binary mixture theory of Jenkins and Mancini[36] assumed Maxwellian distributions for the single particle velocity distributions and the molecular chaos with dense corrections and calculated the average values. That is, the pair distribution functions take the form of a product of two Maxwellian distribution functions at two distinct positions and these products are multiplied by a radial distribution function.

Though Jenkins and Mancini[36] did not assume equipartition of granular energies, they considered the difference in temperatures to be small. Here we are not concerned with the influence of this small difference and take it to be zero.

Ignoring contributions to the species stress that are quadratic in the diffusion velocity, $v_i = u_i - u$, or are associated with the rate of deformation of the mixture and assuming that the only external force is associated with the gravitational acceleration $-g$, the balance of momentum of species i has the form

$$\rho_i \dot{u}_i = -p_i' - n_i m_i g + \phi_i, \tag{5.3}$$

where the dot indicates a time derivative with respect to the mean velocity of i, the prime denotes a derivative with respect to z, p_i is the partial pressure, and ϕ_i is the rate per unit volume at which momentum is provided to i in interactions with the other species. Because the interactions are equal and opposite, $\phi_B = -\phi_A$.

The interaction terms are given by Jenkins and Mancini [36] as

$$\boldsymbol{\phi}_i = K_{ij} n_i T \left[\left(\frac{m_j - m_i}{m_{ij}} \right) (\ln T)' + \left(\ln \frac{n_i}{n_j} \right)' + \frac{4}{r_{ij}} \left(\frac{2 m_i m_j}{\pi m_{ij} T} \right)^{1/2} (v_j - v_i) \right], \tag{5.4}$$

for $i \neq j$. The quantity $v_j - v_i$ is the relative motion of the two species. Using (5.4), it can be written as[32]

$$v_A - v_B = -\frac{n^2}{n_A n_B} D_{AB} d_A^{(DMAX)},$$

where the diffusion coefficient D_{AB} is

$$D_{AB} \equiv \frac{3}{2 n g_{AB}} \left(\frac{2 T m_{AB}}{\pi m_A m_B} \right)^{1/2} \frac{1}{8 r_{AB}^2},$$

and the diffusion force of species A is

$$
\begin{aligned}
& d_A^{(DMAX)} \\
\equiv\ & -\frac{\rho_A}{n\rho T}p' \\
& +\frac{(\ln T)'}{n}\left(n_A + 2M_{AB}K_{AB}n_A + K_{AA}n_A\right) \\
& +\frac{1}{n}\left(\frac{1}{T}\frac{\partial p_A}{\partial n_A} - K_{AB}\right)n_A' \\
& +\frac{1}{n}\left(\frac{1}{T}\frac{\partial p_A}{\partial n_B} + \frac{n_A}{n_B}K_{AB}\right)n_B'. \qquad (5.5)
\end{aligned}
$$

From the momentum balances of species A and the mixture, we have, using the chain rule,

$$
\begin{aligned}
p_A^{'} &= \frac{\partial p_A}{\partial \nu_A}\nu_A^{'} + \frac{\partial p_A}{\partial \nu_B}\nu_B^{'} + \frac{\partial p_A}{\partial T}T' \\
&= -\rho_A g + \phi_A,
\end{aligned}
$$

and

$$
\begin{aligned}
p^{'} &= \frac{\partial p}{\partial \nu_A}\nu_A^{'} + \frac{\partial p}{\partial \nu_B}\nu_B^{'} + \frac{\partial p}{\partial T}T' \\
&= -\rho g.
\end{aligned}
$$

Because we are dealing with steady, fully-developed and rectilinear flows, the difference in the diffusion velocity is equal to zero. We solve for $\nu_A^{'}$ and $\nu_B^{'}$ and obtain a matrix equation

$$
\begin{pmatrix} \nu_A^{'} \\ \nu_B^{'} \end{pmatrix}
= -\frac{1}{\tilde{D}} \begin{pmatrix} \frac{\partial p}{\partial \nu_B} & -\frac{\partial p_A}{\partial \nu_B} - K_{AB}\frac{n_A}{\nu_B}T \\ -\frac{\partial p}{\partial \nu_A} & \frac{\partial p_A}{\partial \nu_A} - K_{AB}\frac{n_A}{\nu_A}T \end{pmatrix}
\times \begin{pmatrix} \rho_A g + K_{AB} n_A \delta m T' + \frac{\partial p_A}{\partial T}T' \\ \rho g + \frac{\partial p}{\partial T}T' \end{pmatrix},
$$

where

$$
\begin{aligned}
\tilde{D} &= \left(\frac{\partial p_A}{\partial \nu_A} - K_{AB}\frac{n_A}{\nu_A}T\right)\frac{\partial p}{\partial \nu_B} \\
&\quad - \left(\frac{\partial p_A}{\partial \nu_B} + K_{AB}\frac{n_A}{\nu_B}T\right)\frac{\partial p}{\partial \nu_A}.
\end{aligned}
$$

Because A and B appear symmetrically, we look at the equation for B. With the relation $\nu_i = 4\pi n_i r_i^3/3$, we have

$$
\begin{aligned}
n_B^{'} &= \frac{1}{\tilde{D}}\frac{3}{4\pi r_B^3}\frac{\partial p}{\partial \nu_A} \\
&\times \left[\rho_A g + \left(K_{AB} n_A \delta m + \frac{\partial p_A}{\partial T}\right)T'\right] \\
&-\frac{1}{\tilde{D}}\frac{3}{4\pi r_B^3}\left(\frac{\partial p_A}{\partial \nu_A} - K_{AB}\frac{n_A}{\nu_A}T\right) \\
&\times \left(\rho g + \frac{\partial p}{\partial T}T'\right). \qquad (5.6)
\end{aligned}
$$

5.3 Arnarson and Willits (RET)

Jenkins and Mancini[37] extended their previous mixture theory by using a perturbed form of dense Maxwellian distribution and by evaluating results from the revised Enskog theory of López de Haro *et al.*[46] and applying them to inelastic spheres. Arnarson and Willits[7] retraced this line of approach and corrected mistakes made in Jenkins and Mancini[37].

As a summary of their result[6], we have the difference in the species diffusion velocities

$$v_A - v_B = -\frac{n^2}{n_A n_B} D_{AB} \left[d_A^{(RET)} + K_T^{(A)} \left(\ln T \right)' \right], \tag{5.7}$$

where the diffusion coefficient D_{AB} is the same as that of Jenkins and Mancini[36] and the diffusion force, $d_A^{(RET)}$, of species A is slightly different from (5.5) of Jenkins and Mancini because of the appearance of the gradients of chemical potentials in place of the gradients of partial pressure:

$$\begin{aligned} & d_A^{(RET)} \\ \equiv \; & -\frac{\rho_A}{n\rho T} p' \\ & + \frac{(\ln T)'}{n} \left(n_A + 2 M_{AB} K_{AB} n_A + K_{AA} n_A \right) \\ & + \frac{n_A}{nT} \left(\frac{\partial \mu_A}{\partial n_A} n_A' + \frac{\partial \mu_A}{\partial n_B} n_B' \right). \end{aligned} \tag{5.8}$$

The difference in the diffusion velocities has an extra term in the theory of Arnarson and Jenkins: the thermal diffusion coefficient, $K_T^{(i)} \equiv a_{i0}/n t_{i0}$, where a_{i0} and t_{i0} are coefficients arising in the Chapman-Enskog procedure. The details on these coefficients can be found in Arnarson and Jenkins.[6]

The chemical potential functions μ_i are given by Reed and Gubbins[57] as

$$
\begin{aligned}
&\frac{\mu_i}{T} \\
= \;& \ln n_i - \ln(1-\nu) + \frac{4\pi r_i^3 p}{3T} \\
&+\frac{3\xi_2 r_i}{1-\nu} + \frac{3\xi_1 r_i^2}{1-\nu} + \frac{9\xi_2^2 r_i^2}{2(1-\nu)^2} \\
&+3\left(\frac{\xi_2 r_i}{\nu}\right)^2 \left[\ln(1-\nu) + \frac{\nu}{1-\nu} - \frac{\nu^2}{2(1-\nu)^2}\right] \\
&-\left(\frac{\xi_2 r_i}{\nu}\right)^3 \left[2\ln(1-\nu) + \frac{\nu(2-\nu)}{1-\nu}\right].
\end{aligned}
$$

Upon differentiating the total pressure with respect to z, we have

$$
p' = \frac{\partial p}{\partial n_A} n_A^{'} + \frac{\partial p}{\partial n_B} n_B^{'} + \frac{\partial p}{\partial T} T' = -\rho g. \tag{5.9}
$$

Setting (5.7) equal to zero and employing the total momentum balance (5.9), we can solve for n_A' and n_B' :

$$
\begin{aligned}
n_A' &= -n\frac{T'}{T}\left(\frac{1}{T}\frac{\partial p}{\partial n_A}\right)^{-1} \\
&\quad \times \left[\beta + \left(\frac{1}{T}\frac{\partial p}{\partial n_B}\right)\left(n\frac{T'}{T}\right)^{-1} n_B' + \frac{p}{nT}\right], \\
n_B' &= \frac{1}{D}\frac{n}{n_A}\frac{1}{T^2}\frac{\partial p}{\partial n_A}\left[\rho_A g + n_A\right. \\
&\quad \left.\times (1 + K_{AA} + 2M_{AB}K_{AB})\, T' + nT' K_T^{(A)}\right] \\
&\quad -\frac{1}{D}\frac{n}{T^2}\frac{\partial \mu_A}{\partial n_A}\left(\rho g + \frac{p}{T}T'\right),
\end{aligned} \tag{5.10}
$$

where $\beta \equiv \rho g / nT'$, $M_{AB} \equiv m_A / m_{AB}$ and D is

$$
D \equiv \det \begin{pmatrix} \frac{n}{T}\frac{\partial \mu_A}{\partial n_A} & \frac{n}{T}\frac{\partial \mu_A}{\partial n_B} \\ \frac{1}{T}\frac{\partial p}{\partial n_A} & \frac{1}{T}\frac{\partial p}{\partial n_B} \end{pmatrix}.
$$

5.4 Comparison

5.4.1 Correspondence of terms

We have so far derived expressions for the density gradient of a species (5.6) from DMAX and (5.10) from RET[7].

We first note that each term is either multiplied by g or T'. That is, the density distribution of each species can be controlled by changing g and T'. We also observe that there is a correspondence of each term in (5.6) and (5.10). For example, $\rho_A g$ and ρg appear in both of the expressions. We provide a table that shows the correspondence.

DMAX	RET
$\left(K_{AB} n_A \delta m + \frac{\partial p_A}{\partial T}\right) T'$	$n_A T' \left(1 + K_{AA} + 2 M_{AB} K_{AB}\right) + n K_T^{(A)} T'$
$\frac{\partial p}{\partial T} T'$	$\frac{p}{T} T'$
$\frac{1}{D} \frac{3}{4\pi r_B^3} \frac{\partial p}{\partial \nu_A}$	$\frac{1}{D} \frac{n}{n_A} \frac{1}{T^2} \frac{\partial p}{\partial n_A}$
$\frac{1}{D} \frac{3}{4\pi r_B^3} \left(\frac{\partial p_A}{\partial \nu_A} - K_{AB} \frac{n_A}{\nu_A} T\right)$	$\frac{1}{D} \frac{n}{T^2} \frac{\partial \mu_A}{\partial n_A}$

In the first row, we can check that these expressions differ by $n K_T^{(A)} T'$:

$$
\begin{aligned}
& \left(K_{AB} n_A \delta m + \frac{\partial p_A}{\partial T}\right) T' \\
& - \left(n_A + K_{AA} n_A + 2 M_{AB} K_{AB} n_A + n K_T^{(A)}\right) T' \\
= \; & - n K_T^{(A)} T' .
\end{aligned}
$$

It is clear also that the second row agrees.

To make an explicit comparison of the terms in the third and the fourth rows, we linearize in $\delta r = r_A/r_B - 1$ and $\delta m = (m_A - m_B)\,/\,(m_A + m_B)$. In the linearization, we assume that δr and δm are of the same order and this gives a restriction to our region in r_A/r_B and ρ_{As}/ρ_{Bs} where our analysis remains valid.

After expanding terms in the third row in small δr, we find that they are equal.

When terms in the fourth row are linearized in small δr, we find that they differ slightly:

$$\begin{aligned} & \frac{1}{\tilde{D}}\frac{3}{4\pi r_B^3}\left(\frac{\partial p_A}{\partial \nu_A} - K_{AB}\frac{n_A}{\nu_A}T\right) - \frac{1}{D}\frac{n}{T^2}\frac{\partial \mu_A}{\partial n_A} \\ = \; & \frac{1}{T}\frac{1}{(1+4G+4H\nu)}\nu_A\nu_B\delta r \\ & \times\left[\frac{(\nu-6)\,(\nu-4)}{(\nu-1)^4} - \frac{6\,(-2\nu+5)}{(\nu-1)^4}\right]. \end{aligned}$$

The difference in the coefficients of $\nu_A\nu_B\delta r$ is about fifteen per cent for all volume fractions. The appearance of the gradient of chemical potential function μ_A in the theory of Arnarson and Willits[7], instead of the gradient of partial pressure as in Jenkins and Mancini[36], accounts for this difference.

5.4.2 Linearization

When the coefficients of g and T' in (5.6) are linearized in small δr and δm, we find DMAX to give

$$
\begin{aligned}
&\frac{n_B'}{n_B} \\
= \quad & -\frac{m_{AB}g}{2T}\frac{1}{1+4G+4H\nu} - \frac{T'}{T}\frac{1+4G}{1+4G+4H\nu} \\
& -\frac{m_{AB}g}{T}\frac{\nu_A}{1+4G+4H\nu} \\
& \times\left[\frac{6G}{\nu}+\frac{(\nu-6)(\nu-4)\nu}{2(\nu-1)^4}\right]\delta r \\
& +\frac{m_{AB}g}{T}\left[\frac{\nu_A}{\nu}-\frac{\nu_A-\nu_B}{2\nu(1+4G+4H\nu)}\right]\delta m \\
& +\frac{T'}{T}\frac{\nu_A}{\nu}4G\delta m \\
& +\frac{T'}{T}\frac{\nu_A}{\nu}\left\{6G+\frac{(3-\nu)\nu^2}{(1-\nu)^3}-\frac{(1+4G)\nu}{1+4G+4H\nu}\times\right. \\
& \left.\left[\frac{12G}{\nu}+\frac{(\nu-6)(\nu-4)\nu}{(\nu-1)^4}\right]\right\}\delta r, \qquad (5.11)
\end{aligned}
$$

where

$$G(\nu)=\frac{(2-\nu)\nu}{2(1-\nu)^3},$$

and $H(\nu)=dG/d\nu$.

Similarly, Arnarson and Jenkins[6] provides the number density gradient (5.10) of RET, when linearized, to be

$$
\begin{aligned}
&\frac{n_B^{'}}{n_B} \\
= \; & -\frac{m_{AB}g}{2T}\frac{1}{1+4G+4\nu H} - \frac{T^{'}}{T}\frac{1+4G}{1+4G+4\nu H} \\
& -\frac{m_{AB}g}{T}\nu_A\frac{6H}{1+4G+4\nu H}\delta r \\
& +\frac{m_{AB}g}{T}\left[\frac{\nu_A}{\nu} - \frac{\nu_A-\nu_B}{2\nu\left(1+4G+4\nu H\right)}\right]\delta m \\
& +\frac{T^{'}}{T}\frac{\nu_A}{\nu}\left(\frac{179}{29}G+\frac{105}{116}\right)\delta m \\
& +\frac{T^{'}}{T}\frac{\nu_A}{\nu}\left\{\frac{5}{58}\left[2+\frac{\nu\left(3-\nu\right)}{2-\nu}-\frac{12G}{5}\right]+2G\times\right. \\
& \left.\left[3+\frac{\nu\left(3-\nu\right)}{2-\nu}\right]-\frac{12\nu H\left(1+4G\right)}{1+4G+4\nu H}\right\}\delta r. \qquad (5.12)
\end{aligned}
$$

5.4.3 Explicit comparisons of coefficients of g and T'

When comparing (5.11) of DMAX and (5.12) of RET, the coefficients of $-m_{AB}g/2T$, $-T^{'}/T$ and $m_{AB}g\delta m/T$ are identical in both cases. The coefficients that differ are plotted in Figure 5.1.

Both DMAX and RET give same qualitative behavior, though RET gives greater values in magnitude for all coefficients, especially at high ν. The deviation in the coefficients of $\left(T^{'}/T\right)\left(\nu_A/\nu\right)\delta m$ can be shown to result from the inclusion of the thermal diffusion coefficient $K_T^{(A)}$. The difference in the coefficient $\left(T^{'}/T\right)\left(\nu_A/\nu\right)\delta r$ is both due to the inclusion of the thermal diffusion coefficient and the appearance of the gradients of chemical potentials in place of the gradients of partial pressures. The difference in the coefficient of $-\left(m_{AB}g/T\right)\nu_A\delta r$ is solely due to the appearance of the gradients of chemical potentials in place of the gradients of partial pressures.

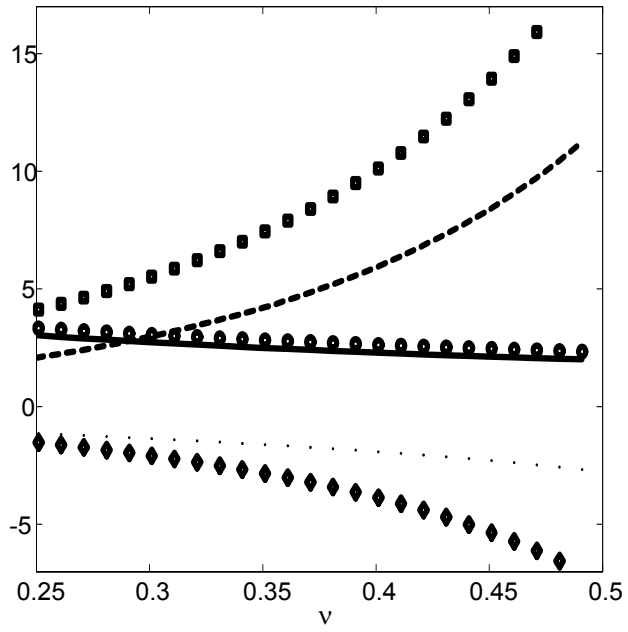

Figure 5.1: Lines: DMAX. Shapes: RET. Solid line, circle: coefficient of -($m_{AB}g/T$)$\nu_A \delta r$. Dashed line, square: coefficient of $(T'/T)\,(\nu_A/\nu)\,\delta m$. Dotted line, diamond: coefficient of $(T'/T)\,(\nu_A/\nu)\,\delta r$.

5.5 Segregation

We characterize segregation by the quantity $x = (n_A - n_B)\,/2n$, which is employed by Arnarson and Jenkins[6]. From the definition of x, it follows that

$$x' = \frac{-n_A n_B' + n_B n_A'}{n^2} = \frac{n_A n_B}{n^2}\left(\ln\frac{n_A}{n_B}\right)'.$$

We note in passing that Arnarson and Willits[7] used a thermal diffusion factor α_{AB} as a measure of thermal segregation and this factor is proportional to x':

$$\frac{n^2}{n_A n_B}x' = -\alpha_{AB}\frac{T'}{T}.$$

From (5.11) of DMAX, we have

$$
\begin{aligned}
& \frac{n^2}{n_A n_B} x' \\
= \; & \frac{m_{AB} g}{T} \frac{\nu}{1+4G+4H\nu} \\
& \times \left[\frac{6G}{\nu} + \frac{(\nu-6)(\nu-4)\nu}{2(\nu-1)^4} \right] \delta r \\
& - \frac{m_{AB} g}{T} \delta m \\
& - \frac{T'}{T} 4G \delta m \\
& - \frac{T'}{T} \left\{ 6G + \frac{(3-\nu)\nu^2}{(1-\nu)^3} - \frac{(1+4G)\nu}{1+4G+4H\nu} \right. \\
& \left. \times \left[\frac{12G}{\nu} + \frac{(\nu-6)(\nu-4)\nu}{(\nu-1)^4} \right] \right\} \delta r. \qquad (5.13)
\end{aligned}
$$

Similarly from (5.12) of RET, we have

$$
\begin{aligned}
& \frac{n^2}{n_A n_B} x' \\
= \; & \frac{m_{AB} g}{T} \frac{6\nu H}{1+4G+4\nu H} \delta r \\
& - \frac{m_{AB} g}{T} \delta m \\
& - \frac{T'}{T} \left(\frac{179}{29} G + \frac{105}{116} \right) \delta m \\
& - \frac{T'}{T} \left\{ \frac{5}{58} \left[2 + \frac{\nu(3-\nu)}{2-\nu} - \frac{12G}{5} \right] + 2G \right. \\
& \left. \times \left[3 + \frac{\nu(3-\nu)}{2-\nu} \right] - \frac{12\nu H(1+4G)}{1+4G+4\nu H} \right\} \delta r. \qquad (5.14)
\end{aligned}
$$

We can make simple comparisons of these two expressions. To achieve this, we examine a situation when there is no segregation: $x' = 0$.

Let us first assume that there is no temperature gradient, but only gravity is present. Jenkins and Yoon[41] studied this simple case of uniform temperature under gravity, based on DMAX of Jenkins and Mancini[36] and provided a simple criterion for the direction of segregation for given ratios of radii and material densities of particles. Figure

5.2 shows that both DMAX and RET agree fairly well, with at most twenty per cent of difference at higher volume fraction, as also noted by Arnarson and Jenkins.[6]

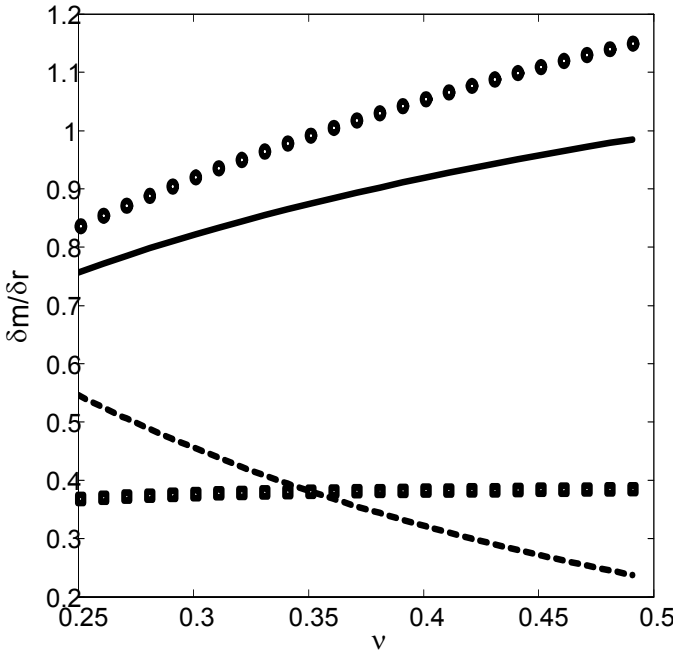

Figure 5.2: Lines: DMAX. Shapes: RET. Solid, circle: when $T' = 0$. Dashed, square: when $g = 0$.

Now, let us assume that gravity is absent, but temperature gradient is present. Figure 5.2 shows that the difference between two theories is larger in this case than in the previous case. In the vicinity of $\nu = 0.34$, the predictions are similar, but the difference can be as great as forty per cent near the very dense or dilute limit.

5.6 Conclusion

From the study of a binary mixture under gravity in the absence of temperature gradient, Jenkins and Yoon[41] showed that DMAX does quite well in predicting segregation. The intention of this study was to see how RET, a more refined theory of a binary

mixture, compares DMAX. Thus, we compared these theories by looking at expressions for the density variation of a species and we identified what differences exist between these theories. One difference was accounted for by the appearance of thermal diffusion coefficient $K_T^{(A)}$ in the theory of Arnarson and Willits. The other difference was from the appearance of the gradients of chemical potentials in place of the gradients of partial pressures.

Linearization in δr and δm allowed us to make quantitative comparisons. Some of the coefficients of g and T' in n_B'/n_B agreed completely, while some agreement was only qualitative. The quantitative differences were significant enough to result in differences even in the qualitative prediction of segregation.

Segregation was studied by examining a measure of segregation, $x = (n_A - n_B)/2n$. To compare the expression of each theory for x', we selected two special cases: 1) $g \neq 0$ and $T' = 0$ and 2) $g = 0$ and $T' \neq 0$. The predictions in the first case agreed quite well in both theories, with at most twenty per cent difference at high ν. This shows that DMAX can be used in place of RET when studying a binary mixture with no temperature gradient.

On the other hand, in the presence of temperature gradients, the two theories did not agree as well. If the volume fraction is near 0.34, the theories gave predictions close to each other. However, the difference could be as large as forty per cent for more dense or more dilute flows.

These comparisons show that when the binary mixture is reasonably dense (not too dense near phase transitions or too dilute), DMAX can be used in place of RET. However, to study more dense flows, RET is the appropriate theory to employ. DMAX is not appropriate to study dilute flows because the transport coefficients depend on the dense corrections made in the pair distribution function.

Chapter 6

FLOWS OF GRANULAR PARTICLES ON AN INCLINED PLANE: KINETIC THEORY APPROACH

The flow of granular particles down an inclined plane has been studied for a number of years by many researchers[5][4][20][56], for these flows serve as a guide in learning about more complicated geophysical flows. Anderson and Jackson[5] have compared solutions from collisional kinetic theory, collisional-frictional theory, which accounts for sustained contacts, and experiments. Ancey[4] and Drake[20] approached the same problem experimentally, whereas Hanes and Walton[27] studied the system using numerical simulations. Recently, some interesting characteristic features have been observed for these flows in a steady, fully developed state.

In physical experiments, Pouliquen[55] has looked at steady fully developed flows of particles flowing down an inclined plane between two side walls. Particles are glued on the plane to make it more "rough." In the experiments, frictional and inelastic spheres of equal sizes were used. It is found that steady fully developed (SFD) flow is possible, only for a certain range of the inclination angle ϕ. At larger angles, the flows accelerate and at smaller angles, the flows either come to a halt or become non-steady. Moreover, given ϕ, there is a minimum height, h_{stop}, below which no SFD flow can exist. Silbert et al.[63] find that SFD flows have a constant density through their depth, the volume fraction being roughly $\nu = 0.59$.

More remarkable is the fact that for all the systems they have looked at, with flow particles of different sizes and materials and with different bottom boundary conditions,

all of the data from all systems could be collapsed using the scaling relation between the depth averaged velocity $\langle u \rangle$ and height h of the flow:

$$\frac{\langle u \rangle}{\sqrt{gh}} = \beta \frac{h}{h_{stop}(\phi)}, \tag{6.1}$$

where $\beta = 0.136$ in the experiments and 0.147 in the simulations, independent of the system.

This present paper aims to investigate whether kinetic theory[33] can reproduce these features and if not, to see whether some modification of kinetic theory might.

It is noteworthy that the observed flows are rather dense, near $\nu = 0.59$. At this volume fraction, the key assumptions of binary collision and molecular chaos are known to fail[54], but these are key assumptions in the kinetic theory. However, as numerical simulations by Luding et al.[49] point out, even when the assumption of molecular chaos fails, kinetic theory can succeed in giving correct predictions.

While the kinetic theory used in this paper does not deal with frictional particles (though small friction can be accounted for, with an "effective" restitution coefficient[42]), the particles that have been used in experiments and simulation are highly frictional. The lack of friction in the simple theory implies that it cannot treat rotational kinetic energy. This energy has been shown to be a significant portion of the total kinetic energy near the bottom boundary[20].

6.1 Kinetic theory

Kinetic theory of granular particles[33] deals with spherical particles that are non-frictional, but which dissipate energy in collisions. Effects from interstitial fluids are not taken into account. In an assembly of granular particles, momentum is transferred either by particles moving between collisions or by collisions between particles. The

collisions are characterized by restitution coefficient, e. Collisions are assumed to be instantaneous.

Furthermore, in modelling collisions, the theory only allows for binary collisions, which is plausible for low density flows, but not obviously so for high density flows.

A more important assumption is that of molecular chaos, which says two colliding particles have no correlation in their velocities and/or positions. Again, such an assumption seems sound at low densities, but is shown to fail in flows with higher densities[49][54].

With the assumptions as stated above, kinetic theory predicts several mean field variables: volume fraction ν, mean velocity u, normal stress p, shear stress S, granular temperature $T = v^2/3$ where v^2 is the mean-square speed of the fluctuating component of the particle velocity, and granular heat flux q. The mean fields are defined as averages over velocity space using a distribution function that is a small perturbation of Maxwellian.

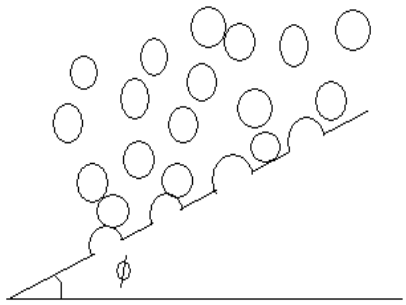

Figure 6.1: Flows on a bumpy incline.

Below, we summarize the results from kinetic theory for spherical particles of diameter σ and material density ρ_s such that the flow density is $\rho = \rho_s \nu$, for steady fully developed flows (SFD) down an incline. Since the flow is fully developed, the flow only

varies along z-axis, normal to the flow. Thus, the only spatial derivative that remains is d/dz, denoted by a prime.

Normal and tangential momentum balances give

$$p' = -\rho g \cos\phi$$

and

$$S' = -\rho g \sin\phi.$$

Constitutive relations express p and S in terms of other field variables T, ν and u :

$$p = \rho T \left(1 + 4G\right) \tag{6.2}$$

and

$$S = \frac{\sqrt{\pi}}{6}\rho\sigma T^{1/2}\left[\frac{5}{16G} + 1 + \frac{4}{5}\left(1 + \frac{12}{\pi}\right)G\right]u'.$$

where

$$G\left(\nu\right) = \begin{cases} \nu\left(2-\nu\right)/\left[2\left(1-\nu\right)^3\right], \text{ if } \nu < 0.49 & \text{Carnahan-Starling} \\ 5.6916\left(0.64-0.49\right)\nu/\left(0.64-\nu\right), \text{ if } \nu \geq 0.49 & \text{Torquato.} \end{cases}$$

Here G/ν is the radial distribution function for hard-spheres at equilibrium[14][65]. We note that the term, $4G$, appearing in the equation for pressure, is a correction to the ideal gas equation of state due to the volume occupied by particles.

The fluctuation energy balance is written as

$$0 = -q' + Su' - \gamma,$$

where γ is the collisional dissipation term

$$\gamma = \frac{24}{\sqrt{\pi}}(1-e)\frac{\rho T^{3/2}}{\sigma}G,$$

and the granular heat flux q, is given as the granular flow analog of Fourier's law

$$q = -\kappa T'$$

with the thermal conductivity given by

$$\kappa = \frac{15\sqrt{\pi}}{16}\rho\sigma T^{1/2}\left[\frac{5}{24G} + 1 + \frac{6}{5}\left(1 + \frac{32}{9\pi}\right)G\right].$$

Finally, the momentum balances are used to get $S/p = \tan\phi$.

In the next section, we discuss boundary conditions for these equations.

6.2 Inclined flows

As shown in Figure (6.1), we deal with particles flowing down an inclined plane, covered with bumps of the same sizes as the particles.

6.2.1 Top boundary condition

Because the flow has a free boundary at the top, it is necessary to impose a condition that specifies the location of the top of the flow. The top of the flow is taken to be where the mean free time between collisions, τ, is greater than or equal to the duration of a typical free trajectory, ζ[35]. That is, with

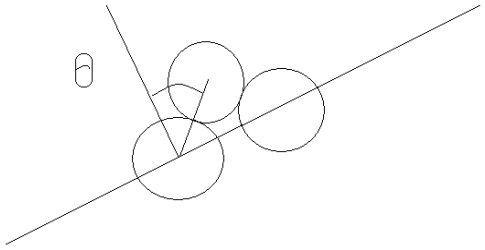

Figure 6.2: θ : measure of bumpiness

$$\begin{aligned} \tau &= \frac{\sigma\sqrt{\pi}}{24\nu T^{1/2}} \\ \zeta &= \frac{2T^{1/2}}{g\cos\phi} \\ \nu T &= \frac{\sigma g\cos\phi\sqrt{\pi}}{48} \end{aligned}$$

and $p \simeq \rho_s \nu T$ when ν is small in (6.2). When the pressure p is non-dimensionalized by $\rho_s \sigma g$, the non-dimensional pressure is found to be roughly 0.035 at the top.

6.2.2 Bottom boundary condition

The inclined plane, covered with hemispheres with a diameter equal to that of the flow particles, is characterized by the average distance between these wall particles. In other words, we characterize the bumpiness of the plane, by how much a flow particle can penetrate among wall particles. One such measure would be the angle θ, the average maximum penetration of a flow particle between wall particles, as shown in the Figure (6.2). Larger θ would give a bumpier plane.

The restitution coefficient in a collision between a flow particle and a wall particle is denoted by e_w. Although we could allow the size of the wall particles to differ from flow particles, for the sake of simplicity, we limit ourselves to the case when the flow and the wall particles have the same diameter.

Such a bumpy boundary has been considered before[40][58] and we refer to this work for details. Note that in contrast to molecular liquids, this boundary permits slip at its surface. By adjusting the values of e and e_w, the bumpy boundary can be made to either absorb or provide fluctuation energy to the flow; we call the corresponding boundary conditions dissipative or energetic, respectively.

6.3 Profiles of solutions

After making all the variables dimensionless by appropriate combinations of ρ_s, σ and g, we solve the flow equations of the kinetic theory with the boundary conditions described in the previous section. We abuse our notations by using the same symbols for dimensionless quantities as their dimensional counterparts and plot some typical solutions for both dissipative and energetic boundaries. The interest lies particularly in reproducing the features seen in experiments and simulations: constancy of density (ν around 0.59), existence of h_{stop} and the scaling relation

$$\frac{\langle u \rangle}{\sqrt{gh}} = \beta \frac{h}{h_{stop}\left(\phi\right)},$$

Consequently, we focus our attention on these points when looking at solutions.

As in the experiments, we specify the mass flux rate $\dot{m}$, the angle of inclination ϕ, e and e_w. The depth of the flow changes as $\dot{m}$ and ϕ change.

6.3.1 Dissipative boundary

Figures (6.3) and (6.4) show a typical solution with a dissipative boundary and parameters $e = 0.95$, $e_w = 0.80$, $\theta = 1.231$, $\dot{m} = 43.00$ and $\phi = 0.2170$.

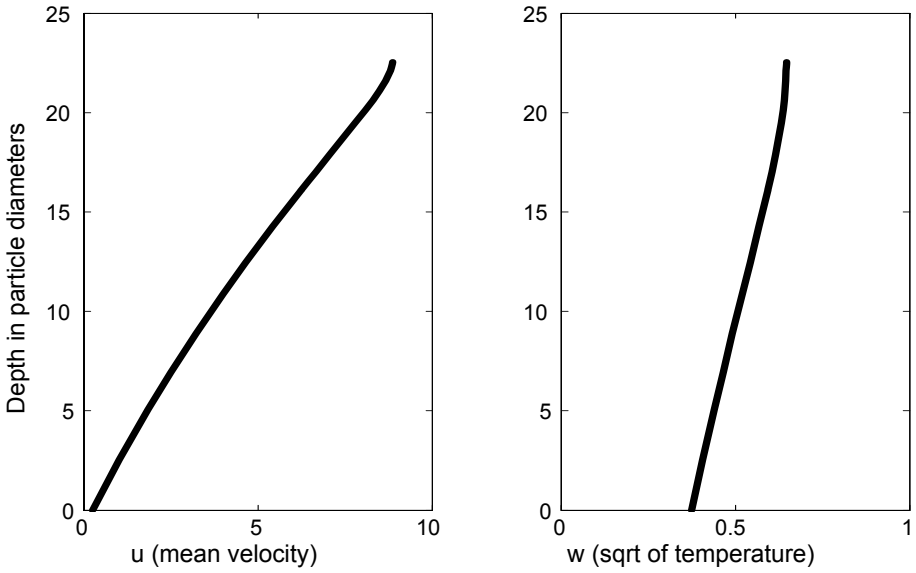

Figure 6.3: Dissipative boundary with parameters $e = 0.95$, $e_w = 0.80$, $\theta = 1.231$, $\dot{m} = 43.00$ and $\phi = 0.2170$. a) Mean velocity of the flow versus particle depth. Velocity increases almost linearly with the height and there is a small slip at the base. b) Temperature is lower at the base because more energy is dissipated at the base than in the flow.

6.3.2 Energetic boundary

Figures (6.5) and (6.6) show a typical solution with an energetic boundary and the parameters $e = 0.92$, $e_w = 0.9486$, $\theta = 0.5712$, $\dot{m} = 32.14$ and $\phi = 0.2260$.

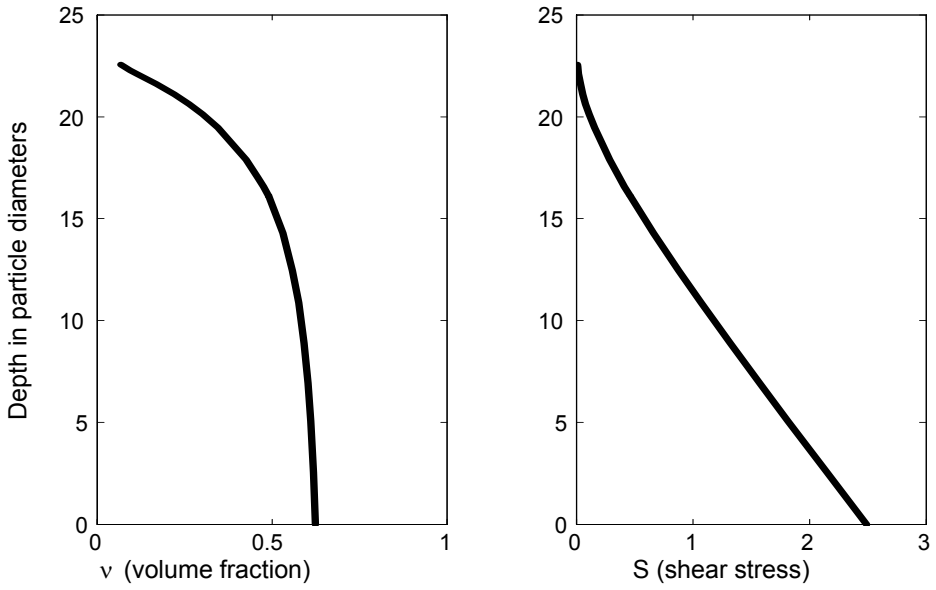

Figure 6.4: Dissipative boundary with parameters $e = 0.95$, $e_w = 0.80$, $\theta = 1.231$, $\dot{m} = 43.00$ and $\phi = 0.2170$. a) The volume fraction ν is not quite constant, but decreasing with height. At the base, $\nu \approx 0.63$, which is rather high compared to what is observed in experiments and simulations. b) The shear stress decreases almost linearly with the height.

6.3.3 Features of the solutions

For both of the boundary conditions, the volume fraction is found to be substantially larger ($\nu \approx 0.63$) than what is observed in experiments ($\nu \approx 0.59$). One explanation is that our radial distribution function (RDF) reaches its singularity at $\nu = 0.64$ and this RDF has been derived for frictionless hard-spheres in equilibrium. However, when frictional and deformable spherical particles are sheared, as in experiments and simulations, it is not clear whether our choice of RDF is applicable.

Given ϕ, we lower the flow height by gradually decreasing the mass flux rate. Though solutions with energetic boundaries exhibit constant density, which is one of the features

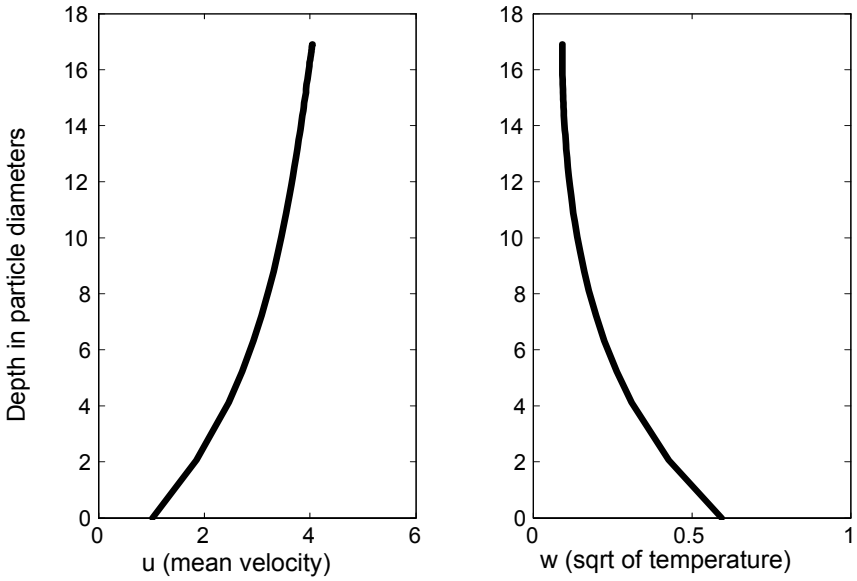

Figure 6.5: Energetic boundary with the parameters $e = 0.92$, $e_w = 0.9486$, $\theta = 0.5712$, $\dot{m} = 32.14$ and $\phi = 0.2260$. a) Mean velocity increases with height, in a non-linear way. Slip also exists at the base. b) Temperature is greater at the base, indicating that the boundary is providing agitation to the flow.

we are after, they fail to provide us with h_{stop}. That is, no matter how small the mass flux rate may be, the flow height continues to decrease to zero and it does not show any existence of h_{stop}.

On the other hand, the dissipative boundary solutions do show h_{stop}. One intuitive explanation for this boundary to have h_{stop} is that when the flow becomes too shallow, the boundary absorbs the fluctuation energy at a greater rate than at which fluctuation energy is generated by gravity among flow particles. Thus, energy can no longer be balanced and SFD flow can not exist when the flow becomes shallower than a certain limit.

Because we are interested in the end in recovering the scaling relation (6.1), we are in need of h_{stop} and thus discard energetic boundary condition for our analysis. Two-

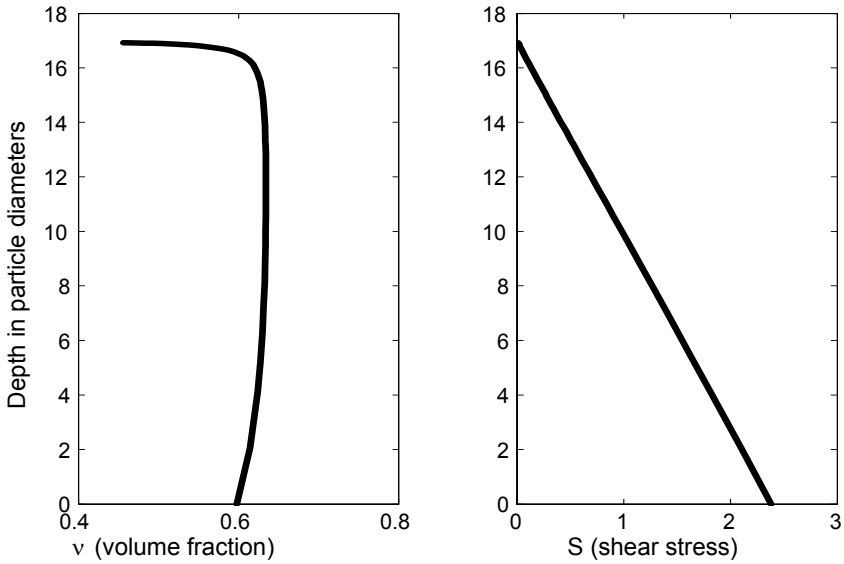

Figure 6.6: Energetic boundary with the parameters $e = 0.92$, $e_w = 0.9486$, $\theta = 0.5712$, $\dot{m} = 32.14$ and $\phi = 0.2260$. a) Volume fraction is rather constant around $\nu \approx 0.63$ throughout the height and decreases rapidly at the top. b) The shear stress decreases linearly.

dimensional inclined flow experiments performed by Berton *et al.*[11] seem to suggest that the temperature profile from the dissipative boundary condition agrees qualitatively with their measurements.

6.3.4 Scaling

For a dissipative boundary with parameters $e = 0.95,\ e_w = 0.80$ and $\theta = 1.2310$, we obtain the following h_{stop} curve:

With Figure (6.7), we try to see whether solutions from kinetic theory can reproduce the scaling relation by plotting h/h_{stop} on x-axis and $\langle u \rangle / \sqrt{h}$ on y-axis.

The solutions suggest that for given e and e_w, there is a finite range for ϕ outside of which no solutions exist.

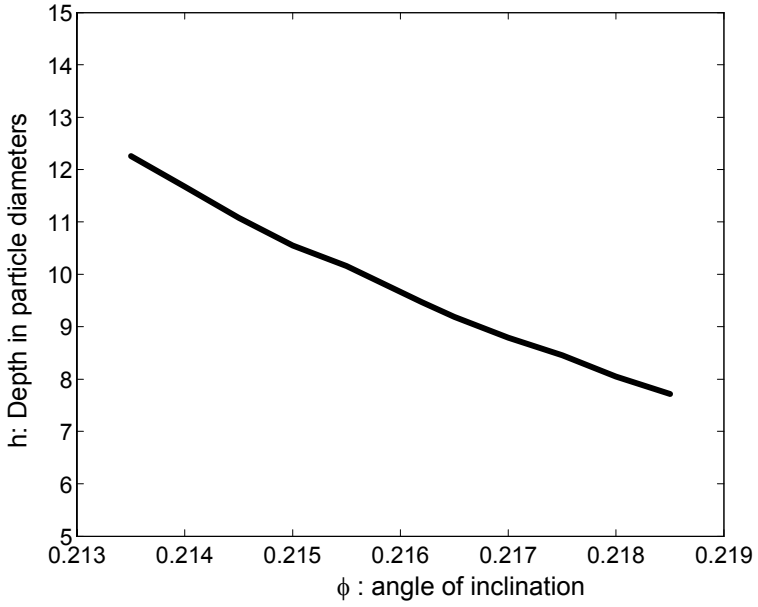

Figure 6.7: Dissipative BC with parameters $e = 0.95,\ e_w = 0.80$ and $\theta = 1.2310$. h_{stop} decreases with ϕ, as does in experiments. Below the curve, no SFD flow is possible. In experiments, as ϕ decreases to its lower bound, h_{stop} diverges, which is not seen in our solutions.

It is clear from Figure (6.8) that kinetic theory with dissipative boundary condition fails to satisfy the scaling relation of Pouliquen. And we saw earlier that energetic boundary condition does not provide us with h_{stop} which is needed for scaling.

There are a few questions that must be addressed at this point. First, is the kinetic theory not applicable to inclined flows (though the theory shows collisional flow exists on inclined planes) or is the boundary condition inappropriate? Second, is the scaling relation something of a coincidence (though seen in experiments and simulations)? Third, just because the theory does not predict the scaling relation, does it mean other predictions, such as velocity, temperature and density profiles, also are not reliable? Fourth, can we make a simple assumption to modify the theory in order to obtain the

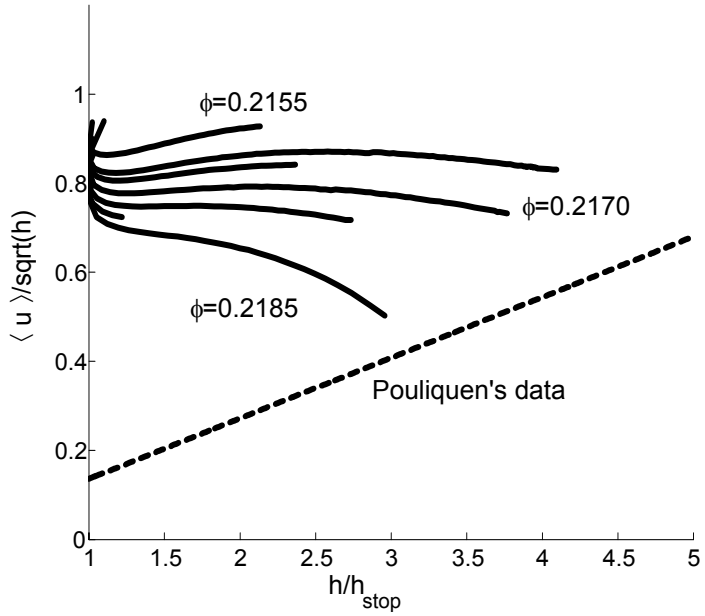

Figure 6.8: Solid lines are from kinetic theory and the dotted line is from Pouliquen's experiments. We see that not only solutions of kinetic theory do not collapse on one straight line, but $\langle u \rangle / \sqrt{gh}$ does not increase with h/h_{stop}.

scaling relation?

We try to answer the first and the last questions, at least in part, in the following section.

6.4 Simplifying the kinetic theory

As the governing equations are complicated functions of volume fraction ν and ν has been suggested to be constant in experiments and simulations, we can make the equations much more tractable by assuming ν is constant.

One immediate problem with this approach is that our expressions for pressure (non-dimensionalized)

$$p' = -\nu \cos\phi \text{ and } p = \nu T\left(1 + 4G\right)$$

tell us how T varies with the height, independent of the boundary condition. We can get around this problem by assuming that $\nu T\left(1 + 4G\right)$, which is provided from kinetic theory, is not total pressure, but some contribution from collisions and transport. The other contribution, which could be from enduring contact, may sum with this to give our hydrostatic pressure[48]. If that is the case, T would still remain undetermined and dependent on boundary conditions. But, we gloss over this fact and concentrate on the rest of the equations.

It turns out then the non-dimensionalized equations can scale out angle dependencies ϕ, from the rest of the equations. With the following scalings,

$$\begin{aligned} \hat{u} &= \frac{u}{\sqrt{\sin\phi}},\ \hat{w} = \frac{w}{\sqrt{\sin\phi}}, \\ \hat{S} &= \frac{S}{\sin\phi},\ \hat{q} = \frac{q}{\left(\sin\phi\right)^{3/2}} \end{aligned}$$

we have our governing equations

$$\begin{pmatrix} \hat{u} \\ \hat{w} \\ \hat{S} \\ \hat{q} \end{pmatrix}' = \begin{pmatrix} \frac{1}{A}\frac{\hat{S}}{\hat{w}} \\ -\frac{1}{B}\frac{\hat{q}}{\hat{w}^2} \\ -\nu \\ \frac{1}{A}\frac{\hat{S}^2}{\hat{w}} - C\hat{w}^3 \end{pmatrix}$$

where

$$\begin{aligned} A &= \frac{\sqrt{\pi}\nu}{6}\left[\frac{5}{16G} + 1 + \frac{4}{5}\left(1 + \frac{12}{\pi}\right)G\right], \\ B &= \frac{15\sqrt{\pi}\nu}{8}\left[\frac{5}{24G} + 1 + \frac{6}{5}\left(1 + \frac{32}{9\pi}\right)G\right] \end{aligned}$$

and $C = 24\,(1-e)\,\nu G/\sqrt{\pi}$ are constants in terms of ν and e. Thus, we have simplified the flow equations a great deal and analytic solutions are possible, if more assumptions are made.

6.4.1 Simple boundary condition

With the simplified set of equations, we impose a very simple boundary condition. At $z = 0$, $q = u = 0$. At $z = H$, $q = S = 0$.

This condition is not meant to represent the bumpy boundary condition that we have considered before, but a simple, yet physically plausible condition which we use to develop intuition about our equations.

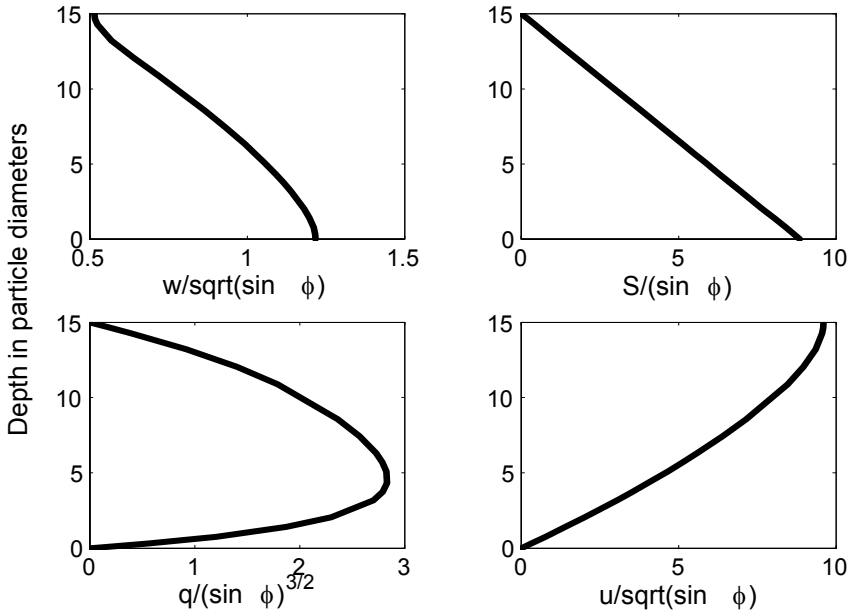

Figure 6.9: A typical solution for the equations with ν = constant, with the simple boundary condition.

The temperature profile shows that the boundary is energetic, from which we would not expect to see h_{stop}. And indeed, there is no h_{stop} for this solution; the flow exists

for any h. However, it is worth noting that when we plot $\langle u \rangle / \sqrt{h \sin \phi}$ (depth averaged velocity divided $\sqrt{\sin \phi}$) on y-axis and h on x-axis, we get a linear relation that is much like the one obtained in experiments.

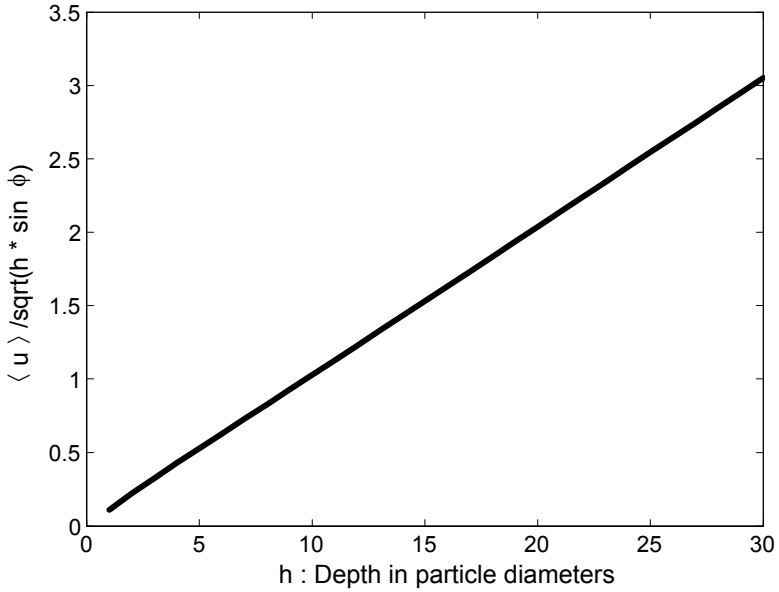

Figure 6.10: $\langle u \rangle / \sqrt{h \sin \phi} \propto h$ or $\langle u \rangle / \sqrt{h} \propto h \sqrt{\sin \phi}$ is obtained with the assumption $\nu =$ constant, whereas this scaling relation failed for the full set of equations.

6.5 Modification of the theory for particles in contact

Here, we briefly mention a different attempt in modifying the kinetic theory that incorporates the source of stresses, not just as a result of collisions, but also as a result of enduring contacts. Recently, Jenkins[34] proposed to introduce a new length scale to the existing kinetic theory and this length scale comes from the number of particles in contact that form a chain. Jenkins[34] argues that the length scale of particle diameter appearing in the expression for the dissipation rate of granular energy should be replaced by a new length scale, called chain length. This chain length, l, is modelled through a

phenomenological evolution equation, based on numerical simulations. In the case of simple shear for disks, l is described as

$$\frac{l}{d} = \frac{1}{2}\frac{d\dot{\gamma}}{T^{1/2}} c G^{1/2},$$

where d is the particle diameter, $\dot{\gamma}$ is the shear rate, T and ν are same quantities as before, but now constant, and c is an arbitrary value to be chosen, which can be estimated for typical values of e and ν. Figure 6.11 and 6.12 illustrate a sample solution for disks from the modified equation for $e = 0.75,\ e_w = 0.95,\ \theta = 0.5512,\ \dot{m} = 45$ and $\phi = 0.260$.

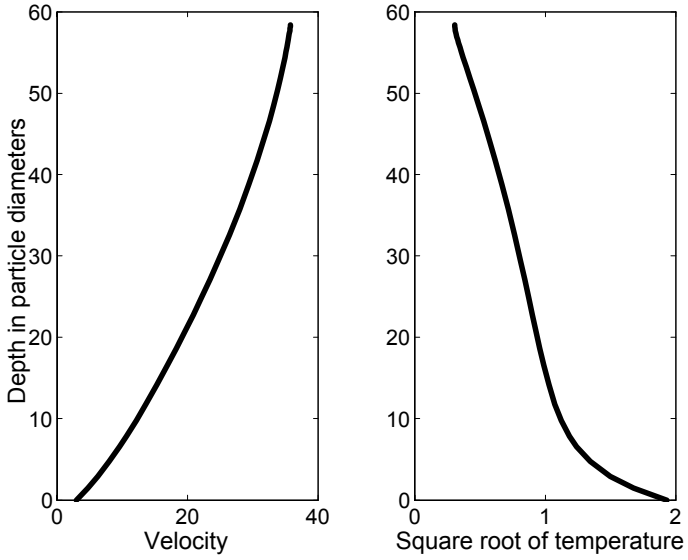

Figure 6.11: Prediction of the chain theory.

As one can see, there are several disadvantages of this approach. One is the unjustified introduction of this new length scale and it replaces an existing length scale only in the expression of the dissipation rate. Another disadvantage is the phenomenological model of l, which depend on two arbitrary parameters. Despite all these disadvantages, this approach deserves special attention because it does agree remarkably well with numerical simulations and captures all the features of an inclined flow, such as the constant

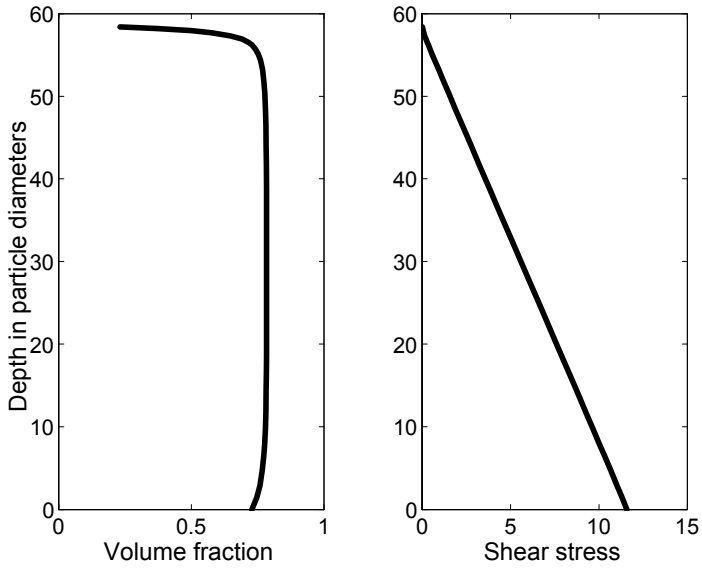

Figure 6.12: Prediction of the chain theory.

density and its dependency on the angle of inclination. When the chain length is taken to represent h_{stop}, this theory provides correct behavior of h_{stop} and the scaling relationship of Pouliquen gets also established, which no theory has been able to accomplish to this date. Those who are interested in this approach are encouraged to refer to the work[34] for more details.

6.6 Summary

We have applied kinetic theory to the situation of granular particles flowing down a bumpy inclined plane. The kinetic theory requires the particles to interact in collisional manner in order for its assumptions to hold. When theory together with bumpy boundary conditions is imposed, it not only predicts the existence of a collisional flow, but also the profiles of velocity, density, granular temperature and others. Depending on the choice of the restitution coefficients between flow particles (e) and between a flow

particle and a wall particle (e_w), the boundary either provides granular heat to the flow (energetic boundary) or takes away such heat (dissipative boundary).

The absence of h_{stop}, the minimum height below which steady fully developed flow is not possible for a given angle of inclination ϕ, for the solutions with energetic boundary shows this boundary to be inadequate in describing the flows seen in experiments and numerical simulations. On the other hand, the dissipative boundary condition does show h_{stop} and its temperature profile resembles more to what is seen in real situations. However, the solutions from this boundary condition do not show constant density through depth, unlike the solutions with energetic boundary. The h_{stop} curve from these solutions qualitatively agree with what is observed in experiments and simulations.

When the solutions from the dissipative boundary condition are tested to see whether the scaling relation suggested by Pouliquen is observed, they fail to scale and they are far from being linear as in experiments and simulations. This suggests that, even though kinetic theory predicts a collisional flow on inclined planes, the theory is inadequate when dealing with inclined flows which tend to be very dense and not as collisional as the theory assumes it to be.

However, when a modification is made to the theory, that is the volume fraction or the density is constant, the theory does show a scaling behavior very similar to that observed by Pouliquen. The boundary conditions employed for these solutions are simple, yet physically plausible. Unfortunately, h_{stop} does not exist for this set of equations. Fortunately, a different modification using a new length scale of chains provides a theory that is consistent with simulations and experiments, though at the cost of rigor.

The failure of the full kinetic theory with bumpy boundary conditions and the somewhat successful results from the modified kinetic theory of chains give us some hope that kinetic theory has still much relevant to say with regard to inclined flows.

Chapter 7

CONCLUSION

We started the study on segregation, using a simple approach based on the theory of dense Maxwellian. We used the difference in mean velocities of species as an indicator of segregation in an idealized case of a binary mixture. By considering the effect of the deviation of species temperatures, we were able to see how the prediction on segregation changed as a result of this; for reasonably high values of e and small differences in sizes and masses, there was little change from the case with equipartition of energies. From then on, with the assumption of equipartition, along with a few other simplifying assumptions, we derived a simple segregation criterion based on sizes and material densities. For disks with representative area fraction, $\nu = 3/4$[41], we have Figure 7.1.

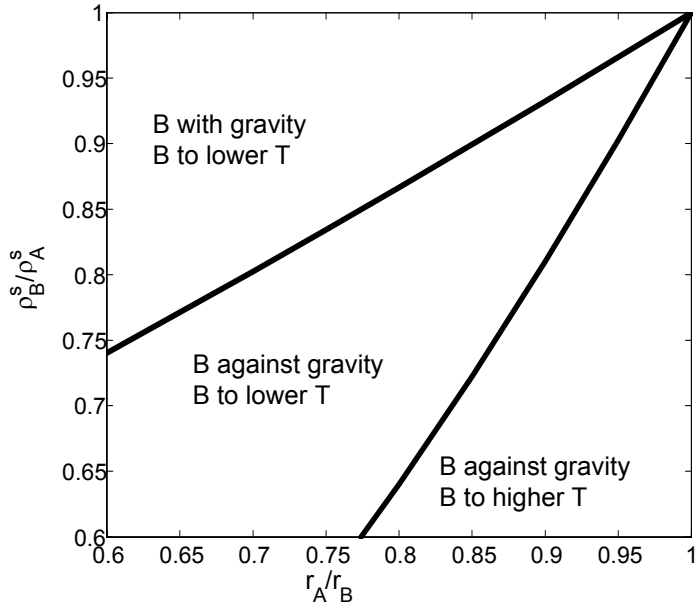

Figure 7.1: Segregation criterion for disks.

Then, we improved the collision model by introducing friction into the theory for

disks. With the friction model that differentiates sticking and sliding collisions, we derived balance equations for linear and angular momentums and translational and rotational fluctuation energies. Assuming that the flow in consideration is in a steady homogeneous shearing state, we acquired an approximate solution for the ratio for translational and rotational temperatures. With this quantity, we were able to absorb rotational motion into translational motion with an effective coefficient of normal restitution.

A more refined version of kinetic theory for disks was introduced for a mixture whose sizes and masses differ little. In this limit, we were able to obtain rather simple expressions for transport coefficients which we used to explicitly solve a boundary value problem of a mixture sheared between two bumpy circular walls. As opposed to the idealized case of segregation in the first problem, this approach allows experimenters to quantitatively compare their findings with our predictions, because the boundary value problem was posed in such a way that it shows all the details of the particles and the boundaries.

When we made explicit comparisons of the theory based on dense Maxwellian with Revised Enskog Theory, we found some notable differences; in the absence of the temperature gradient, both theories agreed very well. However, in the presence of the temperature gradient, with gravity absent, the difference was significant at lower volume fractions. This led to the conclusion that, though the theory on dense Maxwellian is more straightforward and simpler, Revised Enskog Theory should be used when dealing with flows having a high temperature gradient.

In the final chapter, we pushed kinetic theory to the limit by looking at steady fully developed flows on an inclined plane, whose high density made basic assumptions of the kinetic theory invalid. We tried to reproduce three characteristic features of inclined flows, found in physical experiments and numerical simulations. These are the constant

density profile, the existence of a minimum height below which no steady fully developed flows exist and the scaling relation that relates depth averaged velocity, height and this minimum height. After many trials, we came to the conclusion that the kinetic theory, as it stands, is not able to capture these features of inclined flows. Thus, we turned to modify the theory in the hope of salvaging the core of the theory with as few additional assumptions as possible. We briefly mentioned the most promising approach so far, that is the chain theory, and provided a sample solution with this modification.

Here, we conclude our study by looking segregation on an inclined plane using Revised Enskog Theory in conjunction with the output of the chain theory. That is, using the temperature found from the chain theory as the mixture temperature in Revised Enskog Theory and similarly area fraction as mixed area fraction, we solve for the densities of each species. Figure 7.2 is a sample solution, using Figure 6.11 and 6.12, for a mixture of disks with $r_A/r_B = 0.7$, $\rho_B^s/\rho_A^s = 0.6$ with the equal average area fractions of A and B. For this sample, we clearly see that in the final segregated state, bigger particles move to the top and smaller particles to the bottom.

By solving for densities for many different values of r_A/r_B and ρ_B^s/ρ_A^s, we construct Figure 7.3. Open circles represent the set of parameters with which bigger particles are found near the top, dots for parameters where numerical solutions didn't exist and blanks for parameters where the mixture does not clearly separate. Simple approach, as shown in Figure 7.1, based on Maxwellian theory with the temperature profile provided by the chain theory, has little to say about segregation on Region 1 and Region 3. However, it predicts that bigger particles would rise in Region 2, in agreement with the numerical solutions.

This one example does not prove the "correctness" of our simple approach, introduced in the first Chapter. However, it provides a strong support for this criterion of

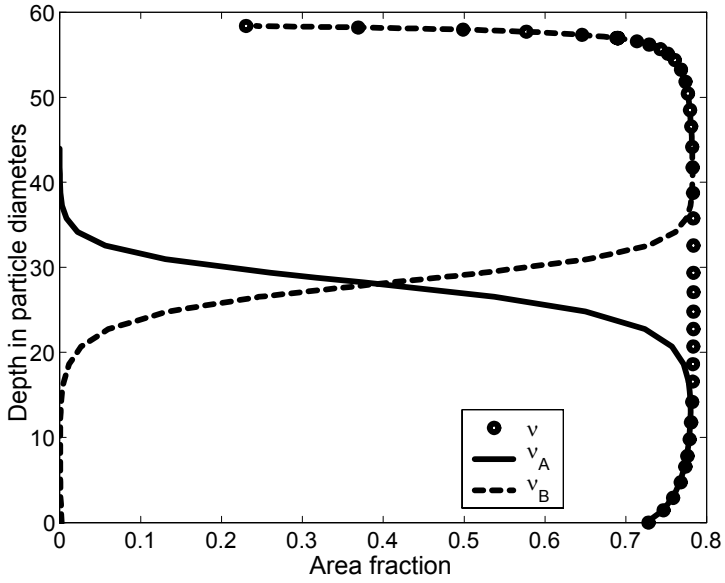

Figure 7.2: Density profile using Revised Enskog Theory.

this simple analysis. It is important to emphasize the differences between these two approaches. One is based on an idealized mixture where a few big particles are dilute in a dense background of smaller particles. By looking at the mean motion of bigger particles with respect to the smaller ones, we obtained this criterion using the kinetic theory based on dense Maxwellian. Only with information on gravity and the qualitative nature of the mixture temperature, the criterion indicates in what direction segregation occurs for a mixture of certain sizes and material densities. On the other hand, the second approach looks at the steady fully developed configuration of the mixture. By numerically solving Revised Enskog Theory, which involves a perturbation from Maxwellian distribution and non-local radial distribution functions and which is more refined than the dense Maxwellian theory, we were able to construct a diagram that shows what the final segregated density profiles are look like for a given set of mixture. It is somewhat assuring to see these two different approaches in agreement.

Overall, the advantage of the segregation criterion based on the simple approach is its

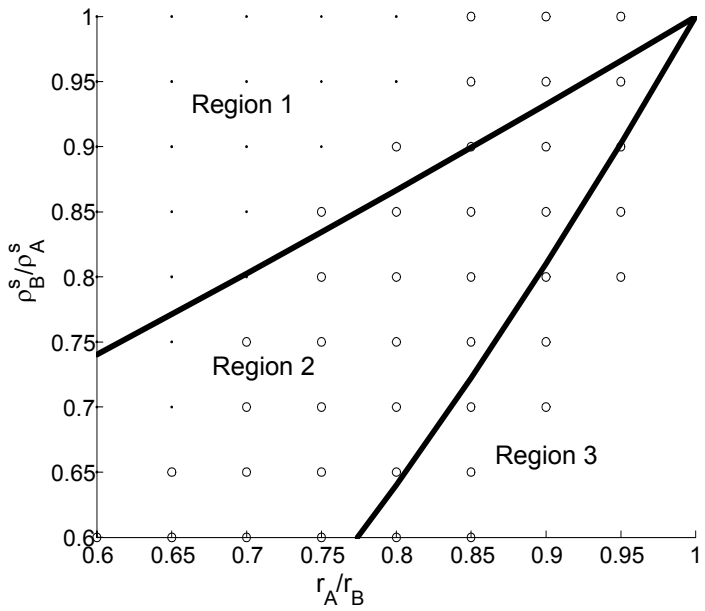

Figure 7.3: Comparison between the simple analysis using dense Maxwellian and the full solutions using Revised Enskog Theory.

simplicity. Its disadvantage is the idealization; that is, though this is a good toy model for theorists, it remains elusive to experimentalists who wish to test the predictions. To meet these needs, it is necessary to solve boundary value problems for a specific geometry, as we have shown, with details on the nature of flow particles and boundary conditions, with friction reconciled in the context of kinetic theory in a simple way.

Appendix A

CALCULATION OF DISSIPATION

A.1 Translational dissipation

A.1.1 Sliding collision

Because $\mathbf{g}\cdot\mathbf{k} = G\cos\Phi$ and $\mathbf{g}\cdot\mathbf{j} = -G\sin\Phi + \sigma s$ from (3.2) and Figure 3.1, we have

$$\begin{aligned}\Delta\frac{1}{2}mC^2 &= -\frac{1}{2}m\hat{e}\,(1-e)\,(\mathbf{g}\cdot\mathbf{k})^2 \\ &\quad + m\mu\hat{e}\,(\mathbf{g}\cdot\mathbf{k})\,(\mathbf{g}\cdot\mathbf{j}) + m\mu^2\hat{e}^2\,(\mathbf{g}\cdot\mathbf{k})^2 \\ &= -\frac{1}{2}m\hat{e}\,(1-e)\,(G\cos\Phi)^2 \\ &\quad + m\mu\hat{e}\,(G\cos\Phi)\,(-G\sin\Phi+\sigma s) \\ &\quad + m\mu^2\hat{e}^2\,(G\cos\Phi)^2\,. \end{aligned} \tag{A.1}$$

A.1.2 Sticking collision

Similarly,

$$\begin{aligned}\Delta\frac{1}{2}mC^2 &= -\frac{1}{2}m\hat{e}\,(1-e)\,(\mathbf{g}\cdot\mathbf{k})^2 \\ &\quad - m\frac{1+\beta_0}{2\,(1+\alpha/4)}\,(\mathbf{G}\cdot\mathbf{j})\,(\mathbf{g}\cdot\mathbf{j}) \\ &\quad + m\left[\frac{1+\beta_0}{2\,(1+\alpha/4)}\right]^2(\mathbf{G}\cdot\mathbf{j})^2 \\ &= -\frac{1}{2}m\hat{e}\,(1-e)\,(G\cos\Phi)^2 \\ &\quad - m\frac{1+\beta_0}{2\,(1+\alpha/4)}\,(-G\sin\Phi)\,(-G\sin\Phi+\sigma s) \\ &\quad + m\left[\frac{1+\beta_0}{2\,(1+\alpha/4)}\right]^2(-G\sin\Phi)^2\,. \end{aligned} \tag{A.2}$$

A.2 Rotational dissipation

A.2.1 Sliding collision

With $(\mathbf{k}\times\mathbf{j})\cdot\mathbf{s}=-s$, we have

$$\begin{aligned}\Delta\frac{1}{2}I\Omega^2 &= m\mu\hat{e}\sigma\left(\mathbf{g}\cdot\mathbf{k}\right)\left(\mathbf{k}\times\mathbf{j}\right)\cdot\mathbf{s}+\frac{\alpha}{4}m\mu^2\hat{e}^2\left(\mathbf{g}\cdot\mathbf{k}\right)^2\\ &= -m\mu\hat{e}\sigma\left(G\cos\Phi\right)s+\frac{\alpha}{4}m\mu^2\hat{e}^2\left(G\cos\Phi\right)^2.\end{aligned}\tag{A.3}$$

A.2.2 Sticking collision

Because $|\mathbf{k}\times\mathbf{G}|=G\sin\Phi$ from Figure 3.1, we have

$$\begin{aligned}\Delta\frac{1}{2}I\Omega^2 &= m\frac{1+\beta_0}{2\left(1+\alpha/4\right)}\sigma\left|\mathbf{k}\times\mathbf{G}\right|\left(\mathbf{k}\times\mathbf{j}\right)\cdot\mathbf{s}\\ &\quad+\frac{\alpha}{4}m\left[\frac{1+\beta_0}{2\left(1+\alpha/4\right)}\right]^2\left(\mathbf{k}\times\mathbf{G}\right)^2\\ &= -m\frac{1+\beta_0}{2\left(1+\alpha/4\right)}\sigma Gs\sin\Phi\\ &\quad+\frac{\alpha}{4}m\left[\frac{1+\beta_0}{2\left(1+\alpha/4\right)}\right]^2\left(G\sin\Phi\right)^2.\end{aligned}\tag{A.4}$$

A.3 Velocity integration

From the definition of $\chi\left[\phi\right]$ in (3.6), we have

$$\begin{aligned}&\chi\left[\phi\right]\left[\frac{n^2g_0\sigma}{\left(2\pi T\right)^2 2\pi\Theta}\right]^{-1}\\ &=\int_0^{\pi/2}\int_c\int_\omega\Delta\phi G\cos\Phi\exp\left[-\frac{1}{2}\left(\frac{C_1^2}{T}+\frac{C_2^2}{T}\right)\right]\\ &\times\exp\left[-\frac{I}{2m}\left(\frac{\Omega_1^2}{\Theta}+\frac{\Omega_2^2}{\Theta}\right)\right]d\mathbf{c}_1d\mathbf{c}_2d\boldsymbol{\omega}_1d\boldsymbol{\omega}_2d\Phi\\ &\equiv\int_0^{\pi/2}Zd\Phi,\end{aligned}\tag{A.5}$$

where

$$Z = \cos\Phi \int_c \int_\omega \Delta\phi G \exp\left[-\frac{1}{2}\left(\frac{C_1^2}{T} + \frac{C_2^2}{T}\right)\right] \times \exp\left[-\frac{I}{2m}\left(\frac{\Omega_1^2}{\Theta} + \frac{\Omega_2^2}{\Theta}\right)\right] d\mathbf{c}_1 d\mathbf{c}_2 d\boldsymbol{\omega}_1 d\boldsymbol{\omega}_2.$$

Note that $\Delta\phi$ depends on either G^2 or Gs. Because the distinction between Ω_i and ω_i is first order in the velocity gradient, to the order of the approximation, we can take $\Omega_i = \omega_i$ in the distribution function.

To evaluate Z, we make a change of variables:

$$\mathbf{C}_1 = (\mathbf{v} + \mathbf{V})/\sqrt{2},\ \mathbf{C}_2 = (\mathbf{V} - \mathbf{v})/\sqrt{2}$$

$$\omega_1 = (p + P)/\sqrt{2},\ \omega_2 = (p - P)/\sqrt{2},$$

which has the Jacobian $J = 1$. This gives

$$Z = K\cos\Phi \int_{\mathbf{v}} \int_p \Delta\phi G \times \exp\left(-\frac{1}{2}\frac{1}{T}v^2\right) \exp\left(-\frac{I}{2m}\frac{p^2}{\Theta}\right) dp d\mathbf{v},$$

where

$$K{=}2\pi T\sqrt{2\pi\frac{m\Theta}{I}}.$$

Note that $s = p/\sqrt{2}$ and $\mathbf{G} = \sqrt{2}\,(\mathbf{v} - p\sigma\mathbf{j}/2)$. Thus, the dependence of $\Delta\phi$ on G and s implies dependence on p and v, but not on P and V.

Now, we introduce another simple change of variable

$$\mathbf{U} = \mathbf{v} - p\frac{\sigma}{2}\mathbf{j}.$$

This gives us

$$\begin{aligned} Z = K\cos\Phi \int_{\mathbf{U}}\int_{p} \Delta\phi\sqrt{2}U \\ \times \exp\left[-\frac{1}{2}\frac{1}{T}\left(U^2 - \sigma pU\sin\Phi + \frac{\sigma^2}{4}p^2\right)\right] \\ \times \exp\left(-\frac{I}{2m}\frac{1}{\Theta}p^2\right) dpd\mathbf{U}. \end{aligned}$$

We can replace $\Delta\phi$ with $G^2$and Gs and thus separate Z into two parts, Ψ_1 and Ψ_2 :

$$\begin{aligned} \Psi_1 \equiv K\cos\Phi \int_{\mathbf{U}}\int_{p} G^2\sqrt{2}U \\ \times \exp\left[-\frac{1}{2}\frac{1}{T}\left(U^2 - \sigma pU\sin\Phi + \frac{\sigma^2}{4}p^2\right)\right] \\ \times \exp\left(-\frac{I}{2m}\frac{1}{\Theta}p^2\right) dpd\mathbf{U} \\ = 3\sqrt{2}K\cos\Phi\pi^2 \frac{16c^2}{\left[4ac - (b\sin\Phi)^2\right]^{5/2}}, \end{aligned}$$

and

$$\begin{aligned} \Psi_2 \equiv K\cos\Phi \int_{\mathbf{U}}\int_{p} Gs\sqrt{2}U \\ \times \exp\left[-\frac{1}{2}\frac{1}{T}\left(U^2 - \sigma pU\sin\Phi + \frac{\sigma^2}{4}p^2\right)\right] \\ \times \exp\left(-\frac{I}{2m}\frac{1}{\Theta}p^2\right) dpd\mathbf{U} \\ = \sqrt{2}K\sin\Phi\cos\Phi\pi^2 \frac{12bc}{\left[4ac - (b\sin\Phi)^2\right]^{5/2}}, \end{aligned}$$

where

$$a \equiv \frac{1}{2T},\ b \equiv \frac{\sigma}{2T},\ c \equiv \frac{I}{2m}\frac{1}{\Theta} + \frac{1}{2}\frac{1}{T}\frac{\sigma^2}{4}.$$

Thus, with $R = T/\Theta$ and $I = m\sigma^2/\alpha$, we can rewrite Ψ_1 and Ψ_2:

$$\begin{aligned} \frac{\Psi_1}{T^3} = \frac{48\sqrt{2}K\cos\Phi\pi^2}{\sigma}\left(\frac{R}{\alpha} + \frac{1}{4}\cos^2\Phi\right)^{-5/2} \\ \times \left(\frac{R}{2\alpha} + \frac{1}{8}\right)^2 \end{aligned}$$

and

$$\frac{\Psi_2}{T^3} = \frac{6\sqrt{2}K\sin\Phi\cos\Phi\pi^2}{\sigma^2}\left(\frac{R}{\alpha}+\frac{1}{4}\cos^2\Phi\right)^{-5/2} \times\left(\frac{R}{2\alpha}+\frac{1}{8}\right).$$

A.4 Dissipation: final expressions

Recall that $\Gamma = -\chi\left[I\Omega^2/2\right]$ and $\gamma = -\chi\left[mC^2/2\right]$. With our knowledge of Ψ_1 and Ψ_2 and (A.1)-(A.4) and (A.5), we can find explicit expressions for the rates of dissipation by evaluating the following integrals. The rotational and the translational rates of dissipation can be found, respectively, from

$$\begin{aligned}
&\chi\left[\frac{1}{2}I\Omega^2\right]\left[\frac{mn^2g_0\sigma}{(2\pi T)^2\,2\pi\Theta}\right]^{-1}\\
&=\int_0^{\Phi^*}\left[-\Psi_2\frac{1+\beta_0}{2\,(1+\alpha/4)}\sigma\sin\Phi\right.\\
&\left.+\Psi_1\frac{\alpha}{4}\frac{(1+\beta_0)^2}{4\,(1+\alpha/4)^2}\sin^2\Phi\right]d\Phi\\
&+\int_{\Phi^*}^{\pi/2}\left(-\Psi_2\mu\hat{e}\sigma\cos\Phi+\Psi_1\frac{\alpha}{4}\mu^2\hat{e}^2\cos^2\Phi\right)d\Phi
\end{aligned}\tag{A.6}$$

and

$$\chi\left[\frac{1}{2}mC^2\right]\left[\frac{mn^2g_0\sigma}{(2\pi T)^2\,2\pi\Theta}\right]^{-1}$$
$$=\int_0^{\Phi^*}\left\{\Psi_1\left[-\frac{1}{2}\hat{e}\,(1-e)\cos^2\Phi-\frac{1+\beta_0}{2\,(1+\alpha/4)}\sin^2\Phi\right.\right.$$
$$\left.\left.+\frac{(1+\beta_0)^2}{4\,(1+\alpha/4)^2}\sin^2\Phi\right]+\Psi_2\frac{1+\beta_0}{2\,(1+\alpha/4)}\sigma\sin\Phi\right\}d\Phi$$
$$+\int_{\Phi^*}^{\pi/2}\left\{\Psi_1\left[-\frac{1}{2}\hat{e}\,(1-e)\cos^2\Phi-\mu\hat{e}\cos\Phi\sin\Phi\right.\right.$$
$$\left.\left.+\mu^2\hat{e}^2\cos^2\Phi\right]+\Psi_2\mu\hat{e}\sigma\cos\Phi\right\}d\Phi. \qquad \text{(A.7)}$$

The integrations from 0 to Φ^* are for sticking collisions and the integrations from Φ^* to $\pi/2$ are for sliding collisions.

A.5 Rotational dissipation

From (3.4), we can replace $(1+\beta_0)\,/\,[2\,(1+\alpha/4)]$ with $\mu\hat{e}/\mu_0$. When (A.6) is fully written out, we have, with $\hat{R}=8R/\alpha$,

$$\begin{aligned}
&\chi\left[\frac{1}{2}I\Omega^2\right]\left[\frac{mn^2g_0}{(2\pi T)^2\,2\pi\Theta}\right]^{-1}\frac{1}{3\sqrt{2}T^3K\pi^2}\frac{16}{\hat{R}+2}\\
&=-2\frac{\mu\hat{e}}{\mu_0}\int_0^{\Phi^*}\frac{\cos\Phi\sin^2\Phi}{\left(\hat{R}/8+\cos^2\Phi/4\right)^{5/2}}d\Phi\\
&+\frac{\alpha}{4}\left(\hat{R}+2\right)\left(\frac{\mu\hat{e}}{\mu_0}\right)^2\int_0^{\Phi^*}\frac{\cos\Phi\sin^2\Phi}{\left(\hat{R}/8+\cos^2\Phi/4\right)^{5/2}}d\Phi\\
&-2\mu\hat{e}\int_{\Phi^*}^{\pi/2}\frac{\cos^2\Phi\sin\Phi}{\left(\hat{R}/8+\cos^2\Phi/4\right)^{5/2}}d\Phi\\
&+\frac{\alpha}{4}\left(\hat{R}+2\right)\mu^2\hat{e}^2\int_{\Phi^*}^{\pi/2}\frac{\cos^3\Phi}{\left(\hat{R}/8+\cos^2\Phi/4\right)^{5/2}}d\Phi.
\end{aligned}$$

This integral can be found using the integral table in Appendix B. The final expression is (3.9).

A.6 Translational dissipation

When (A.7) is fully written out, we have,

$$
\begin{aligned}
&\chi\left[\frac{1}{2}mC^2\right]\left[\frac{mn^2g_0}{(2\pi T)^2\,2\pi\Theta}\right]^{-1}\frac{16}{3T^3K\sqrt{2}\pi^2\left(\hat{R}+2\right)}\\
&=-\left(\hat{R}+2\right)\frac{1}{2}\hat{e}\,(1-e)\int_0^{\Phi^*}\frac{\cos^3\Phi}{\left(\hat{R}/8+\cos^2\Phi/4\right)^{5/2}}d\Phi\\
&+\left(\hat{R}+2\right)\left[-\frac{\mu\hat{e}}{\mu_0}+\left(\frac{\mu\hat{e}}{\mu_0}\right)^2\right]\\
&\times\int_0^{\Phi^*}\frac{\cos\Phi\sin^2\Phi}{\left(\hat{R}/8+\cos^2\Phi/4\right)^{5/2}}d\Phi\\
&+2\frac{\mu\hat{e}}{\mu_0}\int_0^{\Phi^*}\frac{\cos\Phi\sin^2\Phi}{\left(\hat{R}/8+\cos^2\Phi/4\right)^{5/2}}d\Phi\\
&+\left(\hat{R}+2\right)\left[-\frac{1}{2}\hat{e}\,(1-e)+\mu^2\hat{e}^2\right]\\
&\times\int_{\Phi^*}^{\pi/2}\frac{\cos^3\Phi}{\left(\hat{R}/8+\cos^2\Phi/4\right)^{5/2}}d\Phi\\
&-\left(\hat{R}+2\right)\mu\hat{e}\int_{\Phi^*}^{\pi/2}\frac{\cos^2\Phi\sin\Phi}{\left(\hat{R}/8+\cos^2\Phi/4\right)^{5/2}}d\Phi\\
&+2\mu\hat{e}\int_{\Phi^*}^{\pi/2}\frac{\cos^2\Phi\sin\Phi}{\left(\hat{R}/8+\cos^2\Phi/4\right)^{5/2}}d\Phi.
\end{aligned}
$$

The integral can be evaluated with the table in Appendix B and we find the answer to be (3.10).

Appendix B

INTEGRATION TABLE

$$\int_{-\infty}^{\infty} e^{2bx-ax^2}dx = \sqrt{\frac{\pi}{a}}e^{b^2/a}.$$
$$\int_{-\infty}^{\infty} xe^{-a(x-b)^2}dx = b\sqrt{\frac{\pi}{a}}.$$
$$\int_{0}^{\infty} x^4e^{-ax^2}dx = \frac{3}{8a^2}\sqrt{\frac{\pi}{a}}.$$

The following integrals can be evaluated with a simple change of variable.

1.

$$\int \frac{\cos^3\Phi}{\left(R/8+\cos^2\Phi/4\right)^{5/2}}d\Phi$$
$$= \int \frac{\cos\Phi}{\left(R/8+\cos^2\Phi/4\right)^{5/2}}d\Phi - \int \frac{\sin^2\Phi\cos\Phi}{\left(R/8+\cos^2\Phi/4\right)^{5/2}}d\Phi$$
$$= \int \frac{1}{\left(R/8+\left(1-u^2\right)/4\right)^{5/2}}du - \int \frac{u^2}{\left(R/8+\left(1-u^2\right)/4\right)^{5/2}}du$$

where $u = \sin\Phi$

$$= \frac{64}{3}\frac{1}{\left(R+2\right)\left(R+2\cos^2\Phi\right)\sqrt{R/8+\cos^2\Phi/4}}$$
$$\times\left(\frac{3R-4\sin^2\Phi+6}{R+2}\sin\Phi-\sin^3\Phi\right).$$

2.

$$\int \frac{\cos\Phi\sin^2\Phi}{\left(R/8+\cos^2\Phi/4\right)^{5/2}}d\Phi$$
$$= \int \frac{u^2}{\left[R/8+\left(1-u^2\right)/4\right]^{5/2}}du$$

where $u = \sin\Phi$

$$= \frac{64}{3}\frac{\sin^3\Phi}{\left(R+2\right)\left(R+2\cos^2\Phi\right)\sqrt{R/8+\cos^2\Phi/4}}.$$

3.

$$\begin{aligned}
&\int \frac{\cos^2\Phi \sin\Phi}{\left(R/8+\cos^2\Phi/4\right)^{5/2}} d\Phi \\
&= -\int \frac{u^2}{\left(R/8+u^2/4\right)^{5/2}} du
\end{aligned}$$

where $u = \cos\Phi$

$$= -\frac{64}{3} \frac{\cos^3\Phi}{R\left(R+2\cos^2\Phi\right)\sqrt{R/8+\cos^2\Phi/4}}.$$

BIBLIOGRAPHY

[1] Alam, M., Willits, J. T., Arnarson, B. Ö., and Luding, S. 2002. Kinetic theory of a binary mixture of nearly elastic disks with size and mass disparity. Phys. Fluids **14**, 4085.

[2] Alam, M., and Luding, S. 2002. How good is the equipartition assumption for the transport properties of a granular mixture? Gran. Matter **4**, 139.

[3] Alam,M., and Luding, S. 2003 Rheology of bidisperse granular mixtures via event-driven simulations, J. Fluid Mech. **476**, 69.

[4] Ancey, C. 2001. Dry granular flows down an inclined channel: Experimental investigations on the frictional-collisional regime. Phys. Rev. E 65, 011304.

[5] Anderson, K. G., and Jackson, R. 1992. A comparison of the solutions of some proposed equations of motion of granular materials for fully developed flow down inclined planes. J. Fluid Mech. 241, 145.

[6] Arnarson, B. Ö., and Jenkins, J. T. 2004. Binary mixtures of inelastic spheres: simplified constitutive theory. Phys. Fluids **16**, 4543.

[7] Arnarson, B. Ö., and Willits, J. T. 1998. Thermal diffusion in binary mixtures of smooth, nearly elastic spheres. Phys. Fluids **10**, 1324.

[8] Bagnold, R. A. 1954. Experiments on a gravity-free dispersion of large solid particles in a Newtonian fluid under shear. Proc. R. Soc. London Ser. A **225**, 49.

[9] Barajas, L., Garcia-Colin, L.S. and Pina, E. 1973. On the Enskog-Thorne theory for a binary mixture of dissimilar rigid spheres. J. Stat. Phys. **7**, 161.

[10] Barrat, A., and Trizac, E. 2002. Lack of energy equipartition in homogeneous heated binary granular mixtures. Gran. Matter **4**, 57.

[11] Berton, G., Delannay, R., Richard, P., Taberlet, N., and Valance, A. 2003. Two-dimensional inclined chute flows: Transverse motion and segregation. Phys. Rev. E **68**, 051303.

[12] Breu, A. P. J., Ensner, H. M., Kruelle, C. A., and Rehberg, I. 2003. Reversing the Brazil-nut effect: Competition between Percolation and Condensation. Phys. Rev. Lett. **90**, 014302.

[13] Campbell, C. S. 1990. Rapid granular flows. Annu. Rev. Fluid Mech. **22**, 57.

[14] Carnahan, N. H., and Starling, K. E. 1969. Equation of state of non-attracting rigid spheres. J. Chem. Phys. **51** 635.

[15] Chapman, S., and Cowling, T. G. 1970. The mathematical theory of non-uniform gases: an account of the kinetic theory of viscosity, thermal conduction and diffusion in gases. Cambridge University Press, Cambridge.

[16] Chou, C. S., and Richman, M. W. 1998. Constitutive theory for homogeneous granular shear flows of highly inelastic spheres. Physica A **259**, 430.

[17] Clelland, R., and Hrenya, C. M. 2002. Simulations of a binary-sized mixture of inelastic grains in rapid shear flow. Phys. Rev. E **65**, 031301.

[18] Craig, K., Buckholz, R. H., and Domoto, G. 1986. An experimental study of the rapid flow of dry cohesionless metal powders. J. Appl. Mech. **53**, 935.

[19] Dahl, S. R., Clelland, R., and Hrenya, C. M. 2002. The Effects of Continuous Size Distributions on the Rapid Flow of Inelastic Particles. Phys. Fluids **14**, 1972.

[20] Drake, T. G. 1991. Granular flow: physical experiments and their implications for microstructural theories. J. Fluid Mech. **225**, 121.

[21] Feitosa, K., and Menon, N. 2002. Breakdown of Energy Equipartition in a 2D Binary Vibrated Granular Gas. Phys. Rev. Lett. **88**, 198301.

[22] Ferziger, J. H., and Kaper, H. G. 1972. *Mathematical Theory of Transport Processes in Gases.* North-Holland, New York.

[23] Goldhirsch, I. 2003. Rapid granular flows. Annu. Rev. Fluid Mech. **35**, 267.

[24] Foerster, S. F., Louge, M. Y., Chang, H., and Allia, K. 1994. Measurements of the collision properties of small spheres. Phys. Fluids **6**, 1108.

[25] Galvin, J. E., Dahl, S. R., and Hrenya, C. M. 2005. On the role of non-equipartition in the dynamics of rapidly flowing granular mixtures, J. Fluid Mech. **528**, 207.

[26] Hanes, D. M., and Inman, D. L. 1985. Observations of rapidly flowing granular-fluid materials. J. Fluid Mech. **150**, 357.

[27] Hanes, D. M., and Walton, O. R. 2000. Simulations and physical measurements of glass spheres flowing down a bumpy incline. Power Technol. **109**, 133.

[28] Herbst, O., Huthmann, M., and Zippelius, A. 2000. Dynamics of inelastically colliding spheres with Coulomb friction: Relaxation of translational and rotational energy. Gran. Matter **2**, 211.

[29] Hirschfelder, J. O., Curtiss, C. F. , Bird, R. B. 1954. *Molecular theory of gases and liquids.* John Wiley, New York.

[30] Hong, D. C., Quinn, P. V., and Luding, S. 2001. Reverse Brazil Nut Problem: Competition between Percolation and Condensation. Phys. Rev. Lett. **86**, 3423.

[31] Jaeger, H. M., Nagel, S. R., and Behringer, R. P. 1996. Granular solids, liquids and gases. Rev. Mod. Phys. **68**, 1259.

[32] Jenkins, J. T. 1998. Particle segregation in collisional flows of inelastic spheres, in *Physics of Dry Granular Media*, p. 645, Kluwer Academic, Dordrecht.

[33] Jenkins, J. T. 1998. Kinetic theory for nearly elastic spheres, in *Physics of Dry Granular Media*, p. 353, Kluwer Academic, Dordrecht.

[34] Jenkins, J. T. 2006. Dense shearing flows of inelastic disks. In preparation.

[35] Jenkins, J. T., and Hanes, D. M. 1993. The balance of momentum and energy at an interface between colliding and freely flying grains in a rapid granular flow. Phys. Fluids A: Fluid Dynamics **5**, 781.

[36] Jenkins, J. T., and Mancini, F. 1987. Balance laws and constitutive relations for plane flows of a dense, binary mixture of smooth nearly, elastic, circular disks. J. Appl. Mech. **54**, 27.

[37] Jenkins, J. T., and Mancini, F. 1989. Kinetic theory for binary mixtures of smooth, nearly elastic spheres. Phys. Fluids A **1**, 2050.

[38] Jenkins, J. T., and Richman, M. W. 1985. Grad's 13-moment system for a dense gas of inelastic spheres. Arch. Rat. Mech. Anal. **87**, 355.

[39] Jenkins, J. T., and Richman, M. W. 1985. Kinetic theory for plane flows of a dense gas of identical, rough, inelastic, circular disks. Phys. Fluids **28**, 3485.

[40] Jenkins, J. T., and Richman, M. W. 1986. Boundary conditions for plane flows of smooth, nearly elastic, circular disks. J. Fluid Mech. **171**, 313.

[41] Jenkins, J. T., and Yoon, D. K. 2002. Segregation in binary mixtures under gravity. Phys. Rev. Lett. **88**, 194301.

[42] Jenkins, J. T., and Zhang, C. 2002. Kinetic theory for identical, frictional, nearly elastic spheres. Phys. Fluids **14**,1228.

[43] Knight, J. B., Jaeger, H. M., and Nagel, S. 1993. Vibration-Induced Size Separation in Granular Media: The Convection Connection. Phys. Rev. Lett. **70**, 3728.

[44] Koch, D. L., and Sangani, A. S. 1999. Partial pressure and marginal stability limits for a homogeneous monodisperse gas-fluidized bed: kinetic theory and numerical simulations. J. Fluid Mech. **400**, 229.

[45] Liu, J., and Rosato, A. D. 2005. General features of granular Couette flow and intruder dynamics. J. Phys.: Condens. Matter **17** S2609.

[46] López de Haro, M., Cohen, E. G. D., and Kincaid, J. M. 1983. The Enskog theory for multicomponent mixtures: I. Linear transport theory. J. Chem. Phys. **78**, 2746.

[47] Louge, M. Y., Jenkins, J. T., Xu, H., and Arnarson, B. Ö. 2001. Granular segregation in collisional shearing flows, in *Mechanics for a new Millenium*.

[48] Louge, M. Y. 2003. Model for dense granular flows down bumpy inclines. Phys. Rev. E **67**, 061303.

[49] Luding, S., Muller, M., and McNamara, S. 1998. The validity of 'Molecular Chaos' in granular flows, in *World Congress on Particle Technology*.

[50] Lun, C. K. K., Savage, S. B., Jeffrey, D. J., and Chepurniy, N. 1984. Kinetic theories for granular flow: inelastic particles in Couette flow and slightly inelastic particles in a general flow field. J. Fluid Mech. **140**, 223.

[51] Lun, C. K. K. 1991. Kinetic theory for granular flow of dense, slightly inelastic, slightly rough spheres. J. Fluid Mech. **233**, 539.

[52] Mancini, F. 1986. Transport Theory for dense binary mixtures of smooth, round, nearly elastic particles (Ph.D. thesis, Cornell University, Ithaca, NY).

[53] Mitarai, N., and Nakanishi, H. 2005. Bagnold Scaling, Density Plateau, and Kinetic Theory Analysis of Dense Granular Flow. Phys. Rev. Lett. **94**, 128001.

[54] Poschel, T., Brilliantov, N. V., and Schwager, T. 2002. Violation of molecular chaos in dissipative gases. Int. J. Mod Phys C **13**, 1263.

[55] Pouliquen, O. 1999. Scaling laws in granular flows down rough inclined planes. Phys. Fluids **11**, 542.

[56] Rajchenbach, J. 2003. Dense, rapid flows of inelastic grains under gravity. Phys. Rev. Lett. **90**, 144302.

[57] Reed, T. M., and Gubbins, K. E. 1973. *Applied Statistical Mechanics*. McGraw-Hill, New York.

[58] Richman, M. W. 1988. Boundary conditions based upon a modified Maxwellian velocity distribution for flows of identical, smooth, nearly elastic spheres. Acta Mech. **75**, 227.

[59] Richman, M. W. 1993. Boundary conditions for granular flows at randomly fluctuating bumpy boundaries. Mech. Mater. **16**, 211.

[60] Rosato, A., Strandburg, K. J., Prinz, F., and Swendsen, R. H. 1987. Why the Brazil nuts are on top: size segregation of particulate matter by shaking. Phys. Rev. Lett. **58**, 1038.

[61] Savage, S. B., and Sayed, M. 1984. Stresses developed by dry cohesionless. granular materialssheared in an annular shear cell. J. Fluid Mech. **142**, 391.

[62] Sela, N., and Goldhirsch, I. 1998. Hydrodynamic equations for rapid flows of smooth inelastic spheres, to Burnett order. J. Fluid Mech. **361**, 41.

[63] Silbert, L. E., Landry, J. W., and Grest, G. S. 2003. Granular flow down a rough inclined plane: Transition between thin and thick piles. Phys. Fluids **15**, 1.

[64] Taberlet, N., Losert, W., and Richard, P. 2004. Understanding the dynamics of segregation bands of simulated granular material in a rotating drum. Europhys. Lett. **68**, 522.

[65] Torquato, S. 1995. Nearest-neighbor statistics for packings of hard spheres and disks. Phys. Rev. E **51**, 3170.

[66] van Beijeren, H., and Ernst, M. H. 1973. The modified Enskog equation. Physica **68**, 437.

[67] Walton, O. R. 1993. Numerical simulations of inelastic, frictional particle-particle interactions, in *Particle Two-Phase Flow*, ed. M. C. Roco, p. 884, Butterworth, London.

[68] Wildman, R. D., and Parker, D. J. 2002. Coexistence of two granular temperatures in binary vibrofluidized beds. Phys. Rev. Lett. **88**, 064301.

[69] Wildman, R. D., Jenkins, J. T., Krouskop, P. E., and Talbot, J. 2006. A comparison of kinetic theory predictions with experimental and numerical results for a vibrated granular bed containing two size species. *Submitted*.

[70] Willits, J. T., and Arnarson, B. Ö. 1999. Kinetic theory of a binary mixture of nearly elastic disks. Phys. Fluids **11**, 3116.

[71] Xu, H., Louge, M, and Reeves, A. 2003. Solutions of the kinetic theory for bounded collisional granular flows. Continuum Mech. Thermodyn. **15**, 321.

[72] Yoon, D. K., and Jenkins, J. T. 2005. Kinetic theory for identical, frictional, nearly elastic disks. Phys. Fluids **17**, 083301.

[73] Yoon, D. K., Arnarson, B. Ö., and Jenkins, J. T. 2005. Segregation in a sheared binary mixture of nearly elastic, smooth disks under gravity, in *Powders and Grains 2005* , Balkema, Rotterdam.